Photocatalysis of 4-chloro- and 4-nonylphenols using novel symmetric phthalocyanines and an asymmetric porphyrin supported on polyacrylonitrile nanofibres

A thesis submitted in fulfilment of the requirements for the degree of

Master of Science

By

Benjamin Martin Jones

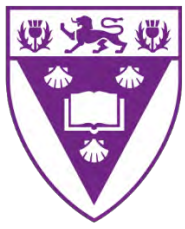

RHODES UNIVERSITY

Where leaders learn

February 2020

Dedication

This thesis is dedicated towards my two pillars

of support from the very beginning, my:

Mother

Sarah Ann Jones

&

Father

Michael Lynn Jones

Acknowledgements

First and foremost, my deepest and sincerest acknowledgements go towards to my supervisor, Distinguished Professor Tebello Nyokong for allowing me the utmost privilege of studying under her mentorship. Thank you for your endless patience, guidance, and support you have provided throughout my postgraduate life at Rhodes University. My endless gratitude goes out to you. I would also like to thank the team of Professor Mack and Dr. Britton, who never hesitated to assist whenever assistance was required. To my colleagues of S22, who I comfortably call my friends, this achievement could not have been accomplished without the endless hours of assistance and constant entertainment that you have supplied! Special mention must go to the one and only Donovan “El Diablo” Mafukidze, your counsel and direction has impacted me incredibly. Little Bean, you are an infinite source of inspiration which I hold so dear to me. Finally, it was never a chore to work around all involved and associated with the Institution of Nanotechnology Innovation. You have really been a family away from home and I thank you from the bottom of my heart. Without the financial support from the National Research Foundation through DST/NRF South Africa Research Chairs Initiative this would not have been possible, and I am eternally grateful.

Abstract

This work explores the synthesis and characterisation of novel symmetrical phthalocyanines and novel asymmetric porphyrins that have been embedded or linked, respectively, and electrospun into fibres for application in the photocatalysis of environmental pollutants. The phthalocyanines contain pyrrole moieties without hetero atom linkers to maintain a rigid structure. The porphyrin contains a carboxy moiety utilized to construct an amide bond between the complex and the polymer prior to the spinning process. The new compounds were characterized by elemental analyses, proton nuclear magnetic resonance (^{1}H NMR), Fourier-transform infrared spectroscopy (FT-IR), MALDI-TOF and UV-vis spectroscopy. The general trends of fluorescence, triplet and singlet oxygen quantum yields are described as well as their appropriate lifetimes. The photocatalytic activity of phthalocyanine embedded fibres were compared against those that had been dyed. Unfortunately, during the degradation process, the dyed fibres leeched compound and the studies could not be continued. It was seen that the porphyrin fibres linked to the polymer showed the most efficient photocatalytic activity against 4-cholorphenol and 4-nonylphenol due to irradiation at lower wavelengths consequently having higher frequencies and transferring more energy.

Table of Contents

List of Abbreviations

ADMA	Tetrasodiuma,a-(anthracene-9,10-diyl)dimethylmalonate
DBU	1,8-diazabicyclo[5.4.0]undec-7-ene
DMF	Dimethylformamide
DMSO	Dimethylsulfoxide
EDC	1-Ethyl-3-(3-dimethylaminopropyl)- carbodiimide/ Endocrine Disrupting Chemicals
EDS	Energy dispersive spectroscopy
FT-IR	Fourier Transform Infrared
^{1}H NMR	Proton nuclear magnetic resonance
HOMO	Highest Occupied Molecular Orbital
ISC	Intersystem crossing
LUMO	Lowest unoccupied molecular orbital
MALDI	Matrix-assisted laser desorption/ionization
MPc	Metallophthalocyanine
NHS	N-hydroxysuccinimide
NMR	Nuclear magnetic resonance
PBS	Phosphate buffer solution
ROS	Reactive oxygen species
SEM	Scanning electron microscopy

TCD	Tip to collector distance
TCSPC	Time-correlated single photon counting
THF	Tetrahydrofuran
UV-vis	Ultraviolet/visible

List of Symbols

α	non-peripheral position
β	peripheral position
τ	lifetime
τ_F	fluorescence lifetime
τ_T	triplet state lifetime
Φ_F	fluorescence quantum yield
Φ_T	triplet state quantum yield
$\Phi\Delta$	singlet oxygen quantum yield
S_1	Singlet excited state
t	time
T_1	triplet excited state

Preamble: This thesis provides an overview on the use of phthalocyanines and porphyrins for the photodegradation of phenolic pollutants. The pollutants chosen are 4-nonylphenol and 4-chlorophenol and were tested against porphyrins and phthalocyanines supported on polyacryonitrile electrospun fibres.

Chapter 1
Introduction

Preamble: This chapter provides an overview on the compounds that are used and relevant literature pertaining to possible applications in which they have been utilized. It also introduces the use of the compounds in conjunction with electrospun fibres. The photophysical properties of the compounds and conjugates will also be introduced.

1.1 Phthalocyanines

1.1.1 A brief history of the molecules

The initial journey of phthalocyanines (Pcs) began by a serendipitous discovery in 1907 by Bruan and Tcherniac when reacting acetic anhydride with a phthalimide [1]. About two decades later, a failed attempt to convert *o*-dibromobenzene into a phthalonitrile resulted in the unearthing of a series of copper phthalocyanine species [2]. Interestingly, these compounds exhibited incredibly high thermal tolerances and stability but were not investigated further. It was not until 1934 when Sir Patrick Linstead studied the chemical and structural properties of iron phthalocyanine [3].

1.1.2 Structure and properties

Phthalocyanines are grouped as a symmetrical, planar 18 π-electron heterocyclic aromatic systems that consist of 4 isoindole moieties (**Figure 1.1**) linked by four aza nitrogen units creating an inner cavity that is often filled with metals [4]. The molecular architecture of these molecules is vastly flexible and can be fine-tuned for different applications. Various substituents can be introduced along the peripheral (β) and non-peripheral (α) positions along with the possibility of the introduction of a central metal as a means of fine tuning their properties.

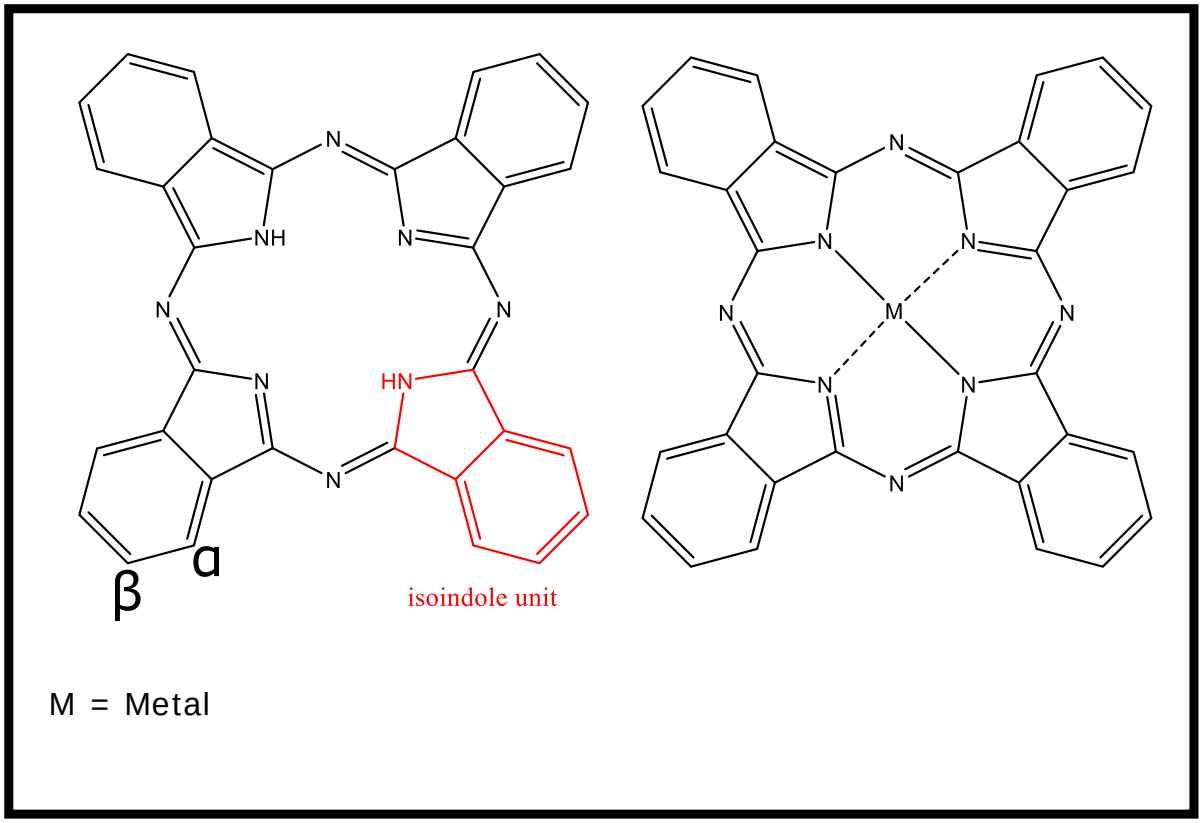

Figure 1.1 – Structure of free base Pc and metallophthalocyanines (MPc)

1.1.3 Applications

Pcs have been reported to have an extremely wide range of applications varying from photodynamic therapy [5], electrochromism [6], photodynamic antimicrobial chemotherapy [7], electrocatalysis [8], dye-sensitized solar cells [9], non-linear optics, [10] and photocatalysis [11]. The latter application with specific regards to phenolic pollutants is the subject of this thesis.

1.1.4 Synthetic Routes

Symmetric phthalocyanines can be synthesized by different routes [12–15]. **Scheme 1.1** illustrates the several differently substituted phthalonitriles that are typically expected in the synthesis of symmetric phthalocyanines [16].

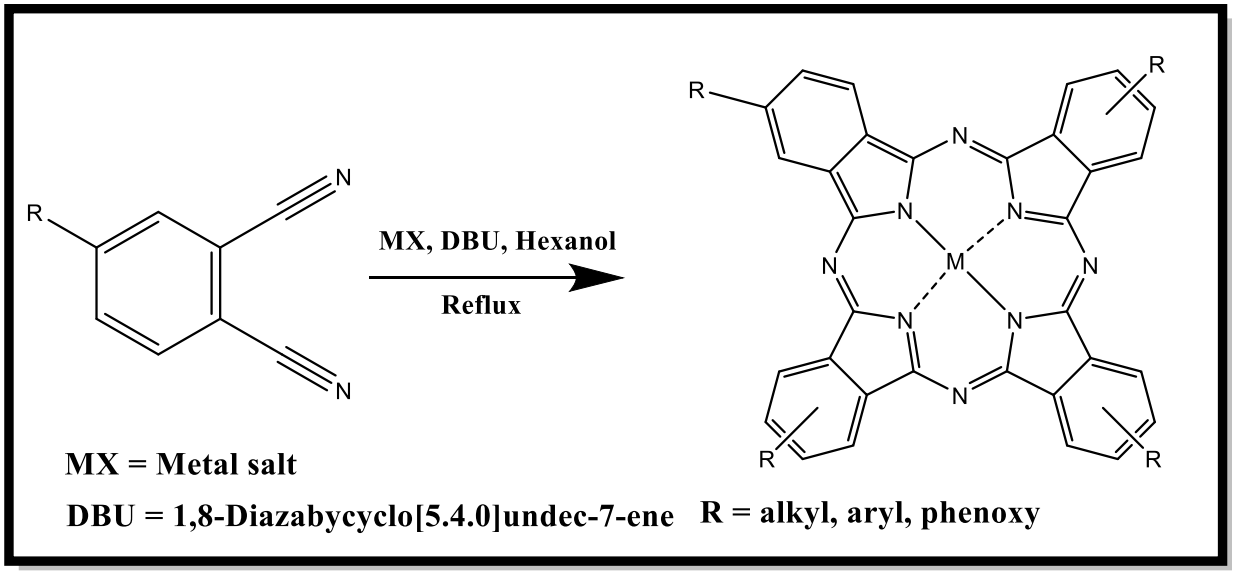

Scheme 1.1. Synthesis of substituted symmetrical phthalocyanine

1.1.5 Electronic Absorption Spectra

The absorption spectra of phthalocyanines has been greatly conceptualised by Gouterman and his four orbital model [17]. In this model, four molecular orbitals are taken into account, being the two highest occupied molecular orbitals (HOMO) and the two lowest unoccupied molecular orbitals (LUMO) [18]. Pcs characteristically display two main spectral absorption bands, namely the Q and the B or Soret bands. The Q band usually resides around 650-1000 nm while the B band is around 300-450 nm (**Figure 1.2**).

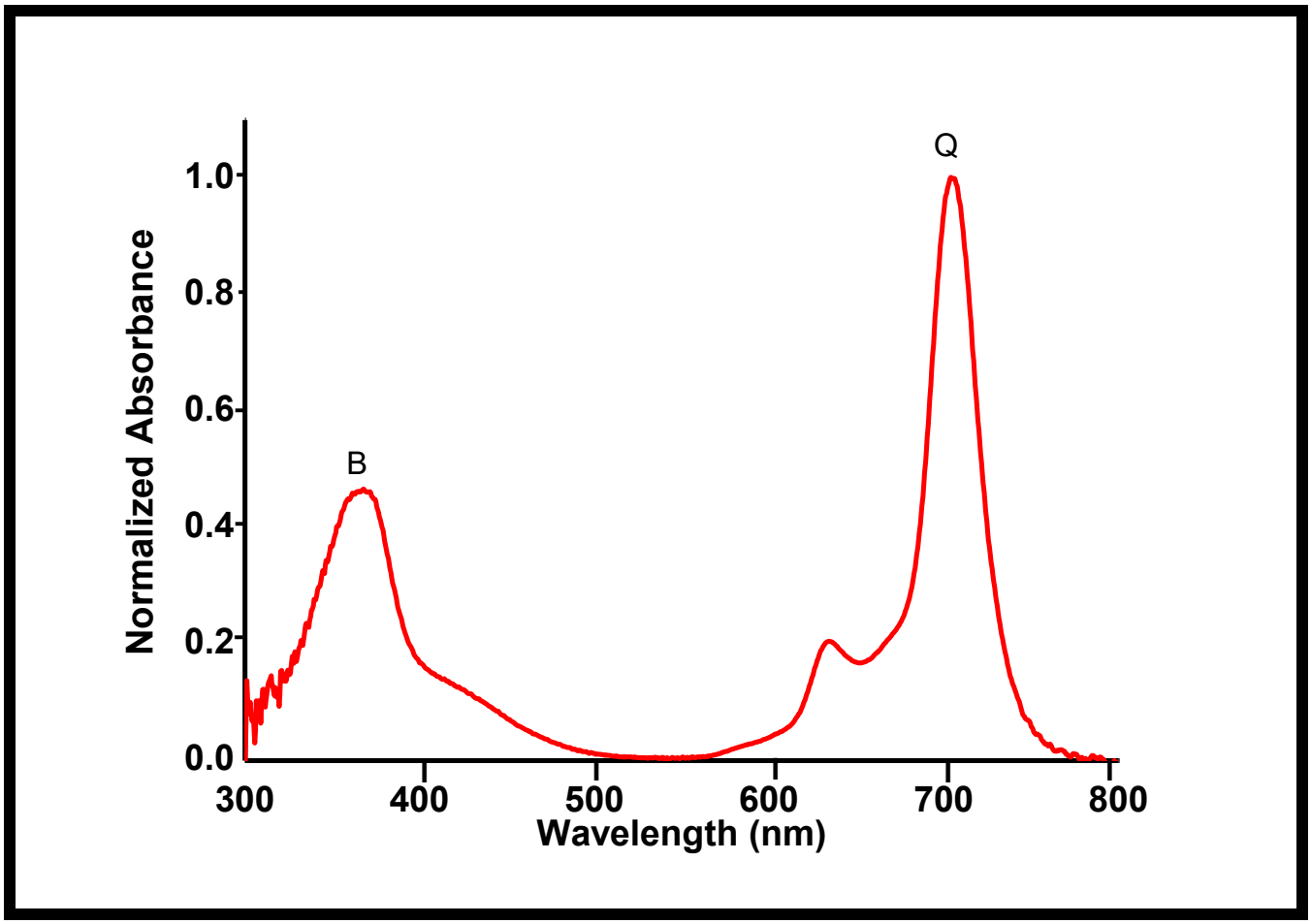

Figure 1.2 – Typical absorption spectra of a phthalocyanine

The Q band stems from the $\pi \rightarrow \pi$ transitions from the a_{1u} orbital of the homo to the e_g orbital of the LUMO [18]. The B bands stem from the transition of the a_{2u} and b_{2u} orbitals to the e_g orbital (**Figure 1.3**). The B band is observed to be significantly less intense and typically broader than the Q band [19].

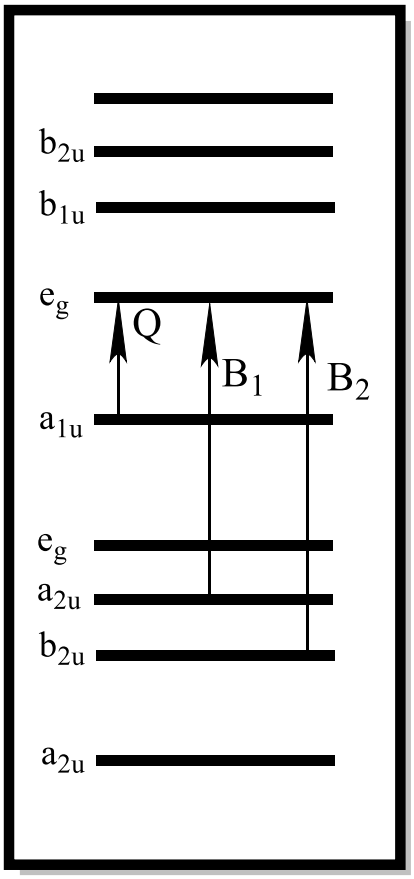

Figure 1.3 – Electronic transitions of a phthalocyanine showing the origin of Q and B bands

1.2 Porphyrins

1.2.1 A brief history of the molecule

The porphyrin's name is derived from the Greek word "porphura" meaning purple, and have been observed for as long back as to when the Phoenicians used the pigment to dye their clothes in 1570 BC [20]. They have been dubbed the "molecules of life" due to the crucial roles which they play in natural systems. A porphyrin is embedded in the structure of heme and it is also part of the structure of chlorophyll, in the form of a reduced porphyrin (chlorin), which allows plants to absorb energy from light (**Figure 1.4**).

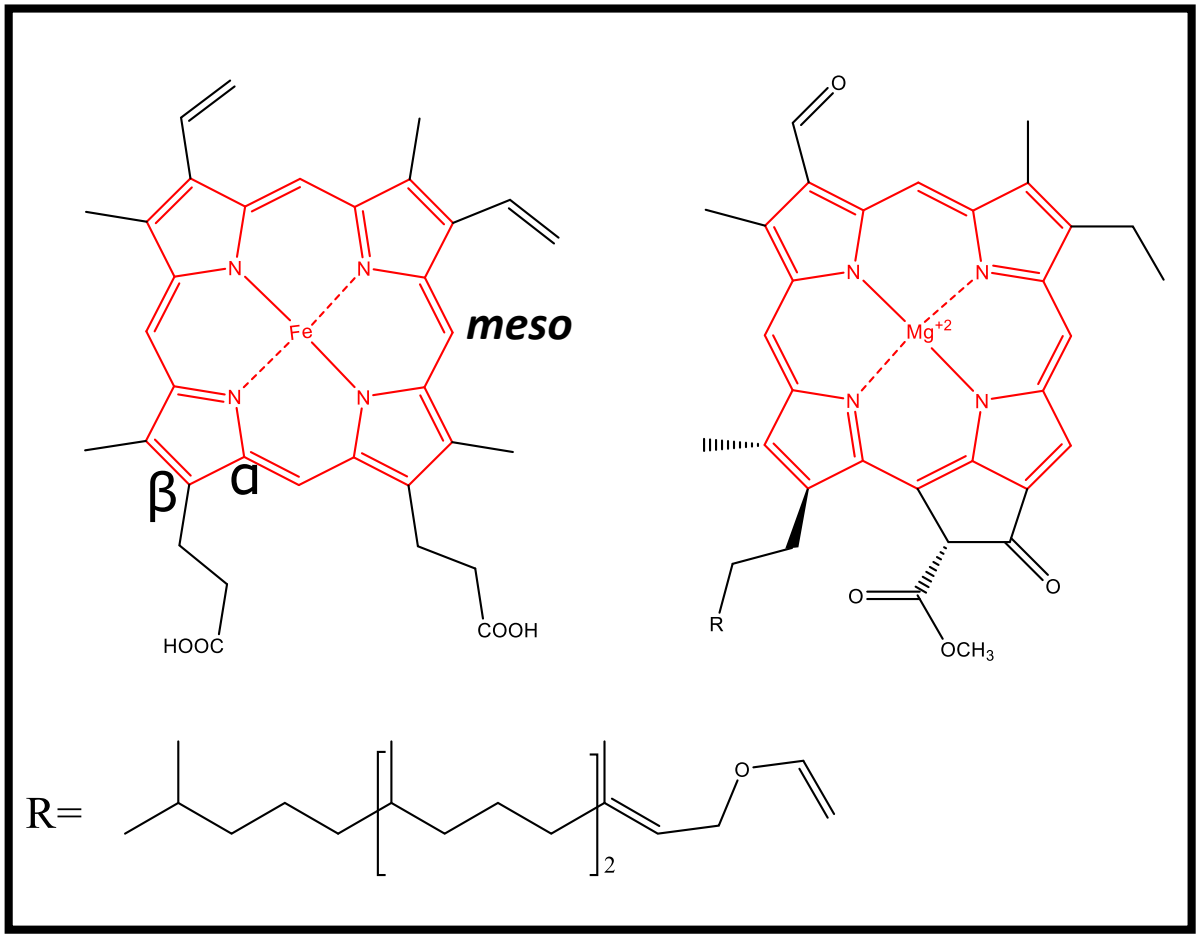

Figure 1.4 – The structure of heme (left) and chlorophyll (right)

1.2.2 Structure and properties

Porphyrins are a group of heterocyclic macrocycle organic compounds, that are made up of four altered pyrrole subunits interconnected at α carbons via methine bridges. It was in 1912 when Küster first proposed the original structure of the compound [21] but it was not confirmed up until 1929 when Zeile and Fisher also proposed the same structure and succeeded in synthesizing heme using pyrrolic starting materials [22]. The unit consists of 26 π-electrons in total, of which 18 π-electrons form the planar, continuous, aromatic ring [23]. The peripheral carbons present on the pyrrole moieties are the α and β carbons while the carbons bridging the pyrroles are known as the *meso* carbons and both are subject to modification [24]. A result of this π conjugated system is that porphyrins typically absorb light in the visible region of the electromagnetic spectrum, consequently deeply colouring them.

1.2.3 Applications

Porphyrins have been extensively applied in various sectors of the scientific domain. Some of these include energy conversion technologies [25], targeted imaging and therapy [26], photocatalysis [27,28], electric and optical sensors [29], photodynamic therapy [30], drug delivery [31] and organic solar cells [32]. Photocatalysis will be discussed in further detail and demonstrated in this work.

1.2.4 Synthetic Routes

There are multiple pathways these structures can be formed [33]. The Adler *et al* synthesis [33] was employed in this work and involves the addition of pyrrole and an aldehyde as illustrated in **Scheme 1.2**. This work utilized multiple aldehydes to afford an asymmetric porphyrin.

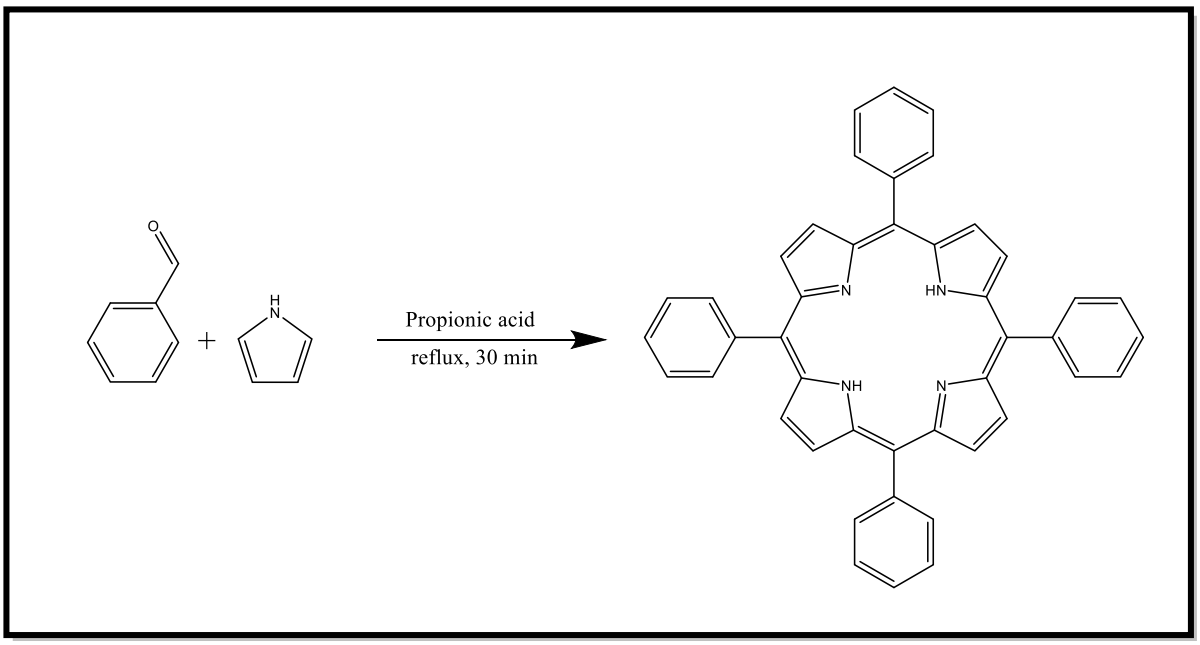

Scheme 1.2 – Adler et al synthesis of a porphyrin

1.2.5 Electronic Absorption Spectra

The absorption spectra of porphyrins may also utilise the concept of Gouterman's model as previously described above [17]. Basic free base porphyrins show a four-banded visible spectrum of moderate intensity in the region of 500 to 650 nm, the Q bands, and a band of extreme intensity around 400 nm known as the Soret band [17]. However, a striking spectral change is exhibited when a free base is converted into a metal porphyrin, whereby there is a collapse of the four-banded spectrum bands into two, and an observed shift in the whole spectrum (**Figure 1.5**) [34].

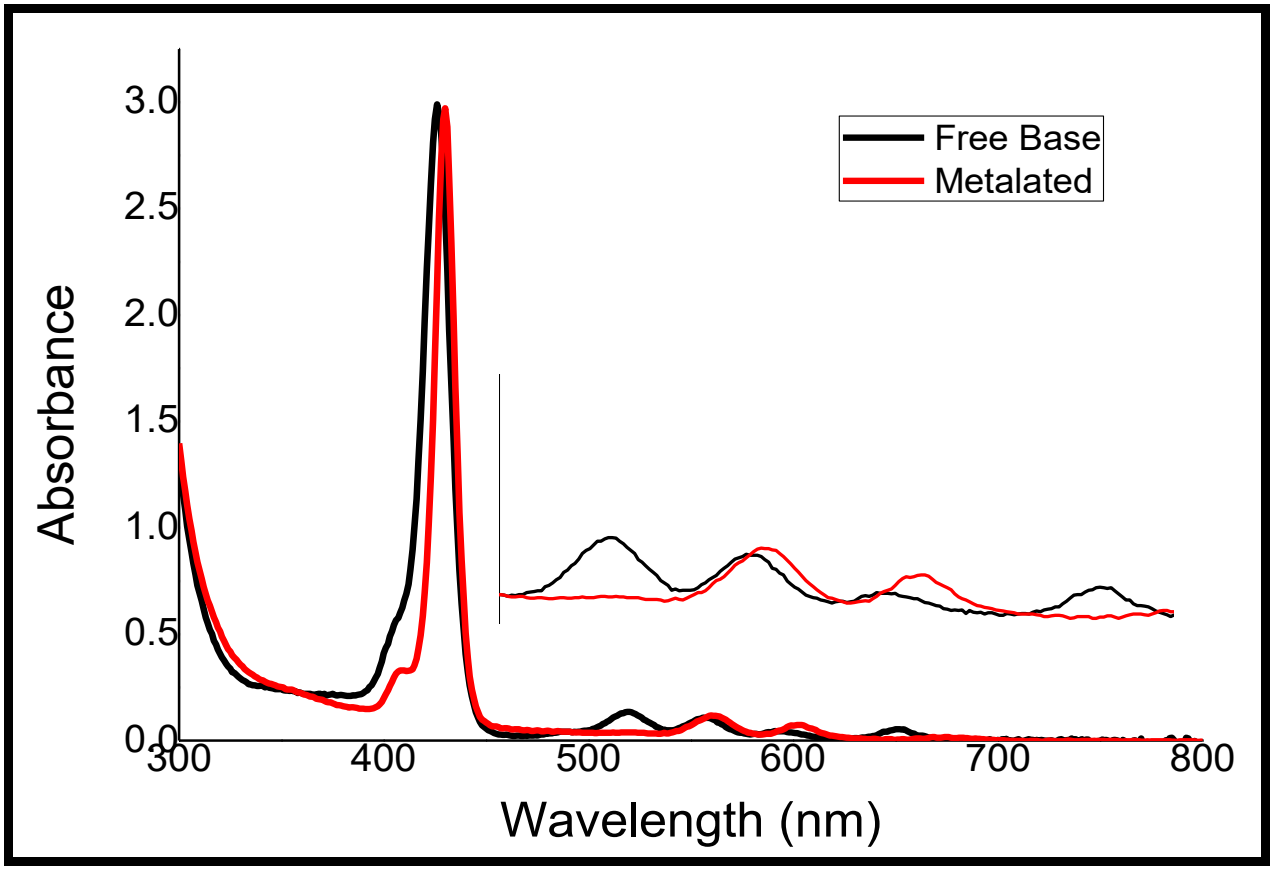

Figure 1.5 – Electronic absorption spectra of a free base porphyrin (black) and a zinc metalated porphyrin (red)

The four Q bands are attributed to $\pi \rightarrow \pi$ transitions namely the a_{1u} (HOMO) orbital to the e_g (LUMO) orbital while the B band is a transition from the a_{1u} to e_g. (**Figure 1.6**) [35,36]. The origin of the four Q bands in free-base porphyrins is due to vibrational excitations. Two bands would be produced owing to transitions from the ground state to two vibrational states. But the presence of the inner NH protons breaks the symmetry and as a result are further split into two more bands. The Q_x and Q_y components are no longer degenerate hence four Q bands are observed.

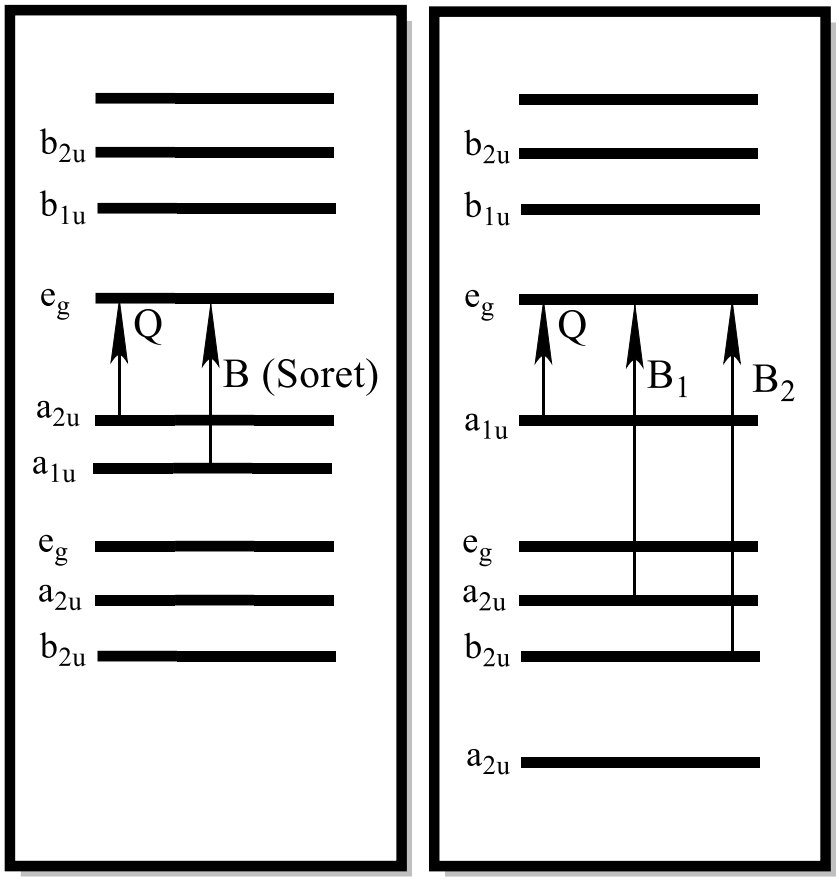

Figure 1.6 – Electronic transitions typically expected from a porphyrin (left) compared to a phthalocyanine (right)

When the absorption bands of a porphyrin are compared to a phthalocyanine, there is an obvious difference in the intensities in the bands. The reason why the Soret band of the porphyrin is much more intense than the Q bands is due to the configuration interactions between the a_{2u} and a_{1u} orbitals (**Figure 1.6**) as they are much closer compared to that of the phthalocyanines and are considered essentially degenerate (**Figure 1.6**) [17]. In addition, this results in both the B and Q transitions almost completely retaining their allowed and forbidden characteristics, respectively [17]. As for the Q band of the phthalocyanine, the degeneracy of these orbitals is lifted (**Figure 1.6**) when there is an addition of the aza linkages and fuzed benzene

rings. This leads to a mixing of the excited states and a significant increase in the Q band [17].

1.3 Photodegradation of Environmental Pollutants

Advanced oxidation process (AOP) such as photocatalysis has gained immense popularity as an agent in the process of degrading recalcitrant pollutants in wastewater [37,38]. The driving force behind this reaction is the generation of reactive oxygen species (ROS) from molecular oxygen which degrade pollutants [39]. Photocatalysis has become increasingly popular as the use of sunlight as a source of energy is not only harmless and cheap, but also broadly available. AOPs also display very rapid reaction rates due to its high oxidation potentials and their non-selectivity. Furthermore, due to the oxidation power of the ROSs, these AOP systems generally do not require a large volume for operation resulting in a much smaller footprint. AOPs have also displayed the ability to mineralize organic materials into stable, inorganic compounds such as water, CO_2, and H_2 gas. Endocrine disrupting chemicals (EDCs) such as 4-nonylphenol (4-*n*-NP) are exogenous substances that directly affect the endocrine system and consequently cause adverse health effects and affect growth and reproduction [40–42]. Unfortunately, 4-*n*-NP (**Figure 1.7**) has been widely detected in various organic wastewaters worldwide [43]. On the other hand, chlorophenols (eg 4-CP) (**Figure 1.7**), are common environmental pollutants as by-products of several manufacturing processes such as pesticides, plastics, dyes and pharmaceuticals [44].

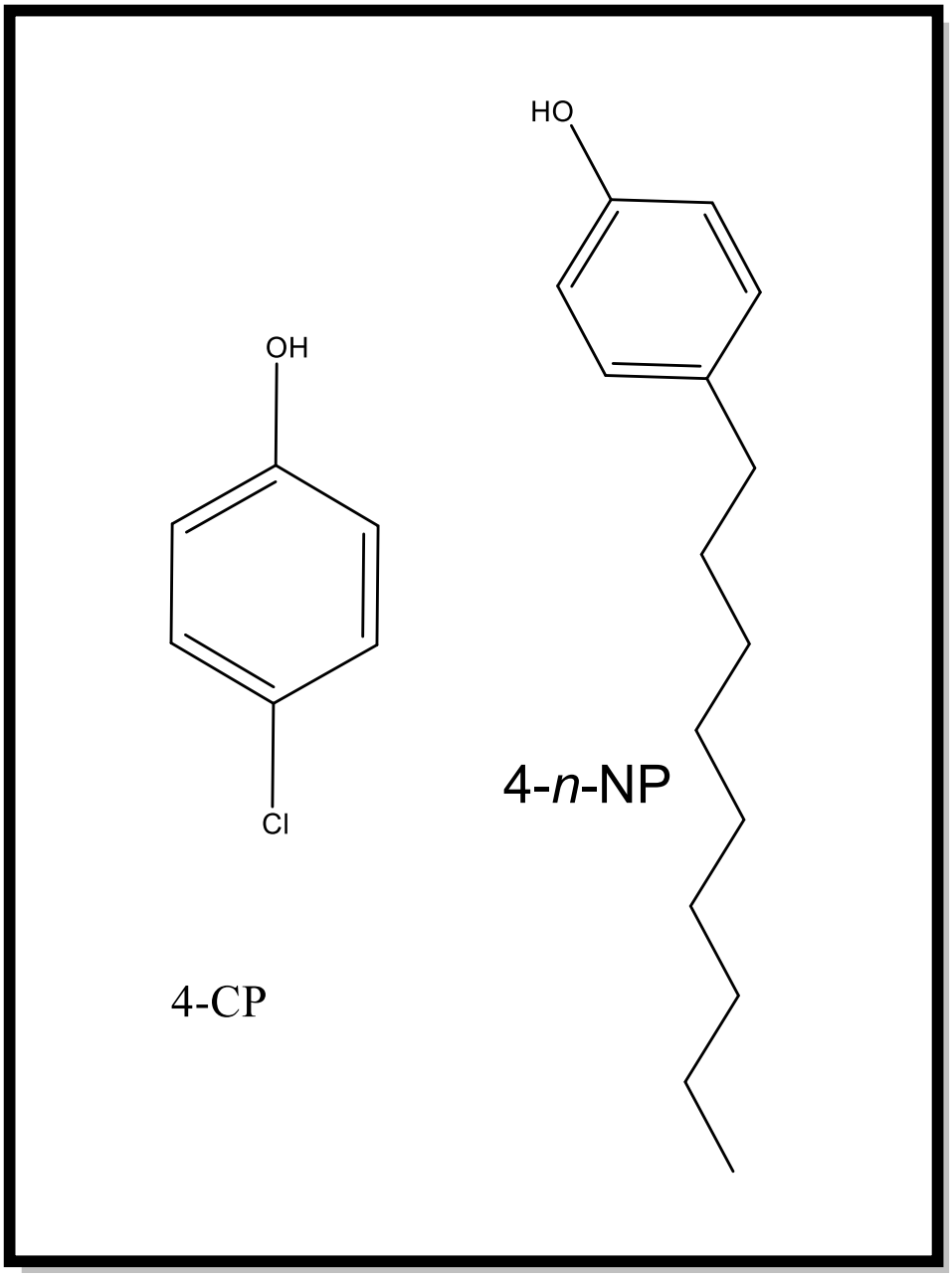

Figure 1.7 - Structure of 4-chloropheno (left)l and 4-nonylphenol (right)

There have been several reported methods of removal of chlorophenols and EDCs such as chemical oxidation, biological methods and photocatalytic processes [45]. This work reports the photodegradation of 4-nonylphenol and 4-chlorophenol using AOP. Previously, phthalocyanines have been used in solution to photodegrade 4-CP [46–48]. Instances where phthalocyanines have been supported on other fibres

showed initial and observed rates of up to 13.1×10^{-7} mol.$L^{-1}min^{-1}$ and 11.1×10^{-3}.min^{-1} with a degradation percentage of 31.9% after 30 min [49]. When supported on polymer membranes, Pcs displayed improved kinetics with initial and observed rates of 3.77×10^{-6} mol$L^{-1}min^{-1}$ and 35.9 L$mol^{-1}min^{-1}$[11]. Porphyrins have also been used against 4-CP using the same process [50,51]. Although the photodegradation of 4-*n*-NP has been attempted before using a phthalocyanine [52] it has never been attempted using a porphyrin before nor with the addition of electrospun fibres, hence this is the subject of this thesis.

1.4 Electrospun fibres

1.4.1 Brief History

The principles of electrostatic attractions date back as early as the 17th century by William Gilbert when he approached a droplet of water on a dry surface with a piece of amber and noted the conical morphology it took [53]. This is the first record of the deformation of a drop which became known as the Taylor cone (**Figure 1.8**) [54]. It was not until 1900 when Cooley filed the first patent of the electrospinning technique where he proposed four different types of indirectly charged heads and a spinneret accompanied by a rotating distributor [55].

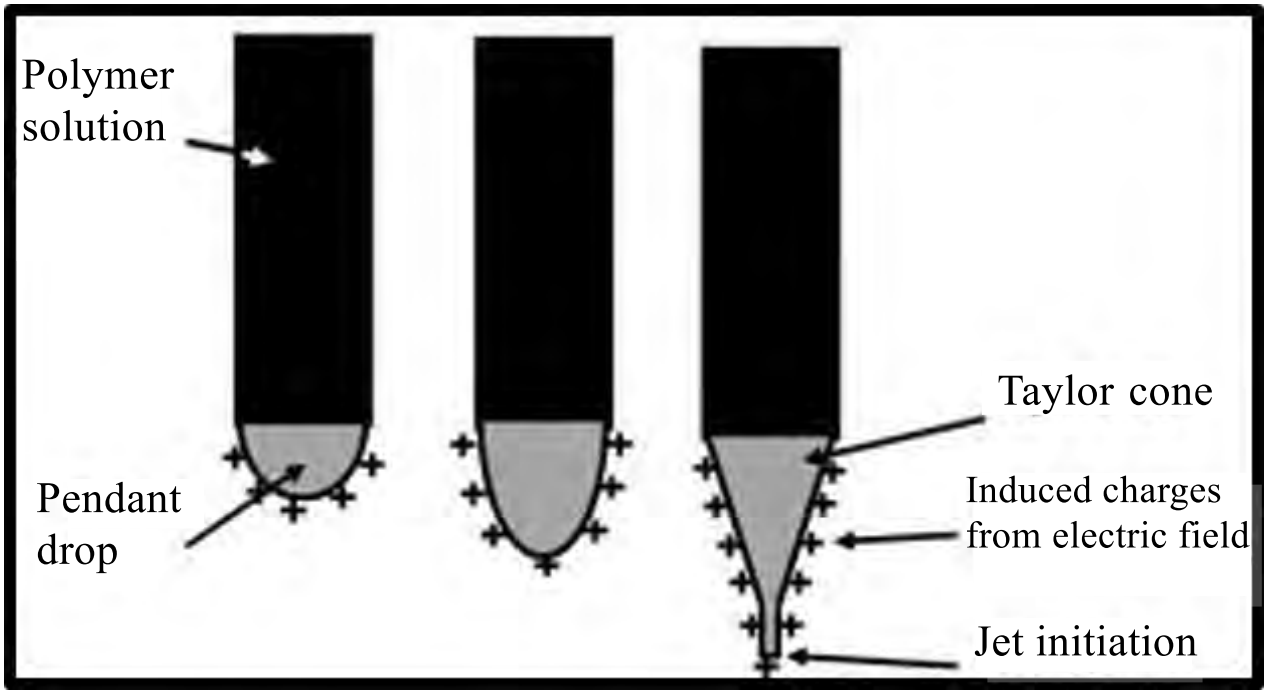

Figure 1.8 – The formation a Taylor cone [54]

1.4.2 Basic Principles

Electrospinning is a reproducible fibre production method which uses electric force to eject threads or jets of a polymer solution with diameters in the order of some hundred nanometres. During the process, a high voltage is applied to the spinneret thus inducing a charge upon the polymer solution. The collecting plate is oppositely charged, inducing a change in potential difference. When a charged polymer is then fed through the spinneret, a jet of threads is ejected from the Taylor cone due to the applied electrostatic force overcoming the surface tension of the polymer (**Figure 1.9**) [56–58]. The morphology of fibres can be varied depending on several controllable parameters, such as: weight percentage (solution concentration), voltage applied, tip to collector distance, solvent and the flow rate [59]. It has also been reported that the relative humidity during the time of spinning influences the morphology of the fibres [60,61].

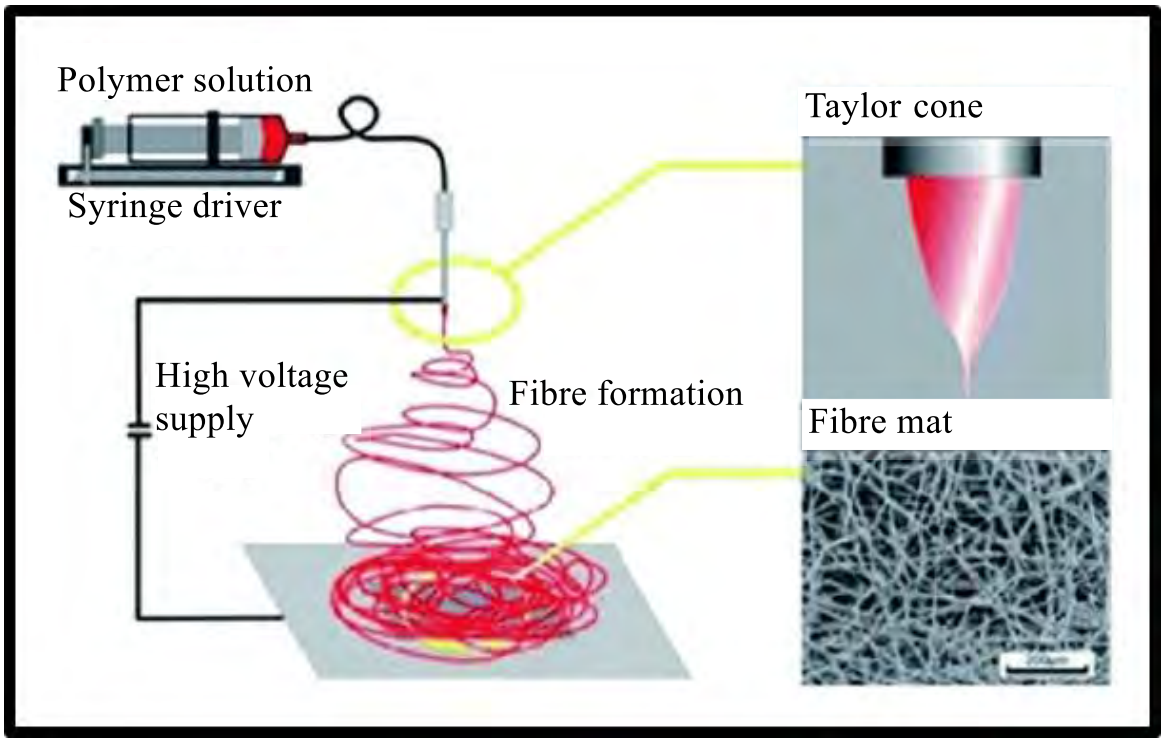

Figure 1.9 – Schematic diagram of the electrospinning process [61]

Electrospinning has been applied across sectors in the modern world including but not limited to: as anti-microbial agents [62], in wound-dressing [63], electrodialysis [64], dye-sensitized solar cells [65], filtration [66] and drug delivery applications [67].

1.4.3 Reported Phthalocyanines/Porphyrins in Electrospun Fibres

In this work, phthalocyanines have been embedded and porphyrins have been covalently linked to electrospun fibres as a means of solid support and for ease of recovery. **Table 1.1** lists examples [68–75] in literature of phthalocyanines or porphyrins that have been involved with electrospun fibres for various applications. As **Table 1.1** shows that there has never been electrospun fibres composed of polyacrylonitrile (PAN) employed against the photocatalysis of phenols making this the first time it has been done. More conventional polymers that have been used before e.g. polystyrene are not as favourable compared to PAN because polystyrene has been shown to have less stability than other fibres [76]. It has also been reported that polystyrene has poor chemical resistance, is susceptible to UV degradation and its chemical composition may impose health effects [77]. Other asymmetric porphyrins have been linked to fibres previously for fluorescence and photocatalytic studies of methyl red [68,69] but this work reports the first time a porphyrin has been linked to polyacrylonitrile and used against the photocatalysis of phenols.

Table 1 - Examples of known electrospun fibres functionalised with phthalocyanines and porphyrins

Compound	Support System	Application	Reference
InOCPc	PAN	Photodegradation of methyl red and PACT	[70]
InTPOPc InAPPc	Polystyrene	Photooxidations of bisphenol A and 4-chlorophenol	[71]
H_2TPCPc	Polystyrene	PACT	[72]
ZnOCPc	Polyamide-6	Photodegradation of orange-G	[73]
MnTPPy	PAN	Superoxide dismutase activity studies	[74]
H_2TPPy	Polystyrene, polyhydroxybutryrate	Gas sensing	[75]
MATPPy	PAN	Fluorescence studies	[69]
FeATPPy	PAN	Photocatalysis of methyl red	[68]

ClInOCPc = chloroindium octacarboxy phthalocyanine, InTPOPc = indium tetrapyridyloxyl phthalocyanine, InAPPC = indium aminophenoxy phthalocyanine, H_2TPCPc = free-base tetraphenylcarboxyphthalocyanine, ZnOCPc = zinc octacarboxy phthalocyanine, MnTPPy = manganese tetrapyridyl porphyrin, H_2TPPy = free-base tetraphenyl porphyrin, MATPPy = methylacrylotetraphenyl porphyrin, FeATPPy = iron aminotetraphenyl porphyrin, PAN = polyacrylonitrile.

1.5 Compounds Synthesized in this Work

The phthalocyanines synthesized in this work are shown in **Figure 1.10**. The substituents were chosen due to their bulky nature as a means of preventing aggregation which is unfavourable for the photodegradation process. Pyrrole also allows for polymerization of phthalocyanine complexes for future applications. This work reports for the first time the direct linkage of the pyrrole to the Pc ring without a hetero atom linker, as it will lead to a more rigid structure. The heavy atoms inserted into the central cavity were chosen as they encourage intersystem crossing from the excited singlet state to the triplet state resulting in an enhancement of the generation of singlet oxygen.

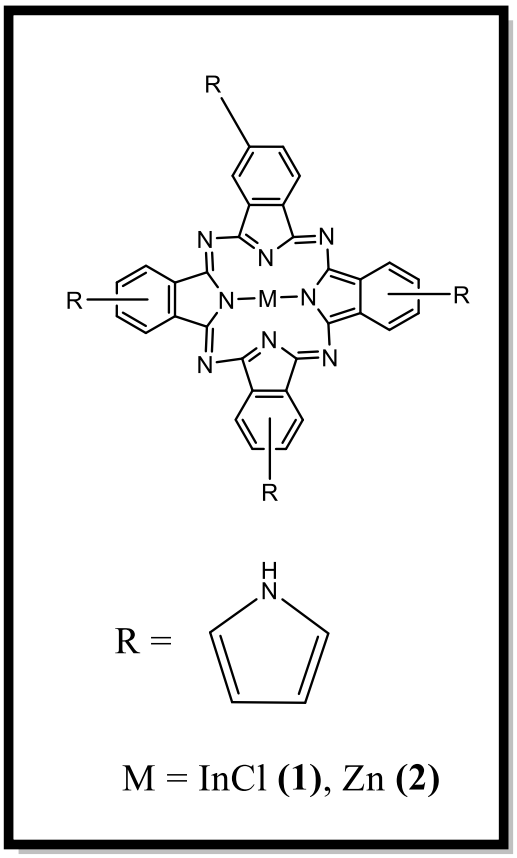

*Figure 1.10 – Structure of phthalocyanines employed in this work – **(1)** = indium tetrapyrrole phthalocyanine, **(2)** = zinc tetrapyrrole phthalocyanine*

The porphyrins employed in this work are shown in **Figure 1.11**. The carboxy moiety was added to allow the formation of an amide bond (**Figure 1.11**). Consequently, this would align the molecules along the polymer backbone due to even spacing from the covalent linking while preventing as much aggregation as possible for reasons aforementioned. The asymmetrical design of the porphyrin was selected as it has been reported that reducing the symmetry in porphyrins results in higher singlet oxygen quantum yields [78]. Compounds **(1)** and **(2)** were used as a comparison of the heavy metal between the photocatalysts. Compound **(3)** was only used as a precursor for compound **(4)** as this compound was used to compare the degradation of 4-*n*-NP and 4-CP.

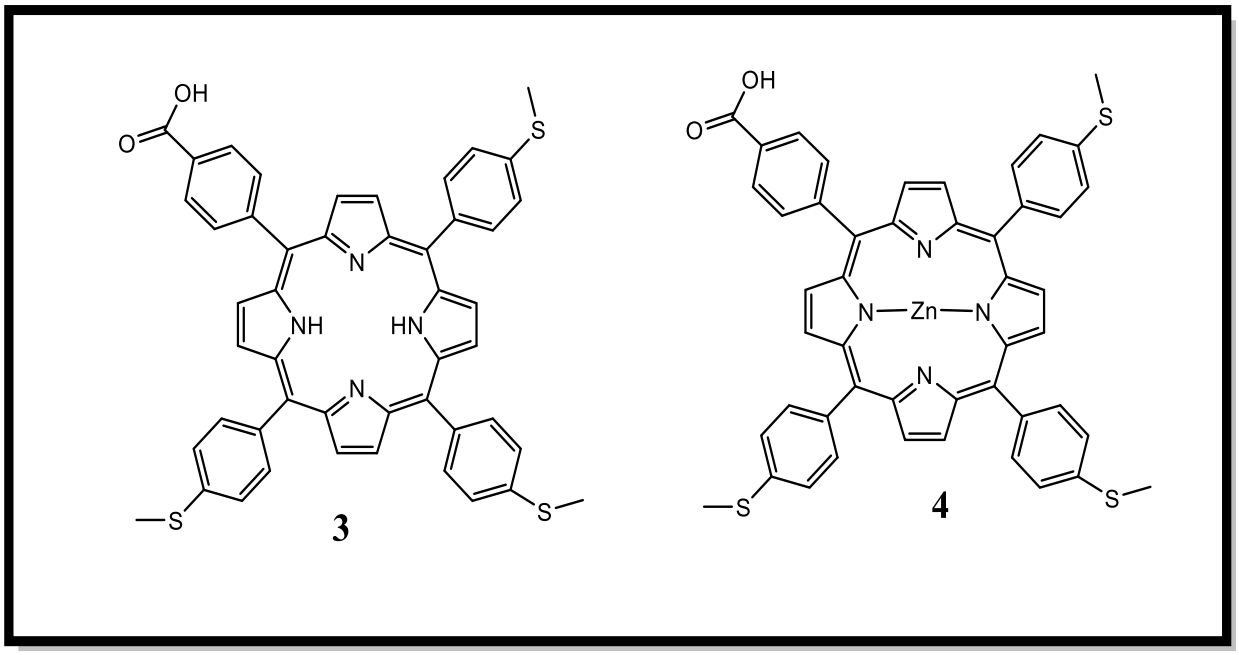

Figure 1.11 – Structure of porphyrins employed in this work

1.6 Photophysical and Photochemical Parameters

When a phthalocyanine or porphyrin is exposed to light a series of processes are initiated that can be excellently illustrated by a simplified Jablonski diagram (**Figure 1.12**) [79].

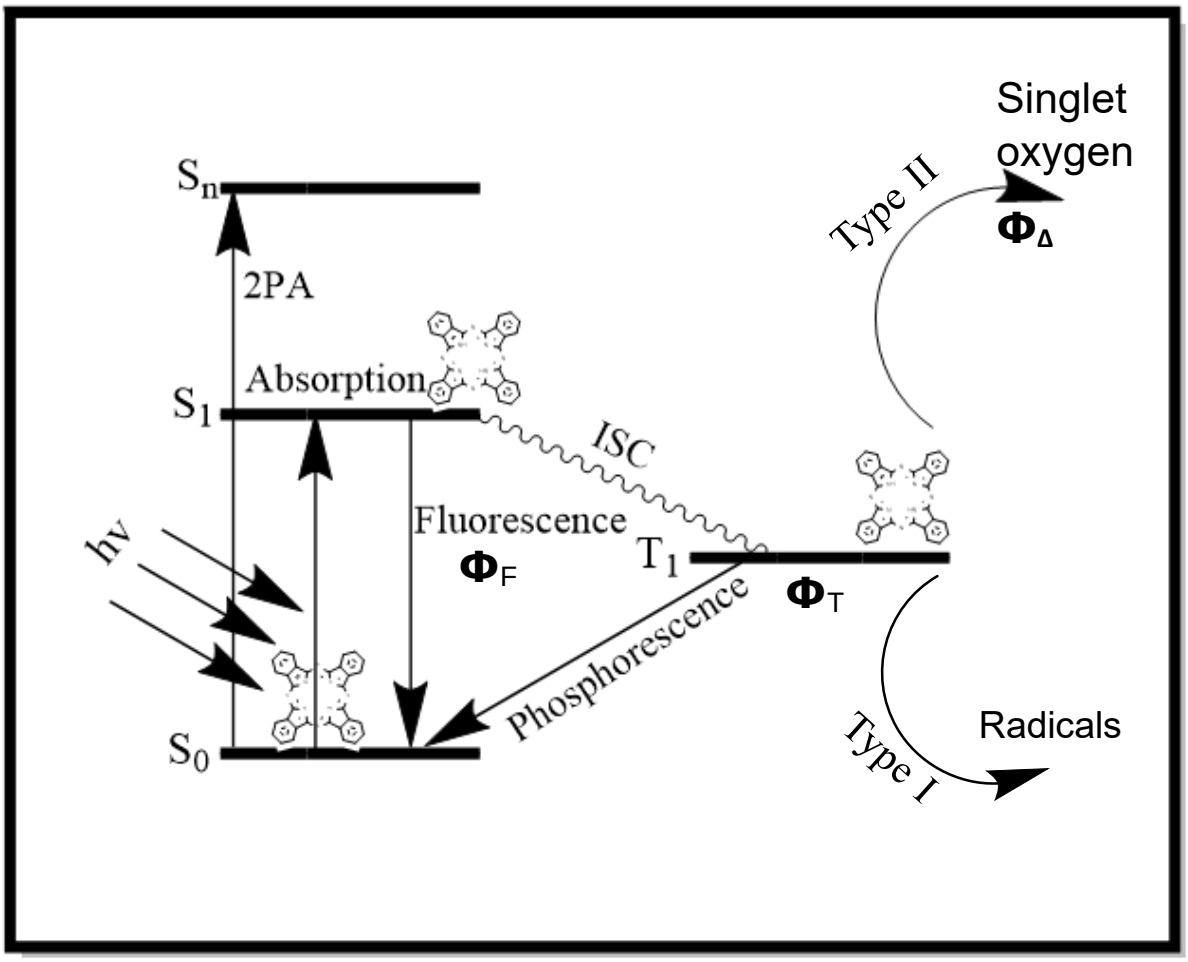

Figure 1.12 – A simplified Jablonski diagram

When a photosensitiser is irradiated with light (hv) it absorbs a photon and is excited from the ground singlet state (S_0) to the excited singlet state (S_1). The molecule can then either dissipate energy by emitting light through a process called fluorescence or undergo intersystem crossing (ISC) to the excited triplet state (T_1). The lifetime of

the triplet state is relatively long, allowing for the energy transfers to molecular oxygen to generate ROS via two pathways [80]. Type I pathway reactions use the electron transfer to produce hydroxyl and free radicals while Type II pathway reactions result in the generation of singlet oxygen.

1.6.1 Fluorescence Quantum Yield (Φ_F) and Lifetime (τ_F)

The fluorescence quantum yield can be defined as the ratio of photons absorbed to photons emitted through fluorescence. The **Φ_F** values (**Figure 1.12**) were all calculated using a comparative method where the emission spectrum of a sample is compared with that of a standard [81,82]. For the phthalocyanines, zinc phthalocyanine (ZnPc) was used as a standard (Φ_F^{Std}) where (**Φ_F** = 0.20 in DMSO) [81]. For the porphyrins, zinc tetraphenyl porphyrin (ZnTPP) was used as a standard where (**Φ_F** = 0.033 in DMF) [83]. **Equation 1.1** was used to calculate the values:

$$\Phi_F = \Phi_F^{Std} \frac{F\, A^{Std}\, n^2}{F^{Std} A\, (n^{Std})^2} \qquad \textbf{(1.1)}$$

where F and F^{Std} are the areas under the emission curves of the sample and standard, respectively, A and A^{Std} are the absorbances of the sample and standard, respectively, and n and n^{Std} are the refractive indices of the solvents used for sample and standard, respectively. The **Φ_F** values were determined for complex **1** and **2** at 620 nm. For complexes **3** and **4**, 421 and 425 nm were used respectively.

Fluorescence lifetimes (τ_F) can be defined as the time that a molecule occupies its excited state before it returns to the ground state through fluorescence. In this work, the method used is a very popular technique known as using time-correlated single-photon counting (TCSPC) [84]. All complexes were excited at their emission maxima.

1.6.2. Triplet Quantum Yield (Φ_T) and Lifetime (τ_T)

The triplet quantum yield (Φ_T) can be defined as the ratio of molecules that successfully undergo intersystem crossing from the excited singlet to triplet state per quanta of light. All triplet quantum yields were determined using a comparative method [85]. For the phthalocyanines, ZnPc (Φ_T^{Std}) was used as a standard (Φ_T = 0.65 in DMSO [85]). The triplet quantum yields and lifetimes were not calculated for the porphyrins due to the compound producing a weak signal. The values were calculated using **Equation 1.2**:

$$\Phi_T^{Sample} = \Phi_T^{Std} \frac{\Delta A_T^{Sample} \cdot \varepsilon_T^{Std}}{\Delta A_T^{Std} \cdot \varepsilon_T} \quad \textbf{(1.2)}$$

where A_T^{Sample} and ΔA_T^{Std} are the changes in the triplet state absorption of the MPc derivative and the ZnPc standard, respectively. $\boldsymbol{\Phi_T^{Std}}$ is the triplet state quantum yield for the standard. ε^{Sample} and ε^{Std} are the triplet state extinction coefficients for the MPc derivatives and the standard, respectively. **Equation 1.2** is generally known as the triplet absorption method. ε_T^{Std} and ε_T were determined from their respective ground state molar extinction coefficient, ε_S and ε_S^{Std}, and the change in absorbance of the triplet state, ΔA_T and ΔA_T^{Std} according to **Equations 1.3a and 1.3b.**

$$\varepsilon_T = \varepsilon_S \cdot \frac{\Delta A_T}{\Delta A_S} \quad \textbf{(1.3a)}$$

$$\varepsilon_T^{Std} = \varepsilon_S^{Std} \cdot \frac{\Delta A_T^{Std}}{\Delta A_S^{Std}} \quad \textbf{(1.3b)}$$

Triplet lifetimes were determined by the exponential fitting of the kinetic curves using the ORIGIN 8 Professional software.

1.6.3 Singlet Oxygen Quantum Yield (Φ_Δ)

The singlet oxygen quantum yield (Φ_Δ) can be defined as the amount of singlet oxygen ($^1O_2$) generated per photon of light absorbed by the photosensitiser [86]. The methods used are either the optical or the chemical method. The optical method involves the observation of a time-resolved phosphorescence decay of singlet oxygen at 1270 nm [87]. The chemical method requires the use of singlet oxygen quenchers that react rapidly with the singlet oxygen generated by the sensitizer in a 1:1 ratio without the possibility of side reactions occurring. The decomposition products of the quencher should not interfere with the detection of singlet oxygen or with the absorption of the photosensitiser [88]. The photosensitiser must remain stable. In this work, 1,3-diphenylisobenzofuran (DPBF) was used for the Pcs and 9,10-dimethylanthracene (DMA) was used for the porphyrins as singlet oxygen quenchers in organic solvents while anthracene 9,10-bis-methylmalonate (ADMA) was used for the studies in water. For the phthalocyanines, ZnPc ($\boldsymbol{\Phi_\Delta^{Std}}$) was used as the standard where ($\boldsymbol{\Phi_\Delta}$ **=** 0.67 in DMSO [85]). For the porphyrins, ZnTPP ($\boldsymbol{\Phi_\Delta^{Std}}$) was used as a standard where $\boldsymbol{\Phi_\Delta}$ = 0.53 in DMF [83]), The $\boldsymbol{\Phi_\Delta}$ can be calculated using **Equation 1.4:**

$$\Phi_\Delta = \Phi_\Delta^{Std} \frac{W.I_{abs}^{Std}}{W^{Std}.I_{abs}} \quad \textbf{(1.4)}$$

where $\Phi_\Delta^{Std}$is the singlet oxygen quantum yield for the standard, W and W^{Std} are the DPBF/DMA photobleaching rates in the presence of the photosensitiser derivatives under investigation and the standard, respectively. I_{abs} and I_{abs}^{Std} are the rates of light absorption by the MPc derivative and standard, respectively.

Due to lack of standards for the fibres, an absolute method described in literature [88] was employed, using ADMA as a quencher. The quantum yield of ADMA (Φ_{ADMA}) was calculated using **Equation 1.5:**

$$\Phi_{ADMA} = \frac{(C_0 - C_t)V}{tI_{abs}} \quad \textbf{(1.5)}$$

where C_0 and C_t are the ADMA concentrations prior to and after irradiation, respectively; V is the solution volume; t is the irradiation time per cycle and I_{abs} is defined by **Equation 1.6**.

$$I_{abs} = \frac{\alpha AI}{N_A} \quad \textbf{(1.6)}$$

where $\alpha = 1\text{-}10^{-A(\lambda)}$, $A(\lambda)$ is the absorbance of the sensitizer on the material at the irradiation wavelength, A is the irradiated area (1.6 cm^2), I is the intensity of light and N_A is Avogadro's constant. Singlet oxygen quantum yields (Φ_Δ) were calculated using **Equation 1.7** [89]:

$$\frac{1}{\Phi_{ADMA}} = \frac{1}{\Phi_\Delta} + \frac{1}{\Phi_\Delta}\frac{k_d}{k_a}\frac{1}{[ADMA]} \quad \textbf{(1.7)}$$

where k_d is the decay constant of singlet oxygen and k_a is the rate constant of the reaction of ADMA with O_2 ($^1\Phi_g$). Φ_Δ is obtained from the plot of 1/ Φ_{ADMA} versus 1/[ADMA].

1.7 Summary of This Thesis

The aims of this thesis are summarized as follows:

1. Synthesise and characterization of novel phthalocyanine and asymmetrical porphyrins.
2. Electrospinning of compounds into fibres.
3. Investigation of photophysical parameters for the compounds alone and when embedded in fibres.
4. Photocatalytic degradation of phenolic pollutants using these fibres.

Chapter 2

Experimental

This chapter provides the materials, instrumentation, synthetic procedure of all porphyrins and phthalocyanines synthesized in this work.

2.1 General Reagents and Solvents

Polyacrylonitrile (PAN, Mw 150,000 g/mol), pyrrole, zinc phthalocyanine (ZnPc), indium (III) chloride, 1,3-diphenylisobenzofuran (DPBF), 4-(methylthio)benzaldehyde, formylbenzoic acid, Zn-5,10,15,20 tetraphenylporphyrin (ZnTPP), N-hydroxysuccinimide (NHS), 1-ethyl-3-(3-dimethylaminopropyl)carbodiimide (EDC), deuterated dimethyl sulfoxide (DMSO-d_6), deuterated chloroform ($CDCl_3$), deuterated acetone (acetone-d_6), propionic acid, dichloromethane (DCM) and sodium hydrogen carbonate were obtained from Sigma-Aldrich. Dimethyl formamide (DMF), dimethyl sulfoxide (DMSO), tetrahydrofuran (THF), ethyl acetate chloroform anthracene 9,10-bis-methylmalonate (ADMA), zinc chloride, and 1,8-diazabicyclo [5.4.0]undec-7-ene (DBU) were purchased from Merck. Phenylene diamine was obtained from the British Drug Houses Laboratory Chemicals group. 4-Nitrophthalonitrile was synthesised according to literature [90]. All solvents were of reagent grade and were freshly distilled before use. Phosphate-buffered solutions (PBS) of pH 10.60 were prepared using appropriate amounts of Na_2HPO_4, KH_2PO_4 and the respective chloride salts in Ultra-pure Type II water was obtained from Elga PURELAB chorus 2 (RO/DI) system.

2.2 Equipment

a) **Ground state electronic absorption spectra** of the complexed were performed on a Shimadzu UV-2550 spectrophotometer for solutions. Solid state spectra were obtained from a Perkin Elmer Lambda 950 UV–Vis NIR spectrophotometer where reflectance measurements were converted into equivalent absorption spectra using the reflectance of holmium as a reference. Solid samples were run in a well-homogenized anhydrous potassium bromide matrix.

b) **Fluorescence emission spectra** were recorded on a Varian Eclipse spectrofluorometer.

c) **Fluorescence lifetime spectra** were measured using a time correlated single photon counting setup (TCSPC), Fluo Time 200, Picoquant GmbH, with a diode laser as the excitation source (LDH-P-670, 20 MHz repetition rate for the phthalocyanines) and (LDH-P-C-420, 20 MHz repetition rate for the porphyrins). Fluorescence was detected under the magic angle with a peltier cooled photomultiplier (PMT) (PMA-C 192-N-M, Picoquant GMbH) and integrated electronics (PicoHarp 300E, Picoquant GmbH). A monochromator with a spectral width of about 4 nm was used to select the required measured emission wavelength. The response function of the system, which was measured with a scattering Ludox solution (DuPont), had a full width at half-maximum (FWHM) of about 300 ns. The ratio of stop to start pulses was kept low (< 0.05) to ensure good statistics. All luminescence decay curves were measured at the maxima of the emission peak. The data were analysed with the program FluoFit (Picoquant GmbH). The support plane approach was used to estimate the errors of the decay times.

d) **Elemental analyses** for carbon, hydrogen, nitrogen and sulphur were done using a Vario-Elementar Microcube ELIII Series.

e) **Mass Spectral** data were obtained using a Bruker AutoFLEX III Smartbeam TOF/TOF Mass spectrometer. The instrument was operated in positive ion mode using a m/z range of 400 – 3000 amu. The voltage of the ion sources was set at 19 and 16.7 kV for ion sources 1 and 2 respectively, while the lens was set at 8.50 kV. The reflector 1 and 2 voltages were set at 21 and 9.7 kV respectively.

The spectra were acquired using α-cyano-4-hydroxycinnamic acid as the MALDI matrix and a 354 nm nitrogen laser as the ionizing source.

f) **^{1}H-nuclear magnetic resonance spectra** (^{1}H-NMR) were recorded in deuterated solvents (DMSO-d_6, $CDCl_3$-d_6) using Bruker AMX 600 MHz spectrometer.

g) **Infrared** (IR) spectra were recorded on a Perkin–Elmer Spectrum 100 ATR FT-IR spectrometer.

h) **The $^1O_2$ generation determination** was quantified using the chemical method, in DMF and water respectively. For the porphyrins photo-irradiations for singlet oxygen were done using the Spectra-Physics^R primoScan OPO series, which is pumped by Spectra-Physics Quanta Ray INDI Lab with maximum 5 pump energy of 750 mJ and output energy of 27 mJ. The irradiation wavelength for singlet oxygen studies was the cross over between the absorbance of the standard ZnTPP and the sample (426 nm). For the phthalocyanines studies were done using a General Electric Quartz line lamp (300W). A 600 nm glass cut off filter (Schott) and a water filter were used to filter off ultraviolet and infrared radiations respectively while a 670 ± 40 nm interference filter was employed. Light intensities were measured with a POWER MAX 5100 (Molelectron Detector Inc.) power meter and was found to be 1.0×10^{19} photons cm^{-2} s^{-1}.

Figure 2.1 – Schematic diagram of lamp setup

i) **Scanning electron microscope** (SEM) images of electrospun fibres were obtained using a JOEL JSM 840 scanning electron microscope.

j) **Energy dispersive spectroscopy** on an INCA PENTA FET coupled to the VAGA TESCAM using 20 kV accelerating voltage.

k) **Time of Flight Secondary Ion Mass Spectrometer** (TOF-SIMS) images were obtained usin0067 an ION TOF GmbH TOF SIMS 5-100 run in micro-raster mode. The raster area was 3000 μm x 3000 μm, and the sample was run in both positive and negative ion modes. The analyser was set to a standard operating mode with a cycle time of 100 μs, whilst the primary beam was a Bi_3 ion cluster gun with a current of 0.4 pA and an energy of 3000 eV (also termed as spectrometry mode). The Bi_3 cluster and electron flood gun was used to get a better ion signal from the sample. Charge compensation was used to account for the electron flood gun. The raw data was processed using the SurfaceLab 6.5 software provided by ION TOF.

l) **Electrospinning** was done on a KD Scientific model 100 series using a 10 mL syringe with a continuous mode of operation. The set flow rate was 0.2 mL/h for all experiments with a syringe tip diameter of 0.1 cm.

m) Laser flash photolysis experiments were performed to determine the triplet decay kinetics. The excitation pulses were produced by a tunable laser system consisting of a Nd:YAG laser (355 nm, 135 mJ/4–6 ns) pumping an optical parametric oscillator (OPO, 30 mJ/3–5 ns) with a wavelength range of 420–2300 nm (NT-342B, Ekspla). Solutions for triplet state studies were degassed with nitrogen for 20 min before measurement. The absorbance of the solution at the Q-band was 1.5 for these studies. Triplet lifetimes were

determined by exponential fitting of the kinetic curves using Origin Pro 8 software.

2.3 Synthesis

2.3.1 Synthesis of precursor 4-(1H-pyrrol-1-yl)phthalonitrile (B), Scheme 3.1

Compound **B** was synthesized as reported in literature [91] but using 4-nitrophthalonitrile instead of fluoro phthalonitrile as follows: 4-nitrophthalonitrile (200 mg, 1.15 mmol) **(A)**, pyrrole (8 mL) and potassium carbonate (7 g, 50.64 mmol) were added to a round bottom flask. DMF (5 mL) was added under inert atmosphere and the mixture left to stir for 48 h. The compound was purified by boiling in water twice and then recrystalising in methanol.

Yield: 82% (w/w); FT-IR [(KBr) vmax/cm^{-1}]: 2160 (C„N stretching), 3141 (CAH stretching). ^{1}H NMR (400 MHz, Acetone d_6) (d, ppm): 8.33–8.31 (q, 1H), 8.13–8.12 (d, 1H), 8.11 (s, 1H), 7.58– 7.55 (q, 2H) 6.43–6.40 (q, 2H).

2.3.2 Synthesis of tetrapyrrole indium phthalocyanine (1), Scheme 3.2

Precursor **B** (200 mg, 1.04 mmol) and indium chloride (193 mg, 0.872 mmol) were added to a round-bottom flask containing 1,8-diazabicyclo[5.4.0]undec-7-ene (DBU) (0.5 mL) and hexanol (5 mL) as the solvent and refluxed under magnetic stirring for 24 h. The product was isolated and purified using silica packed column chromatography using 10% methanol in dichloromethane.

Yield: 40% (w/w); UV/vis (DMSO): λmax/nm (log Ɛ): 371 (4.81), 634 (4.50), 706 (4.17). FT-IR [(KBr) *v*max/cm^{-1}]: 1331 (C-N stretching), 1609 (C=C stretching), 2918 (C-H stretching). Anal. Calc. for $C_{48}H_{28}N_{12}InCl$: C, 62.46; H, 3.06; N, 18.21; Found: C, 64.12; H, 3.50; N, 18.21. ^{1}H NMR (400 MHz, DMSO-d_6) (δ, ppm): 8.61-8.46 (s,

7H), 8.07-8.03 (d, 8H), 6.90-9.87 (s, 3H), 6.71-6.66 (s, 2H) 6.63-6.54 (d, 8H). MALDI TOF-MS: Calculated: 922.13; Found: 887.66[M-Cl+H]$^{+}$.

2.3.3 Synthesis of tetrapyrrole zinc phthalocyanine (2), Scheme 3.2

The synthesis of complex **1** was as outlined for complex **2** but using zinc chloride (175 mg, 0.997 mmol) instead of $InCl_3$, the amounts of the other reagents as well as purification methods were the same.

Yield: 52% (w/w); UV/vis (DMSO): λmax/nm (log Ɛ): 361 (4.93), 623 (4.56), 690 (5.04). FT-IR [(KBr) *v*max/cm^{-1}]: 1309 (C-N stretchin, 1611 (C=C stretching), 2926 (C-H stretching). Anal. Calc. for $C_{48}H_{28}N_{12}Zn$: C, 68.78 H, 3.37; N, 20.05; Found: C, 64.06; H, 3.78; N, 17.98. ^{1}H NMR (400 MHz, DMSO-d_6) (δ, ppm): 8.04 (s, 8H), 8.03 (d, 4H), 7.65-7.64 (t, 8H), 6.37-6.34 (t, 8H). MALDI TOF-MS: Calculated: 838.22; Found: 838.85[M].

2.3.4 Synthesis of 4-(10.15.20-tris(4-methylthio)phenyl)porphyrin-5-yl)benzoic acid (3), Scheme 3.3

Formylbenzoic acid (292 mg, 1.942 mmol) and 4-(methylthio)benzaldehyde (2.96 g, 19.429 mmol) were placed in a 250 mL round bottomed flask. Propionic acid (120 mL) was then added to the mixture which was left to reflux with stirring for 1 h. Pyrrole (1.39 g, 2.008 mmol) was then added. The characteristic purple colour indicated successful cyclotetramerization. The mixture was then left to reflux and under magnetic stirring for a further 2 h. The reaction vessel was then cooled to room temperature, poured into 500 mL water, followed by addition of $NaHCO_3$, until a basic mixture was obtained. The resulting precipitate was filtered under vacuum. The product was added to methanol (200 mL) then boiled, filtered under vacuum and dried. The compound was further purified using column chromatography using first

tetrahydrofuran (THF) followed by DMF as eluents. This process was repeated several times until a pure compound was obtained.

Yield: (58%).FT-IR (KBr, vmax/cm^{-1}): 3501 (O-H), 2949 (C-H), 2914 (C-H), 1712 (C=O), 1594 (C=C), 1265(C-O). ^{1}H NMR 400 MHz, $CDCl_3$) δ (ppm) 8.88 (d, 2H, Ar-Benzene), 8.58 (d, 4H, Py), 8.34 (s, 1H, Py, Ar-Benzene), 8.17 (d, 5H, Ar-Benzene), 8.09 (d, 1H, Ar-Benzene), 7.69 (d, 6H, Ar-Benzene), 6.99 (s, 4H, Py), 6.59 (s, 1H, Ar-Benzene), 2.35 (s, 9H, CH_3), -2.76 (s, 2H, Py). UV/vis (DMF) λmax nm (log ε): 423 (4.13), 516 (2.91), 553 (2.77), 593 (2.47), 649 (2.40). Calc. for $C_{48}H_{36}N_4O_2S_3$ = 72.34, H = 4.55, N = 7.03, S = 12.07 Found: C = 72.54, H = 4.70 N = 7.99, S = 11.86. MALDI-TOF-MS(m/z) Calc: 796.20. Found $(M+1H)^+$ 797.12.

2.3.5 Metallation of 4-(10.15.20-tris(4-methylthio)phenyl)porphyrin-5-yl)benzoic acid (4), Scheme 3.4

Compound **(3)** (200 mg, 0.25 mmol) and zinc chloride (40 mg, 0.30 mmol) were added to a round bottomed flask containing refluxing DMF (5 mL) as a solvent. The reaction was heated under reflux for 5 h until metalation was complete, as judged by collapse of the four Q bands into two in the UV-Vis absorption spectra. The compound was cooled and washed with water and methanol.

Yield: (85%).FT-IR (KBr, vmax/cm^{-1}): 3490 (O-H), 2953 (C-H), 2917 (C-H), 1709 (C=O), 1589 (C=C), 1260(C-O). ^{1}H NMR 400 MHz, $CDCl_3$) δ (ppm) 8.91 (d, 1H, Ar-Benzene), 8.49 (s, 2H, Py), 8.43 (d, 6H, Ar-Benzene), 8.07 (d, 2H, Py), 7.77 (d, 6H, Ar-Benzene), 7.57 (d, 3H, Ar-Benzene), 7.45 (d, 2H, Py), 6.89 (s, 2H, Py), 2.73 (s, 9H, CH_3). UV/vis (DMF) λmax nm (log ε): 430 (4.58), 560 (3.79), 601 (3.55). Calc. for $C_{48}H_{34}N_4O_2S_3Zn$ = 67.01, H = 3.98, N = 6.51, S = 11.18, Found: C = 67.89, H =

4.12, N = 6.15, S = 10.84. MALDI-TOF-MS(m/z) Calc: 858.11. Found $(M+2H)^{2+}$ 860.42.

2.3.6 Partial modification of polyacrylonitrile (PAN) to PAN(COOH), Scheme 3.5

Polyacrylonitrile (5 g) was placed in a 250 mL round bottomed flask. Hydrochloric acid (200 mL of 5 M) was added to the flask. The reaction mixture was heated at reflux temperature for 2 h, cooled, filtered and washed with water to produce the partially modified polymer. The process was monitored using IR as a means of controlling the rate of modification.

2.3.7 Conversion of PAN(COOH) to PAN(NH_2), Scheme 3.5

PAN(COOH) (2g) was left to stir in DMF to form a homogenous mixture. EDC (500 mg, 3.22 mmol) and NHS (500 mg, 4.34 mmol) were then added in excess and the reaction was left to stir for 24 h. Phenylene diamine (500 mg. 4.62 mmol) was dissolved in DMF (12 mL) and added to the polymer solution. The mixture was left to stir for 48 h, following which, it was added (using a Pasteur pipette) to water (500 mL), while stirring vigorously, resulting in the formation of pellets. The pellets were then separated by filtration under vacuum. The product was purified by stirring in 300 mL methanol (10 min), filtered and the boiled in 300 mL ethyl acetate for 10 min and filtered again. The pellets were then dissolved in DMSO and stirred until the mixture was homogenous. Ethyl acetate was slowly added until the polymer precipitated out. The product was then filtered and dried.

2.3.8 Conjugation of (4) to PAN(NH_2), Scheme 3.6

Compound **(4)** (12 mg, 0.0139 mmol) was dissolved in DMF (3 mL). Then EDC (12 mg, 0.0774 mmol) and NHS (12 mg, 0.10 mmol) were added and the solution left to stir for 24 h. PAN(NH_2) (1 g) was added to the vial and the mixture was left to stir for 48 h to form **4**-PAN. The conjugate was then boiled in ethyl acetate until the solution was clear to remove any unreacted (**4**).

2.4 Electrospinning

2.4.1 Phthalocyanine functionalised fibres

Solution for electrospinning were prepared by mixing PAN (10 weight %) in DMF under magnetic stirring for 24 h at room temperature for unfunctionalized fibres. Functionalization of the nanofibres was achieved by adding 40 mg (0.043 mmol, 0.048 mmol) of complexes **1** and **2** to the PAN solutions and then stirring overnight, followed by electrospinning. Solutions for electrospinning were placed in a 20 mL syringe fitted with a hypodermic needle (inner diameter of 0.1 mm). The electrospinning experiments were carried out at a flow rate of 0.2 $mL \cdot h^{-1}$ and a tip to collector distance (TCD) of 15 cm. The solutions were spun at 20 kV onto a grounded collector covered with aluminium foil where the solidified fibres were collected. The electrospinning was conducted at 21.1 °C and 41% humidity. When complexes **1** and **2** were added to PAN before electrospinning, the resulting modified fibres are represented as **1**-PAN (embedded) and **2**-PAN (embedded). Experiments where the prepared unfuctionalized PAN fibres were immersed in solutions of complexes **1** and **2**, are represented as **1**-PAN (immersed) and **2**-PAN (immersed). For the immersion, solutions of complexes **1** and **2**, (40 mg corresponding to 0.043 mmol and 0.048 mmol, respectively) were dissolved in tetrahydrofuran (THF) and the

unfunctionalized PAN fibres were immersed in the solutions for 24 h. Following immersion, the fibres were dried in air for 12 h.

2.4.2 Porphyrin functionalised fibres

The solution for electrospinning were prepared by mixing **4**-PAN (12 %) in DMF under magnetic stirring for 24 h at room temperature. The solution was placed in a 20 mL syringe fitted with a hypodermic needle (inner diameter of 0.1 mm). The electrospinning experiments were carried out at 20 kV, at a flow rate of 0.2 $mL \cdot h^{-1}$ and a tip to collector distance (TCD) of 15 cm. A grounded collector covered with aluminium foil was employed, where the solidified fibres were collected. The electrospinning was conducted at 23.4 °C and 35% humidity.

2.5 Photocatalytic studies

4-CP solutions were prepared with concentrations of 0.20 $mol.L^{-1}$, 0.19 $mol.L^{-1}$, 0.11 $mol.L^{-1}$, 0.10 $mol.L^{-1}$,0.09 $mol.L^{-1}$ for the Pc fibres and 0.20 $mol.L^{-1}$, 0.17 $mol.L^{-1}$, 0.13 $mol.L^{-1}$, 0.10 $mol.L^{-1}$, 0.09 $mol.L^{-1}$ for the porphyrin fibres both in pH 10.60 buffer solution. 4-*n*-NP solutions were prepared with concentrations of 0.17 $mol.L^{-1}$, 0.19 $mol.L^{-1}$, 0.14 $mol.L^{-1}$,0.09 $mol.L^{-1}$,0.07 $mol.L^{-1}$ in pH 10.60 buffer solution. For each concentration, a 3 mL solution was irradiated in a sealed vessel using the Spectra-Physics^{R} laser system described above in the presence of a 1.0 × 2.0 cm fibre strip cut into several smaller fragments. The irradiation period for 4-CP was 5 min per cycle and the 4-*n*-NP period was 2 min per cycle. The change in concentration after each irradiation was monitored using UV-vis spectroscopy by noting the decrease in each absorption band, being ~244 nm for 4-CP and ~225 nm for 4-*n*-NP.

PUBLICATIONS

The results presented in the following chapters have either been published or submitted for publication. These articles are not referenced in this thesis

1. **B. Jones,** J. Britton, D. Mafukidze, T. Nyokong, Photodegradation of 4-chlorophenol using Zn and In phthalocyanines substituted with pyrrole without hetero atoms linkers and supported on polyacrylonitrile electrospun fibres. Polyhedron 178 (2020) 114329.
2. **B. Jones**, D. Mafukidze, T. Nyokong, Fabrication of electrospun fibers from a porphyrin linked to polyacrylonitrile polymer for photocatalytic transformation of phenols. J. Mol. Struct. 1213 (2020) 128191.

Side Publications

1. N. Njemuwa, **B. Jones**, J. Mack, D.O. Oluwole, T. Nyokong, Nonlinear optical dynamics of benzothiazole derivatized phthalocyanines in solution, thin films and when conjugated to nanoparticles. Journal of Photochemistry and Photobiology A: Chemistry 346 (2017) 46-59.

Results and Discussion

The results obtained in this section will be presented in three chapters:

3. Synthesis and spectroscopic characterization

4. Photophysical and photochemical properties

5. Photodegradation and kinetics

Chapter 3

Synthesis and spectroscopic characterization

This chapter provides all relevant characterization for the phthalocyanines, porphyrins and their electrospun fibre counterparts.

3.1 Synthesis and characterisation of phthalocyanines

Scheme 3.1 shows the synthetic route of precursor **(B)**. The formation of the phthalonitrile (**B**) was via a nucleophilic substitution reaction of the pyrrole NH moiety and the nitro group of the 4-nitrophthalonitrile (**A**). The disappearance of the band at 3394 cm^{-1} corresponding to the secondary amine of the pyrrole confirms linkage of the two precursors with the nitrile peak still present in **B** at 2160 cm^{-1}, **Figure 3.1**.

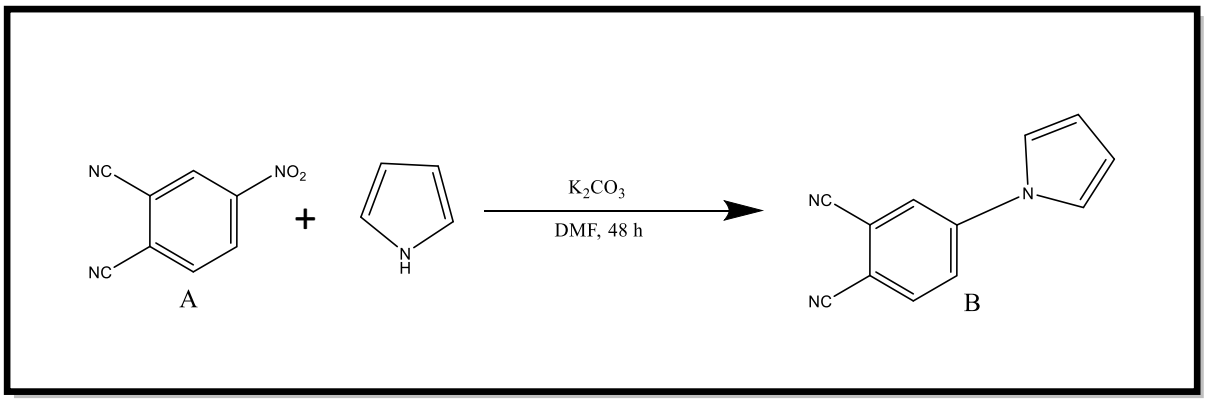

*Scheme 3.1 – Synthetic route for precursor **B***

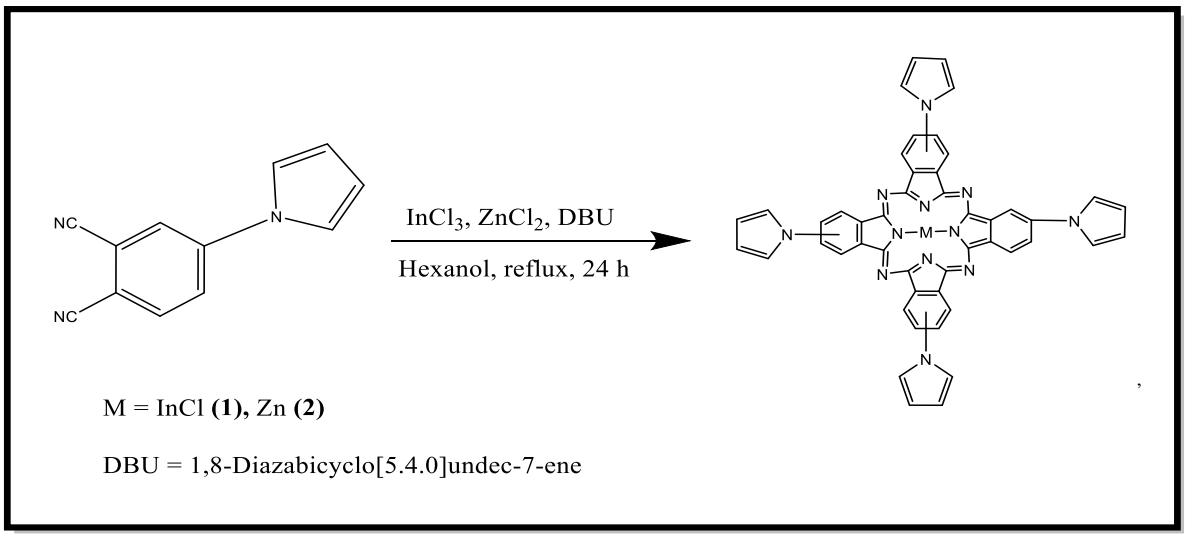

*Scheme 3.2 – Synthetic route for complexes **1** and **2***

Scheme 3.2 shows the synthetic route for complexes **1** and **2**, which involves a cyclotetramerization of the corresponding phthalonitrile **(B)** using hexanol as the solvent and a catalytic amount of DBU. FT-IR spectra (**Figure 3.1**) showed the disappearance of the nitrile peak in precursor **B**, confirming cyclotetramerization and the formation of complexes **1** and **2**.

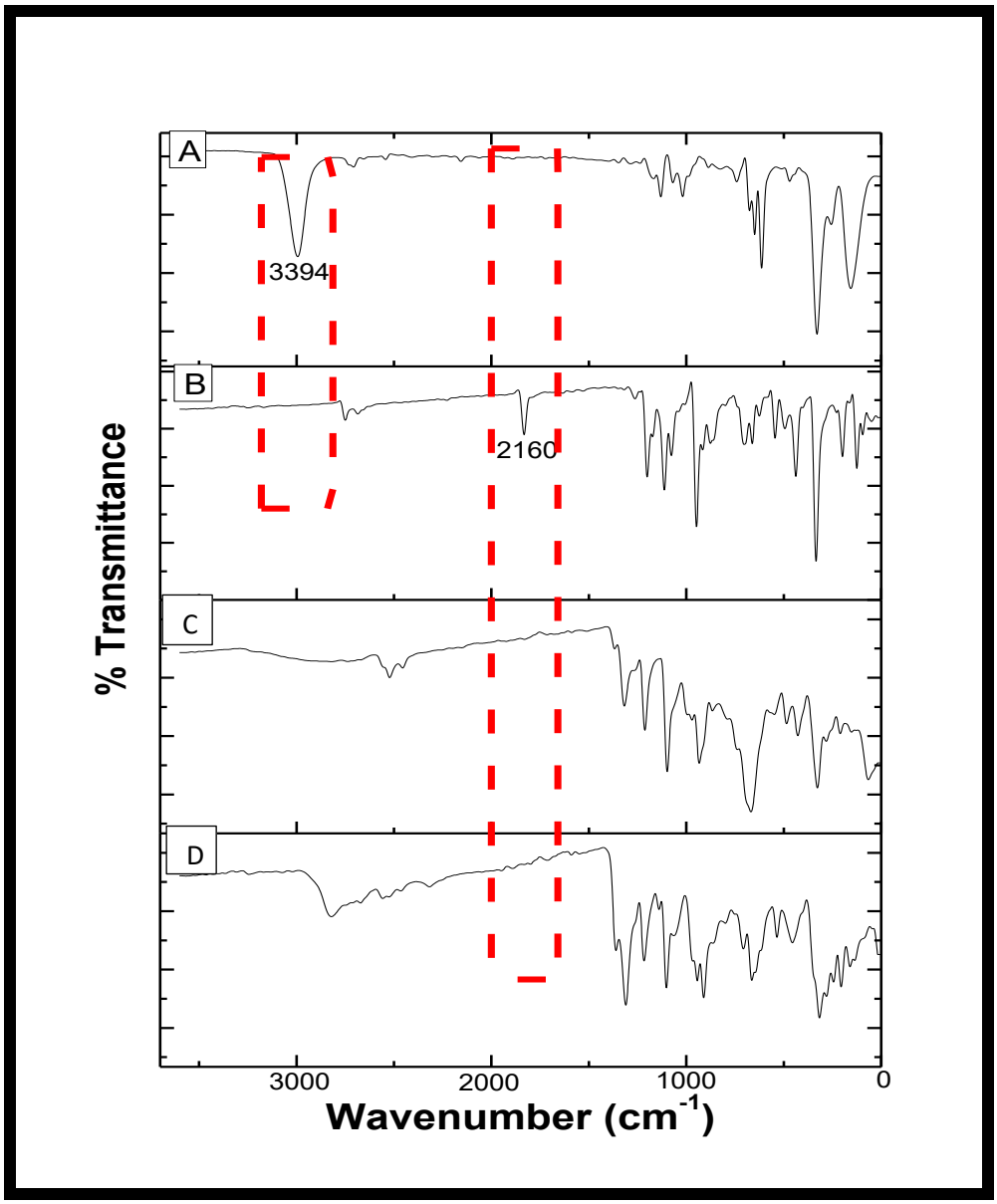

*Figure 3.1 – FT-IR spectra of (A) pyrrole, (B) precursor B, (C) complex **1**, (D) complex **2***

The ^{1}H NMR spectrum for **1** and **2** (**Figures 3.2 and 3.3**) shows aromatic ring proton peaks between 8.61 and 6.54 ppm, and between 8.04 and 6.34 ppm, respectively. Peak integration gave the anticipated total number of protons, confirming the relative purity of the complexes.

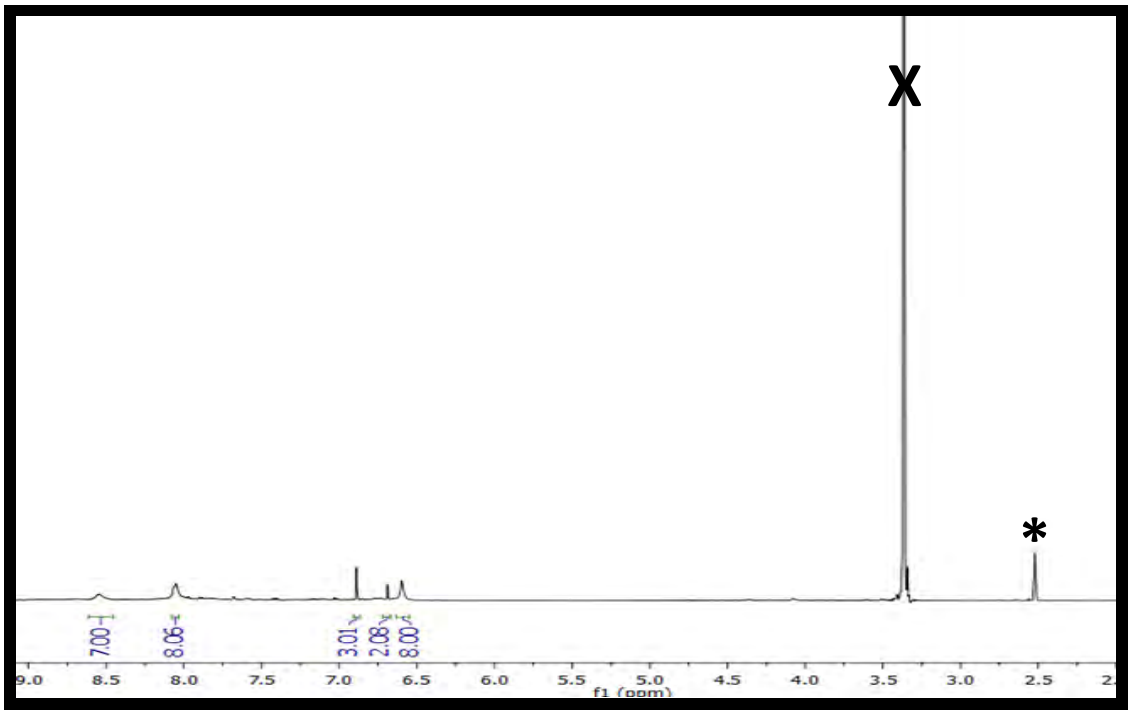

*Figure 3.2 - NMR spectrum for compound **1** (x = Water peak, * = Solvent Peak -DMSO d_6)*

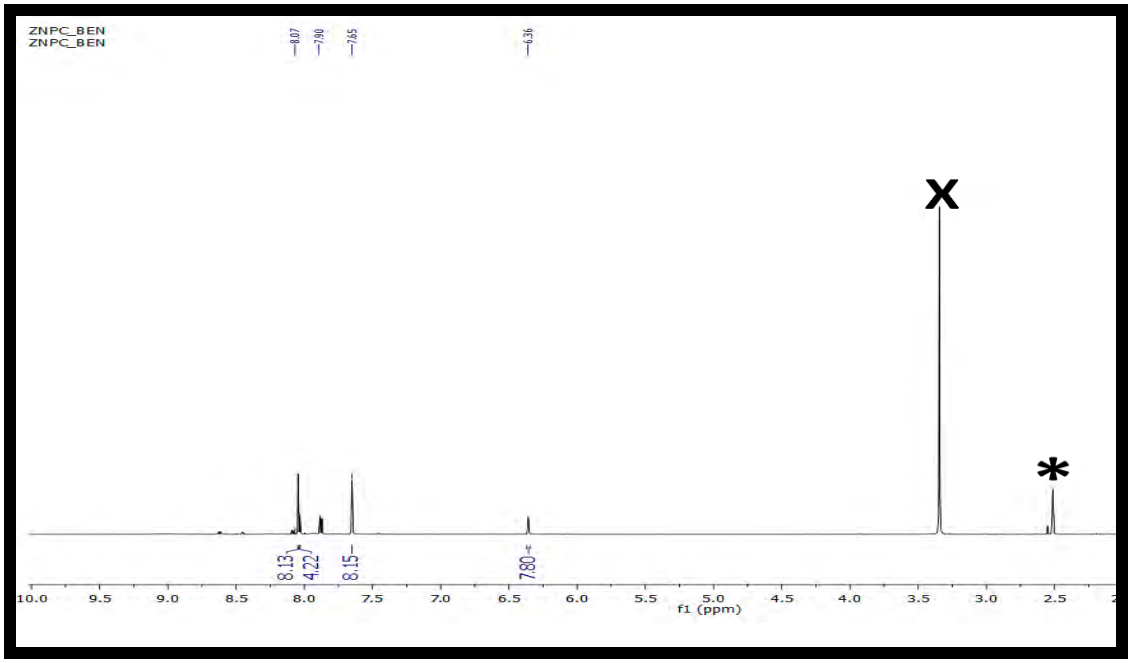

*Figure 3.3 – NMR spectrum for compound **2** (x = Water peak, * = Solvent Peak DMSO d_6)*

Mass spectral data (**Figures 3.4**) and elemental analyses were in agreement with the proposed structures in **Scheme 3.2.**

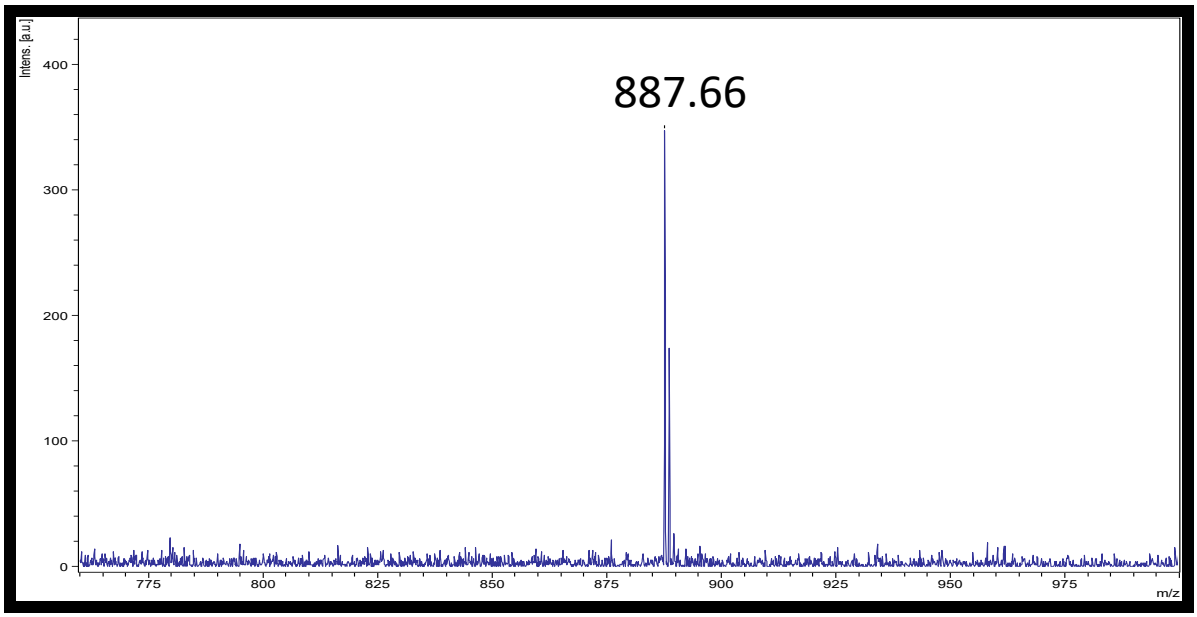

*Figure 3.4 – MALDI-TOF spectra for complex **1***

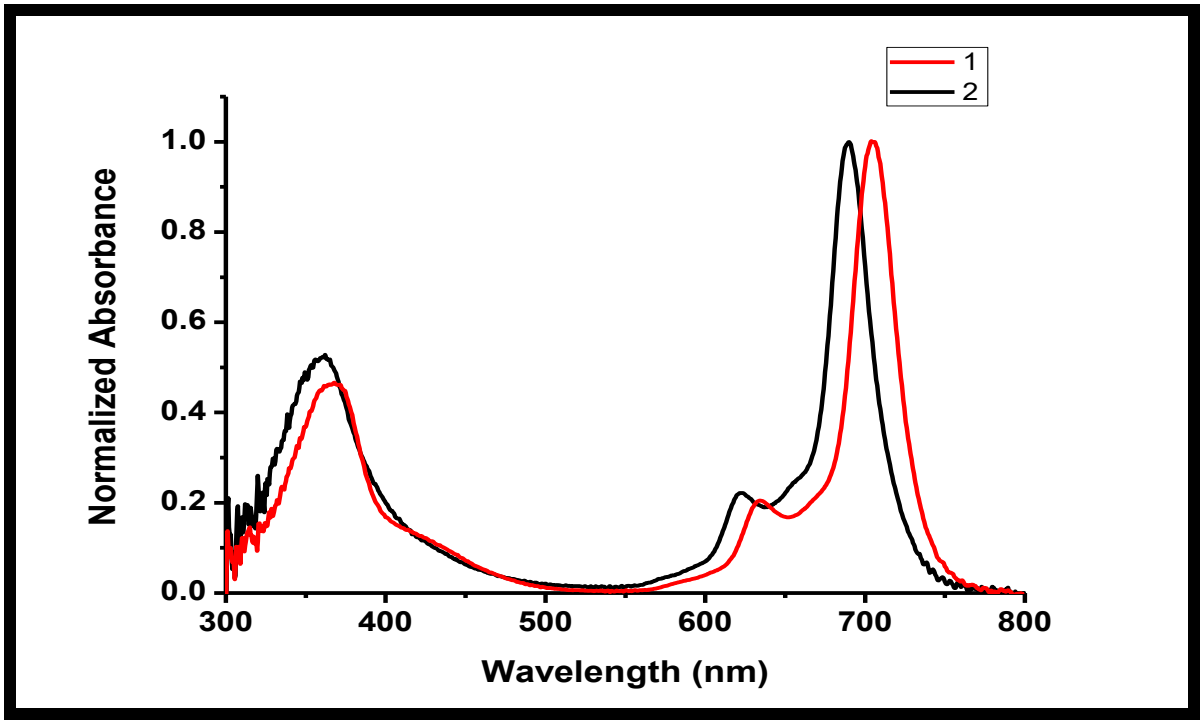

*Figure 3.5 – UV-vis spectra of complexes **1** and **2** in DMSO*

The narrow intense bands in the Q band region (600-750 nm) for compounds **1** and **2** in DMSO (**Figure 3.5**), are characteristic of metallophthalocyanines and are consistent with the presence of monomeric complexes and the absence of aggregation [92]. Due to the non-planar effect of the indium(III) ion, with a relatively bigger ionic radius compared to zinc(II) [93], the Q band of complex **1** is red shifted as compared to complex **2, Table 3.1**.

Table 3.1 – Photophysical properties of complexes and their fibre counterparts

Compound	SEM diameter (nm)	λ max Q Band	λ max B Band
1	-	706	367
2	-	692	361
1-PAN (embedded)	604	716[a]	336[a]
2-PAN (embedded)	690	697[a]	346[a]
1-PAN (immersed)	804	714[a]	355[a]
2-PAN (immersed)	855	696[a]	347[a]
3	-	517, 555, 595, 649	425
4	-	561, 602	430
4-PAN	890	561[a], 602[a]	435[a]

[a]*Solid state spectra.*

3.2 Synthesis and characterisation of porphyrins

Scheme 3.3 illustrated the preparation of **(3)** followed by metalation yielding **(4)** as described above. Compound **(3)** was synthesized used established methods for porphyrins [94]. This involves a reaction between an aldehyde(s) refluxing in propionic acid in open air prior to adding the pyrrole. The formation of the product was confirmed using MALDI-TOF mass spectrometer which showed a close correspondence between the calculated and observed masses.

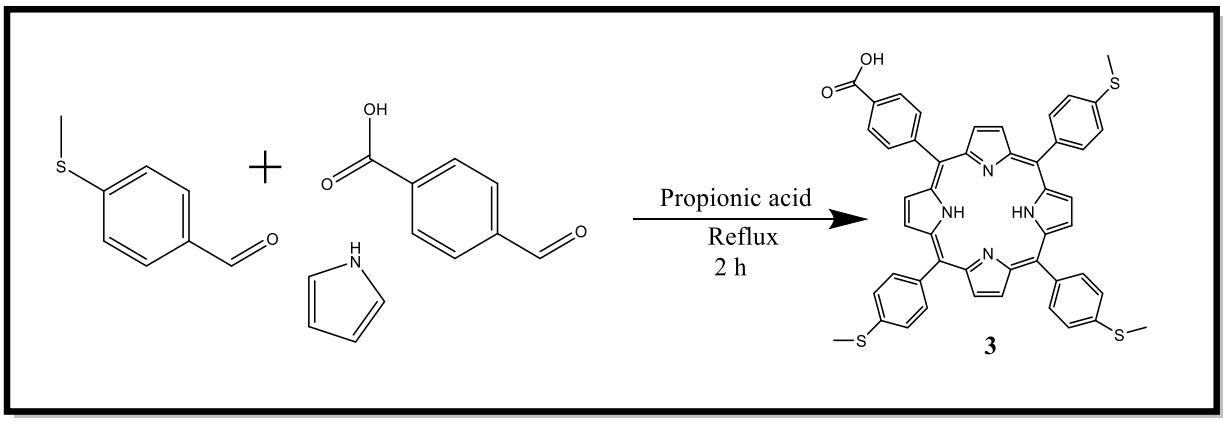

*Scheme 3.3 – Synthetic route of compound **3***

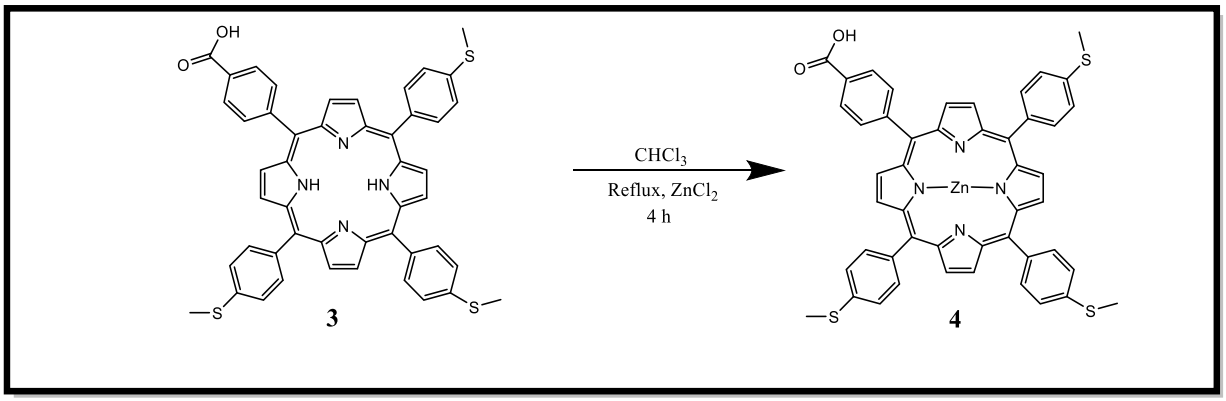

*Scheme 3.4 – Synthetic route of complex **4***

Scheme 3.4 shows the metalation of compound **(3)**. The general procedure for the metalation of porphyrins [33] was adopted as follows: DMF was brought to reflux temperature, then compound **(3)** was added in conjunction with zinc chloride. The confirmation of the product **(4)** was monitored using MALDI-TOF mass spectra (**Figure 3.6**). **Table 3.1** displays the red-shifting effect of inserting a heavy into the central cavity of the porphyrin.

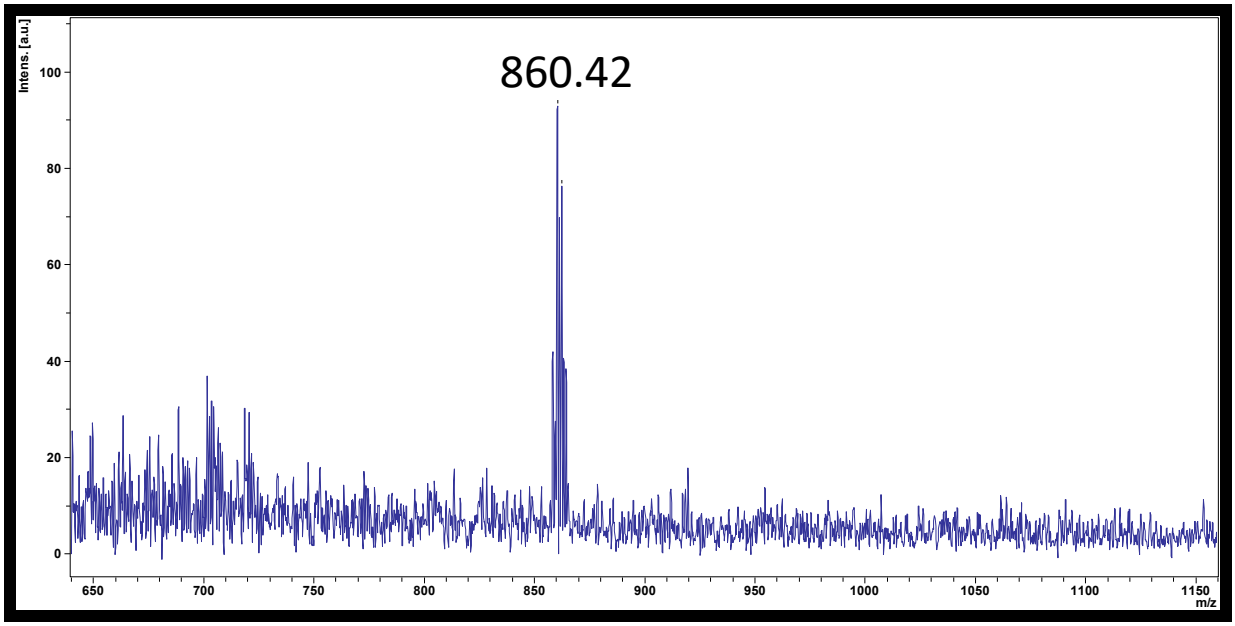

*Figure 3.6 – MALDI-TOF spectra for complex **4***

A collapse of the four Q-bands into 2 Q-bands is indicative that metalation had taken place (**Figure 3.7**) [95].

The ^{1}H NMR spectrum for compound **3** and complex **4** shows aromatic ring protons between 8.88 and 6.59 ppm, and between 8.91 and 6.89 ppm, respectively. Peak integration gave the anticipated number of protons thus confirming the relative purity of the complexes.

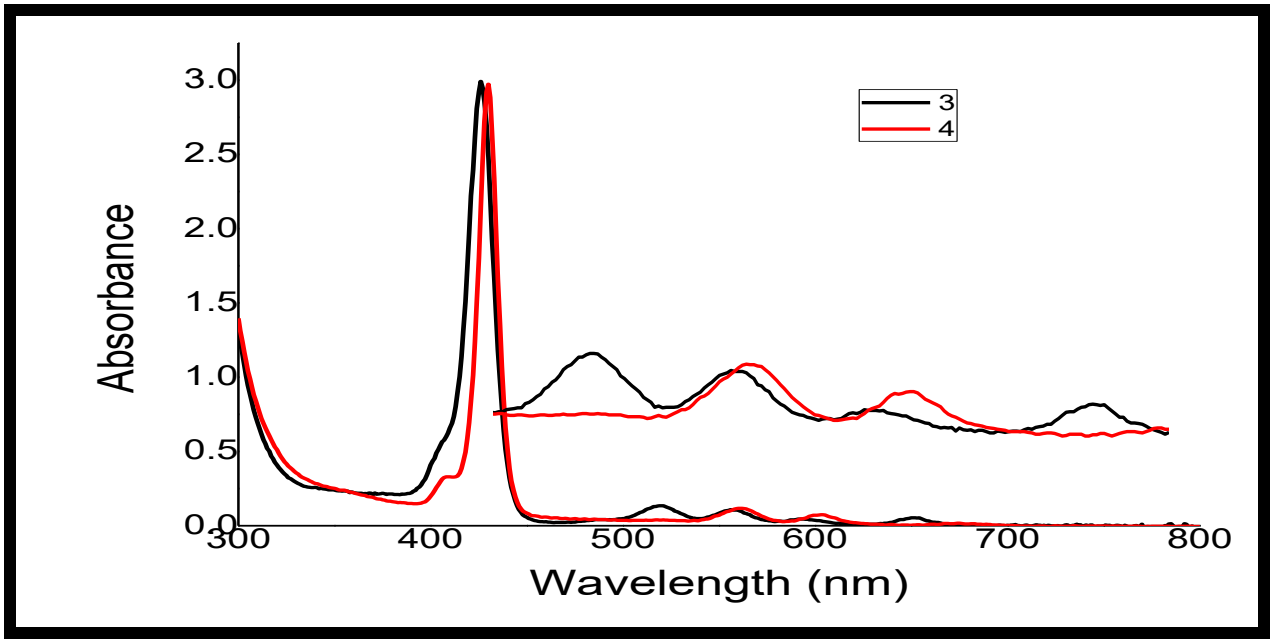

*Figure 3.7 – UV-vis absorption spectra of **3** and **4** in DMF*

3.3 Characterisation of electrospun fibres

3.3.1 Phthalocyanine functionalised fibres

SEM analysis was conducted for the electrospun fibres after embedding them with the compounds to obtain their topography. The images of PAN, **1**-PAN (embedded) (as examples) are shown in **Figure 3.8.** The SEM images reveal that the nanofibres are cylindrical and unbranched with relatively smooth surfaces even after incorporation of the Pcs. The values for the diameters are listed in **Table 3.1**. The diameter for PAN alone is 601 nm. The diameters increased after embedding or immersing with complexes **1** and **2**, **Table 3.1**. There was an observable increase in fibre diameters of the zinc analogues when compared to the indium. This may be due to the nature of the zinc as it exhibits a larger degree of planarity relative to the indium and therefore occupies more surface area. Polymer solution properties such viscosity and conductivity play a significant role in the electrospinning process and the resultant fibre diameter and morphology [60,61]. Pcs are high charge density aromatic macromolecules which may increase conductivity, increasing the fibre diameter during electrospinning. **1**-PAN (immersed) and **2**-PAN (immersed) gave larger diameters than the corresponding embedded PAN fibres, this could be due to the presence of more Pcs on the fibre for the former.

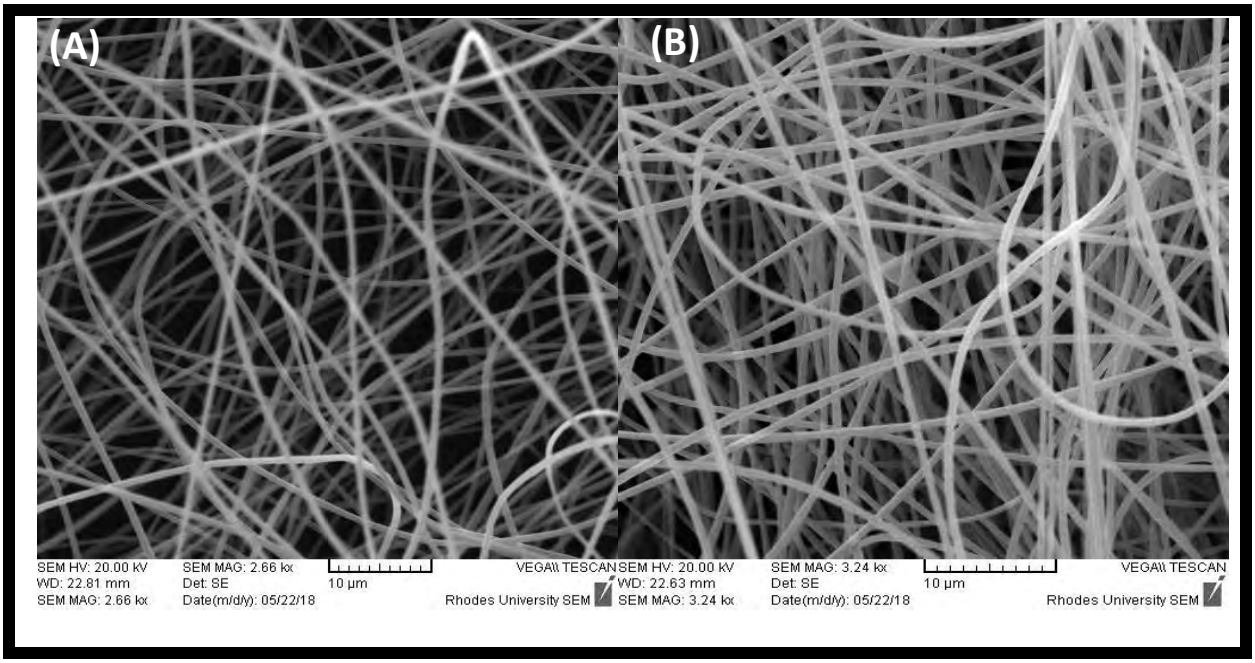

*Figure 3.8 - SEM image of unfuctionalized PAN fibres (A) and **1**-PAN (embedded) (B)*

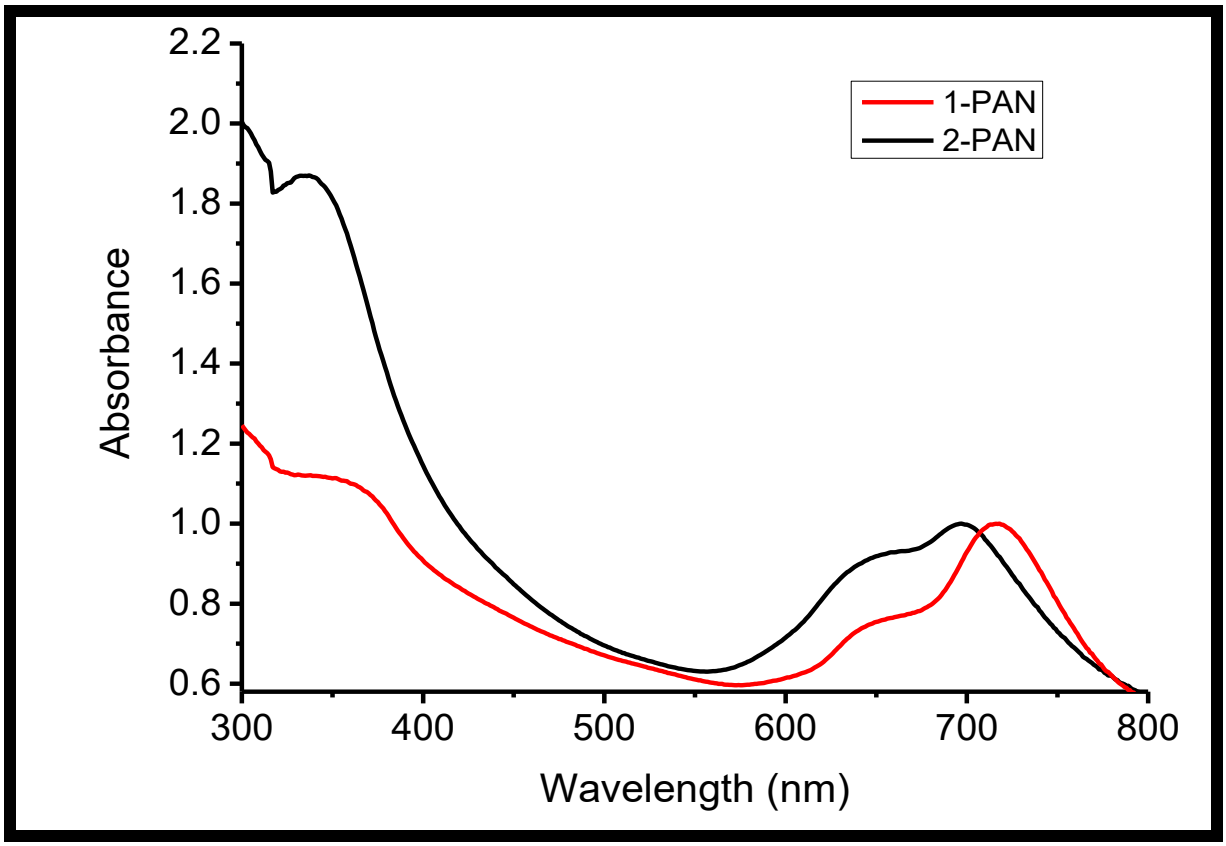

*Figure 3.9 – Solid state spectra of **1**-PAN (embedded) and **2**-PAN (embedded)*

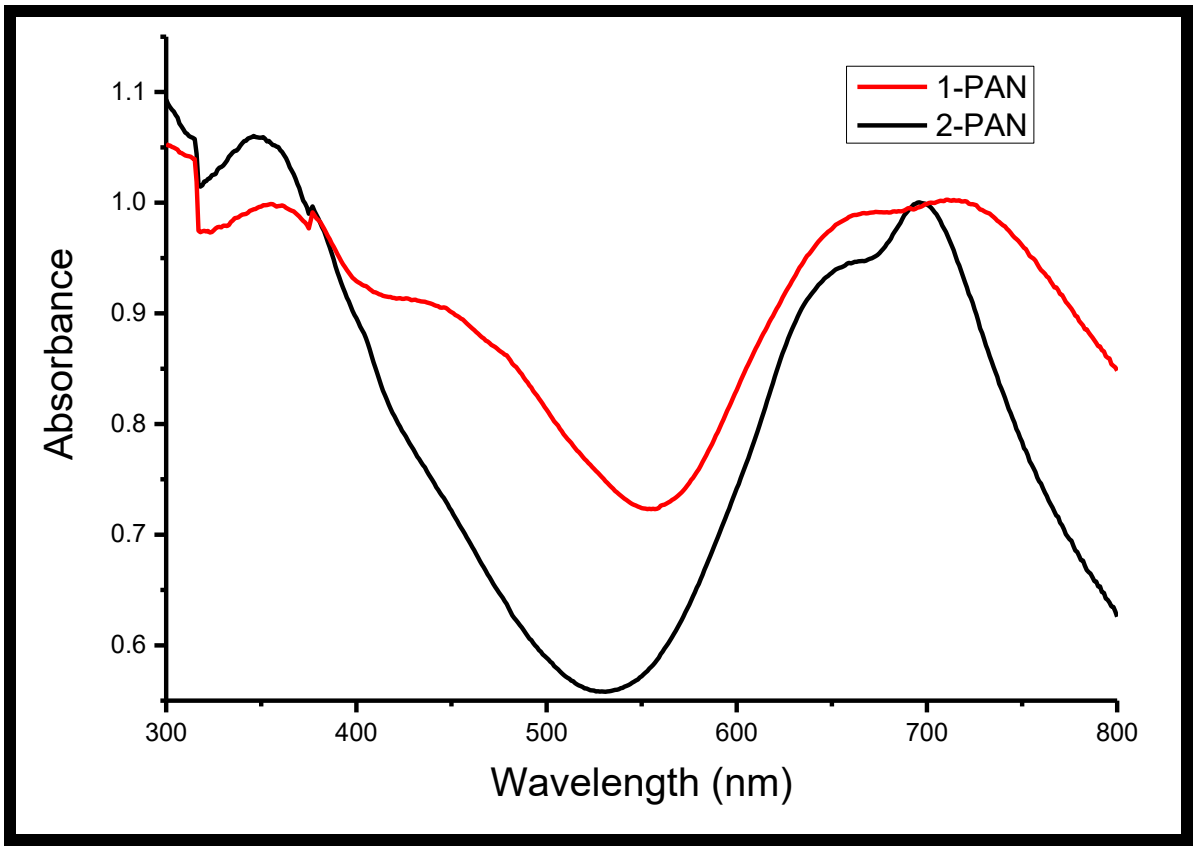

*Figure 3.10 – Solid state spectra of **1**-PAN (immersed) and **2**-PAN (immersed)*

Confirmation of embedded complexes **1** and **2** is shown with solid state spectra, **Figure 3.9**. The spectra are broad due to aggregation, typical of MPc spectra in the solid state [96]. Aggregation is judged by broadening or split in the Q band, with the high energy band being due to the "H" aggregate [92]. The red-shifting is common for Pcs in the solid state [97], as observed in **Table 3.1**. The theory of exciton coupling is often used to explain spectra of phthalocyanines in the solid state [98]. When the interaction of two phthalocyanines is an edge to edge interaction, the theory suggests the Q-band undergoes a red-shift. While if the interaction is a co-facial alignment, a blue-shift of the Q-band is observed [98]. The fact that the Q band is observed for the Pcs, confirms that they remain intact within the fibre following the

electrospinning process. The solid-state spectra of **1**-PAN (immersed) (**Figure 3.10**) reveals more aggregation with the high energy band (due to aggregate) being more intense for compared **1**-PAN (embedded) (**Figure 3.9**). Aggregation would occur if there is a higher loading of the Pc molecules on the fibre. There is no significant difference in the Q band solid state maxima between the embedded and immersed Pcs, **Table 3.1**.

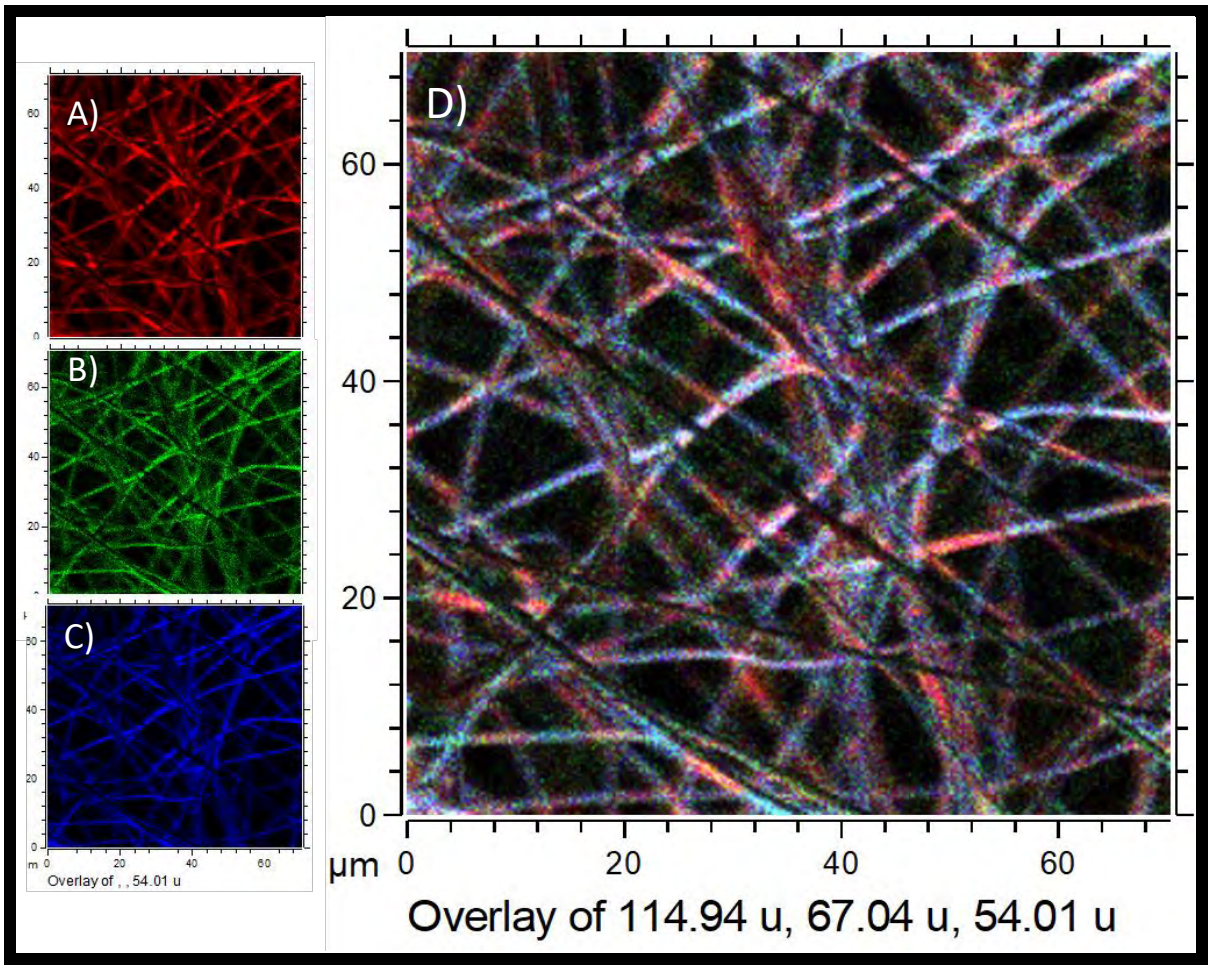

*Figure 3.11 - TOF-SIMS images for complex **1**-PAN (embedded) showing (A) indium ion and (B) pyrrole moiety and (C) C_3H_3N fragment from the PAN. (D) shows a red, green, blue (RGB) plot of the combined compositions.*

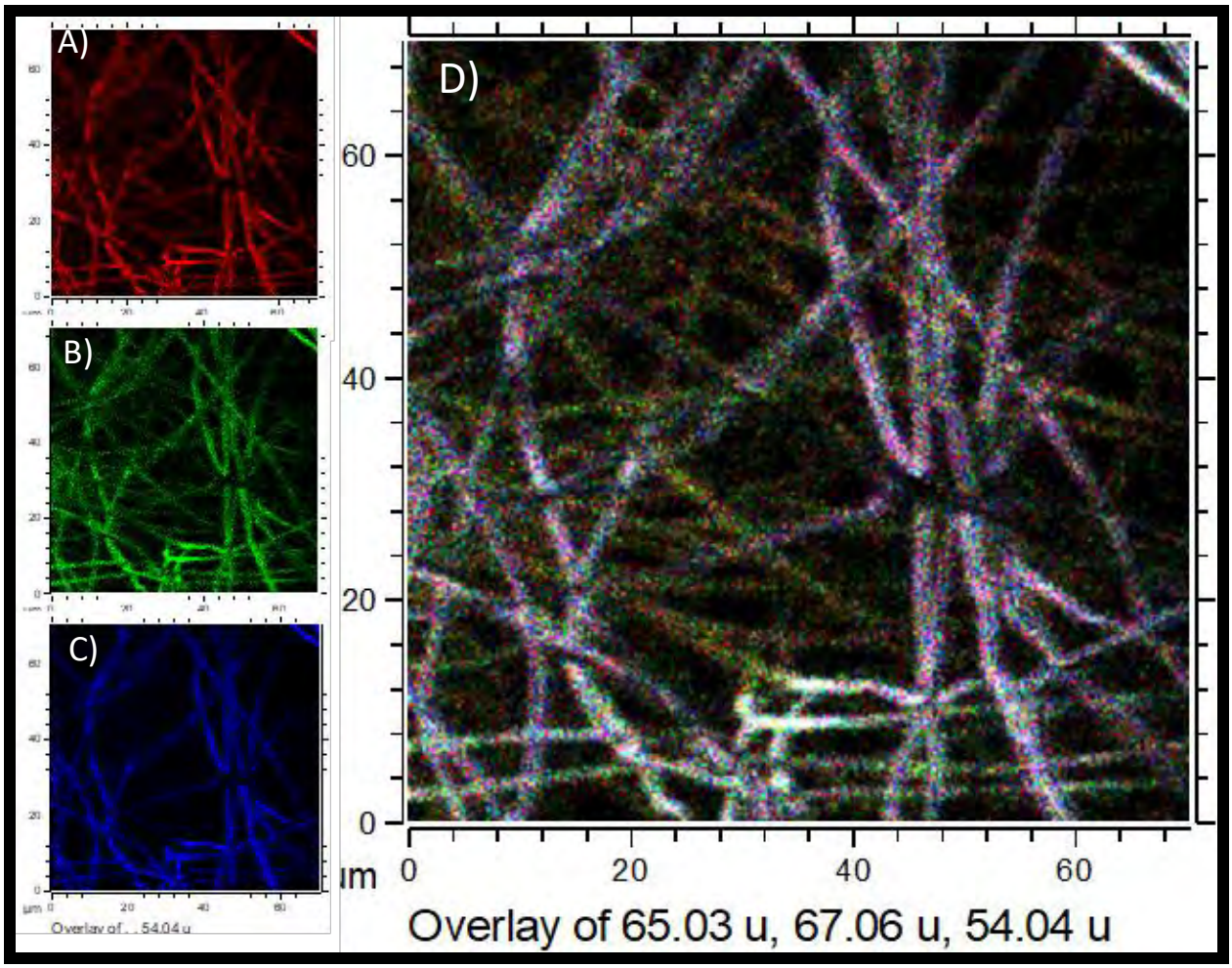

*Figure 3.12 - TOF-SIMS images for complex **2**-PAN (embedded) showing (A) zinc ion and (B) pyrrole and (C) C_3H_3N fragment from the PAN. (D) shows an RGB plot of the combined compositions.*

The topographic compositions of the embedded fibres and dyed fibres were analysed using TOF-SIMS **Figure 3.11** (for complex **1**) and **Figure 3.12** (for complex **2**). The images depict a semi quantitative analysis of the surface modification of the fibres. **Figure 3.11** A, B and C illustrate the relative concentration of the indium, pyrrole moieties and a C_3H_3N fragment from the PAN equating to 114, 67 and 53 amu respectively while **Figure 3.11 D** illustrates the combined concentrations in the form of and RGB (red, green and blue) plot. For complex **2**, Zn, pyrrole and a C_3H_3N

fragment equating to 65, 67 and 53 amu respectively. It can be observed that the dye is evenly distributed throughout each fibre with a few patches of more concentrated areas.

3.3.2 Porphyrin functionalised fibres

To ensure the hydrophobic properties of the polymer were retained, a partial modification was achieved to convert the nitrile group to the desired carboxylic moiety to form PAN(COOH), **Scheme 3.5A**. Then PAN(COOH) was linked to phenylenediamine using EDC/NHS coupling chemistry to form PAN(NH_2), **Scheme 3.5B**. PAN(NH_2) was then linked to complex **4** by EDC/NHS coupling chemistry to form **4**-PAN, **Scheme 3.6**. **4**-PAN was then electrospun into fibres.

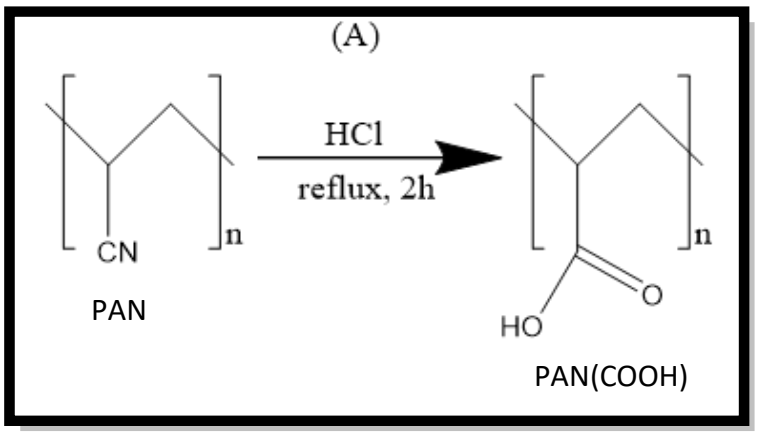

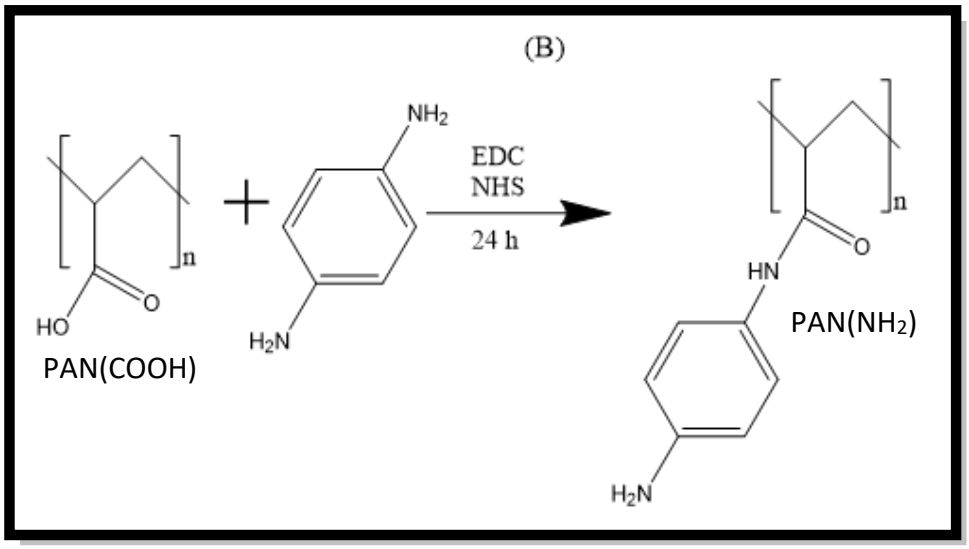

Scheme 3.5 - (A) The partial modification of PAN to PAN(COOH), (B) conversion of PAN(COOH) to PAN(NH_2)

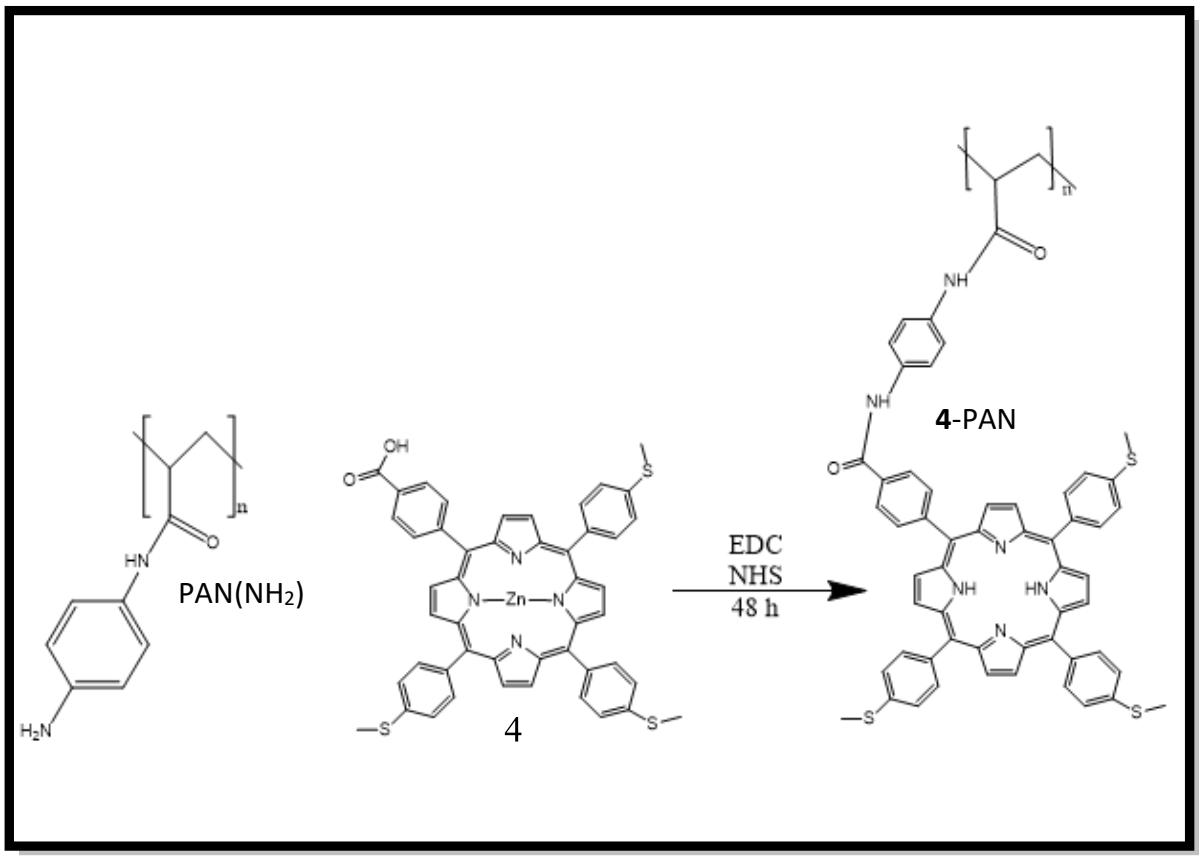

*Scheme 3.6 - Illustration of the conjugation process of **4** to PAN(NH2).*

The linkage of complex **4** to PAN(NH_2) was confirmed using FT-IR **(Figure 3.13)**. A collapse of the NH stretches at 3374 and 3270 cm^{-1} stemming from the NH_2 groups of PAN(NH_2) indicates an amide bond had been successfully formed. The intensification of the carbonyl peak at 1670 cm^{-1} (for **4**-PAN) due to the formation of two amides further corroborates that this process was successful.

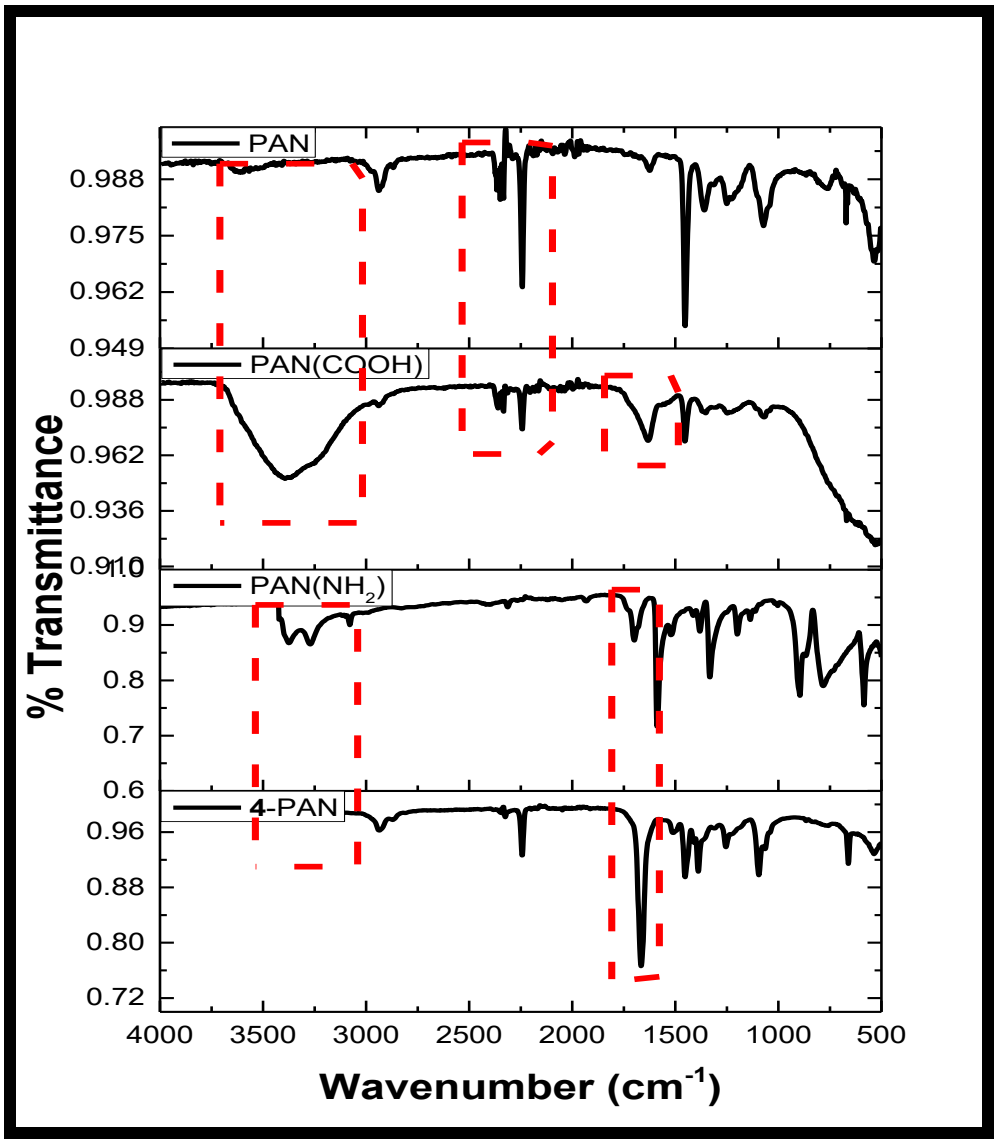

*Figure 3.13 - FT-IR spectra of PAN, PAN(COOH), PAN(NH_2) and **4**-PAN*

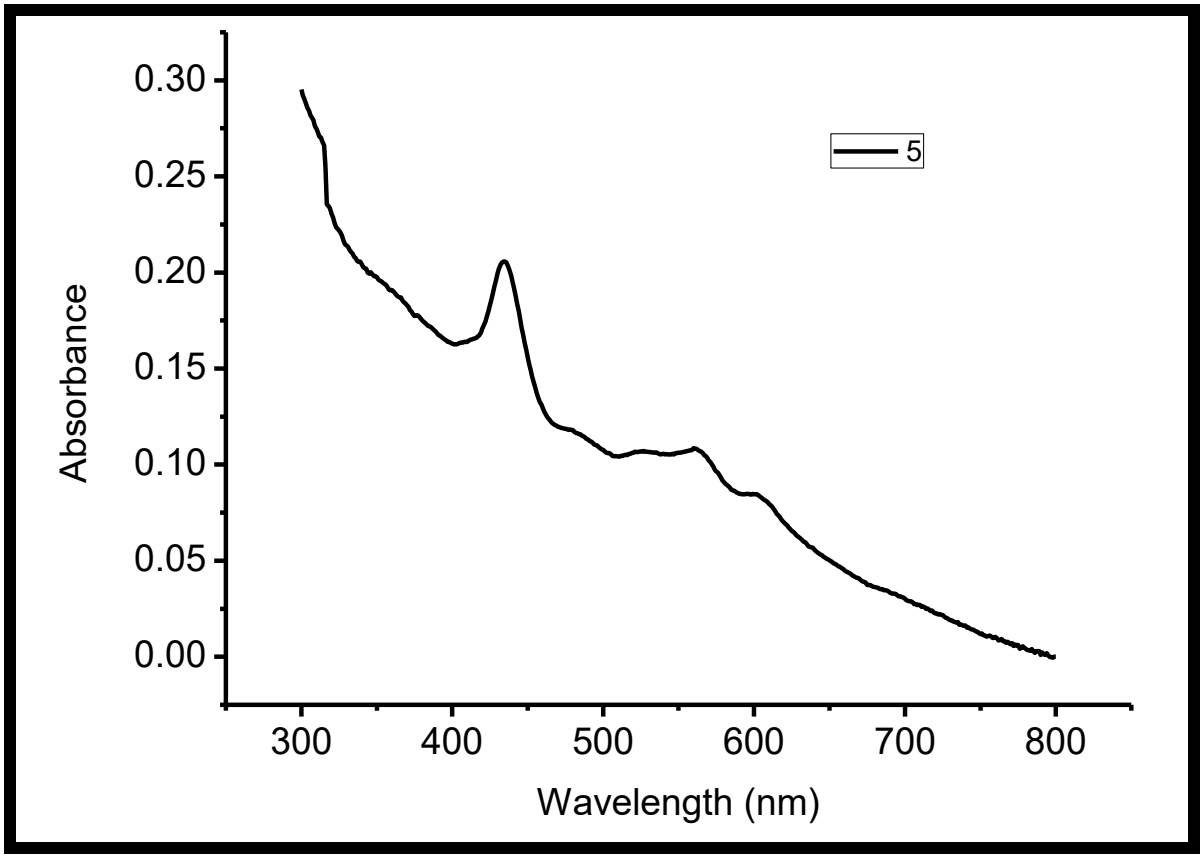

*Figure 3.14 - UV-Vis absorption spectra **4**-PAN in the solid state.*

Further confirmation of complex **4** being linked to PAN is shown with the solid-state spectra (**Figure 3.14**). There is an observed slight red-shift in the Soret band of **4** which is common for porphyrins in the solid-state (**Table 3.1**) [99]. The primary mechanism of forming these aggregates can be described as self-assembly through intrinsic intermolecular interactions [100]. The term “molecular self-assembly” has been defined as the spontaneous association of two or more molecules leading to the generation of well-defined aggregates or of extended polymolecular assemblies through non-covalent interactions, such as hydrogen bonds, metal coordination or π-π interactions [101]. The broadening of the Soret and Q bands are attributed to aggregation due to H or J aggregation (**Figure 3.15**).

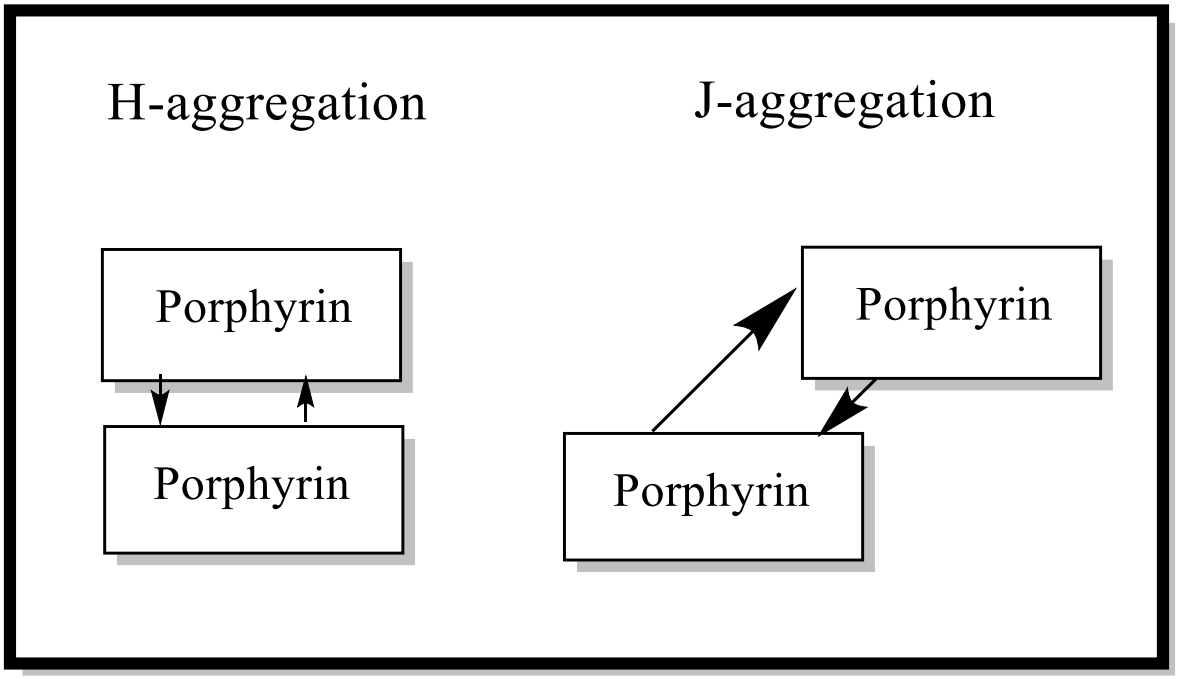

Figure 3.15 – Illustration of the differences between H and J aggregation

A blue shift of the absorption spectra is indicative of H-aggregation while a red shift indicates that J-aggregation is taking place [102]. A red shift confirms J aggregation has taken place.

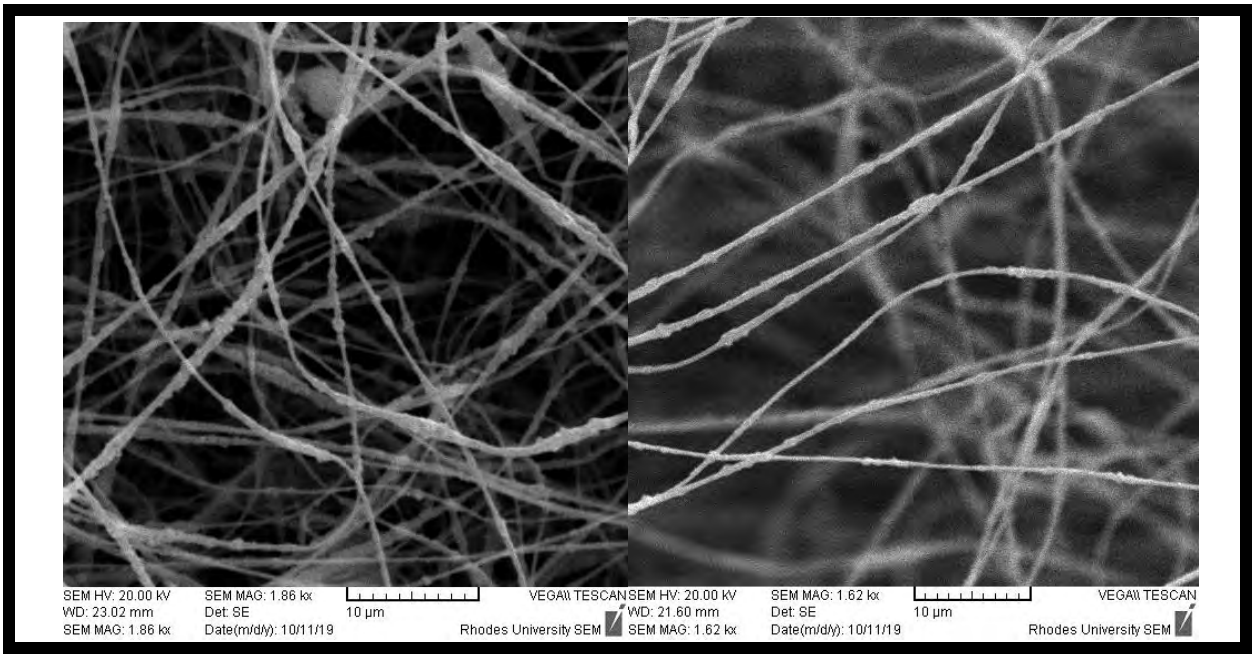

*Figure 3.16 – SEM images of **4**-PAN taken at different times at 10 µm*

SEM was also used to obtain the morphology of the fibres after functionalisation (**Figure 3.16**). The fibres kept their cylindrical shape, but a few beads were formed in the process.

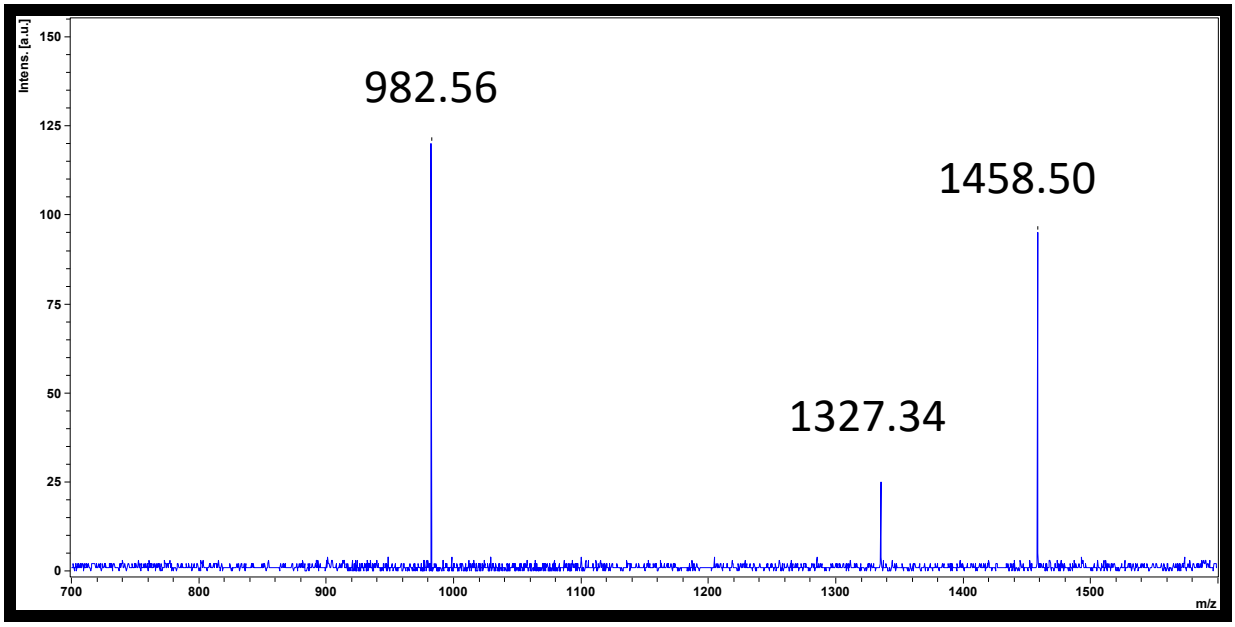

*Figure 3.17 – MALDI-TOF spectra of **4**-PAN*

Figure 3.17 shows MALDI-TOF spectra of **4**-PAN. This was used as an aid to show conjugation to the polymer was successful. Due to the nature of polymer, fragmentation of different mass units of the polymer occurred. However, each peak showed masses greater than the observed mass of **(4)** alone. This could show that **4**-PAN was successfully linked and was ionized with different fragments of the polymer when using MALDI-TOF.

3.4 Conclusions for the chapter

The syntheses and relevant characterisation of the phthalocyanine, porphyrin and their electrospun fibre counterparts were successfully carried out.

Chapter 4

Photophysical and Photochemical Properties

This chapter provides and discusses the photophysical and photochemical parameters and values obtained for the phthalocyanines, porphyrins and their electrospun fibre counterparts

4.1 Phthalocyanines and Their Fibres

4.1.1 Fluorescence Quantum Yields and Lifetimes

The Φ_F values of all Pcs were relatively low due to the heavy atom effect of the In and Zn central metals which encourage intersystem crossing to the triplet state (**Table 4.1**) [85]. The values obtained for complex **1** and **2** were <0.01 and 0.12 respectively in DMSO. The value for complex **1** is expectedly lower than for complex **2** due to indium being a heavier metal than Zn. The Φ_F values for the Pcs in fibres were not calculated as they offer no contribution to the work of this thesis. **Figure 4.1** shows the fluorescence spectra for complex **2** as an example.

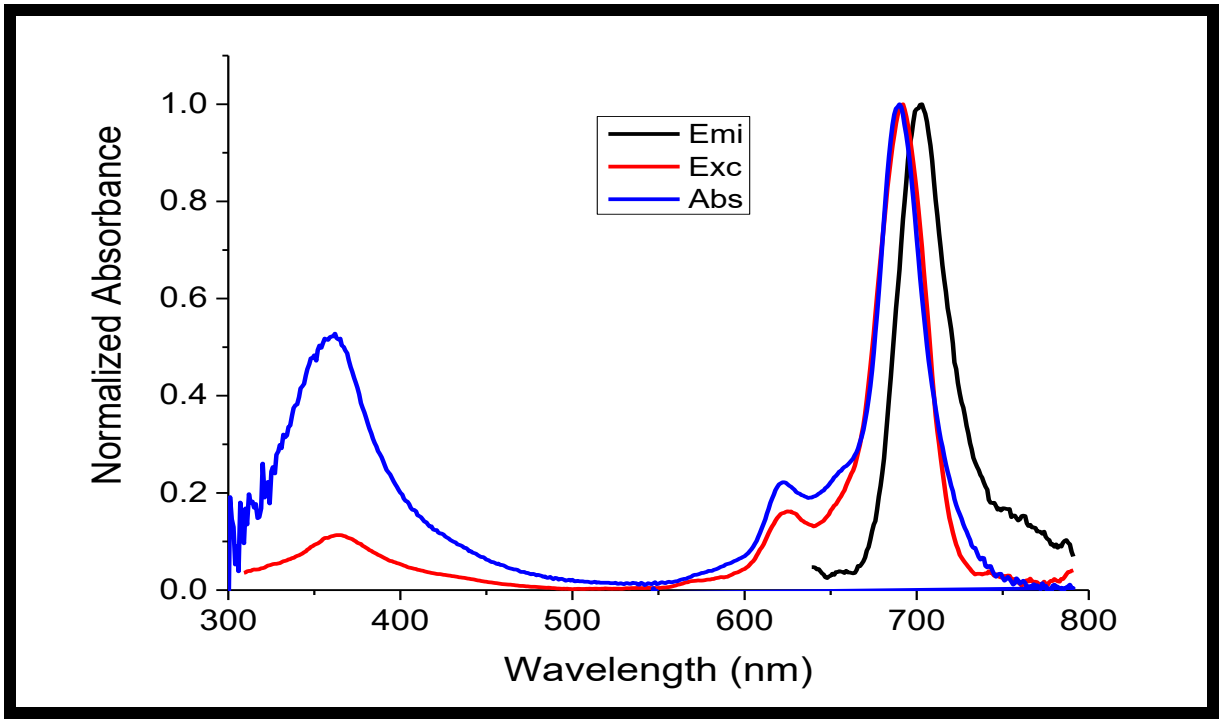

*Figure 4.1 – Fluorescence spectra of complex **2**. Emi = emission, Exc = excitation, Abs = absorption*

The excitation spectrum (**Figure 4.1**) is similar to the absorbance spectrum confirming the molecule being excited is the same molecule absorbing with the

expected mirror image emission spectrum. The fluorescence lifetimes τ_F refer to the average time a molecule stays in its excited state before fluorescing and its value is directly proportional to its quantum yield; i.e. the larger the Φ_F, the longer the lifetime as observed in table **Table 4.1**. For complexes **1** and **2** , the τ_F values were 0.29 and 2.45 ns respectively. The observed decrease is due to the presence of a heavier indium metal than zinc aforementioned. Mono-exponential decay curves were observed for both complexes.

4.1.2 Triplet Quantum Yields and Lifetimes

The efficiency of a phthalocyanine as a photosensitizer is determined by its triplet state quantum yield (Φ_T) and lifetime (τ_T). A high triplet quantum yield is of great importance since it influences the singlet oxygen production. The transient differential spectrum of **2** as an example is shown in **Figure 4.2**, with the insert showing the triplet decay curve. This spectrum is useful in determining the excited-state dynamics of Pcs. The typical broad band between 400 – 600 nm with a peak centred at 515 nm, is attributed to the triplet-triplet state excited absorption ($T_1 \rightarrow T_n$). The negative peaks attributed to the depletion or bleaching of the phthalocyanine ground state were also observed at 710 nm and at 361 nm [103].

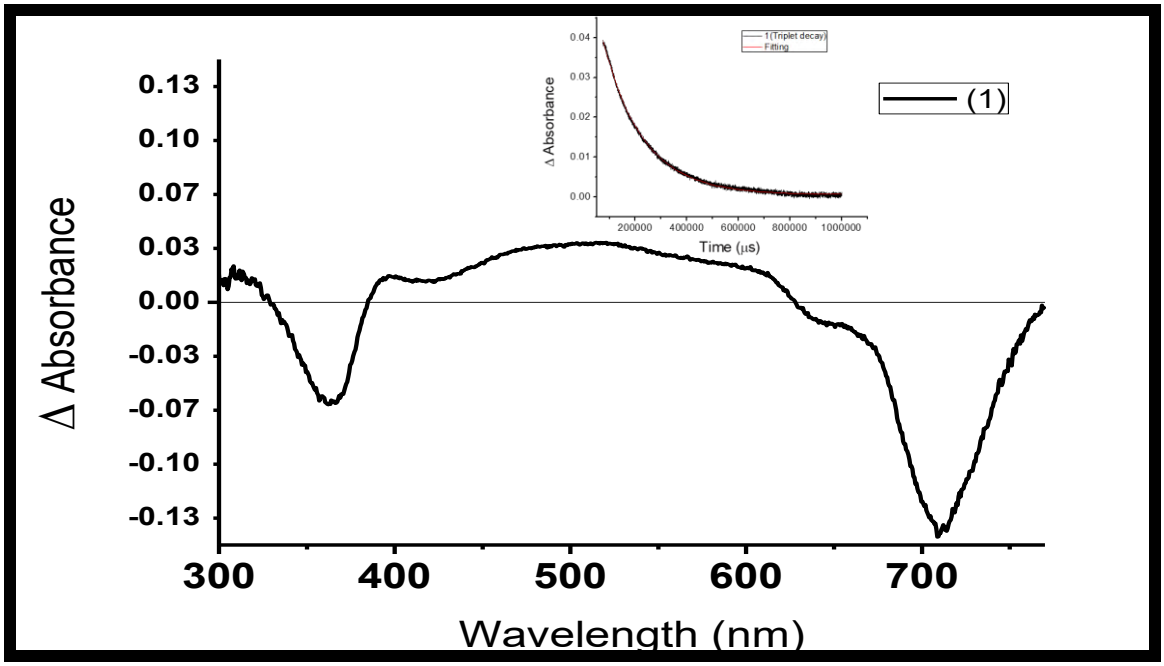

*Figure 4.2 – Transient differential spectrum for complex **1** in DMSO. Insert = triplet decay curve*

The triplet decay curve obeyed second order kinetics which is characteristic of MPcs at higher concentrations due to the triplet-triplet recombination [104]. The Pc complexes displayed high triplet quantum yields (Φ_T = 0.79 for **1** and 0.68 for **2**) (**Table 4.1**), corresponding to the low Φ_F, due to the presence of heavy atoms, Zn and In, as previously explained. The heavy atom effect was also confirmed by larger triplet quantum yield values of the indium complex compared to the zinc counterpart since indium is a heavier atom than zinc. The triplet lifetimes became shorter as the triplet quantum yields increased as expected [105]. It has also been reported that Pcs bearing nitrogen containing substituents quench the triplet state, resulting in shorter lifetimes [106].

4.1.3 Singlet Oxygen Quantum Yield

The Φ_{Δ} values for **1** and **2** were obtained by monitoring the degradation of DPBF as a singlet oxygen quencher in DMSO at ~417 nm. There were no significant changes observed of the Q-bands for the complexes (**Figure 4.3**), indicating that they are photostable. However, the steady decrease of this band at 417 nm was observed and this can be attributed to the production of singlet oxygen. The rate of production of singlet oxygen is directly proportional to the rate of degradation of DPBF.

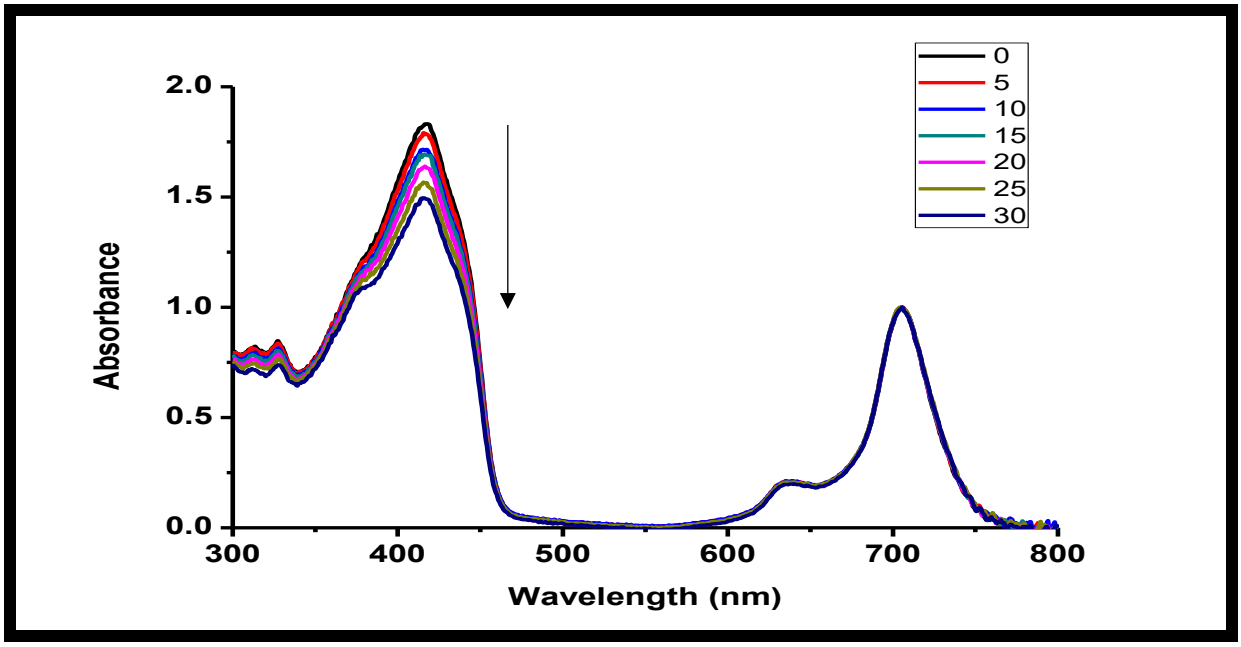

*Figure 4.3 – Absorption spectral changes of DPBF in DMSO in the presence of compound **1** (5 s intervals)*

The Φ_{Δ} values for complex **1** and **2** were 0.35 and 0.21 respectively (**Table 4.1**). The significantly higher values for the In complex is attributed to the heavier central metal as it promotes more intersystem crossing as previously described.

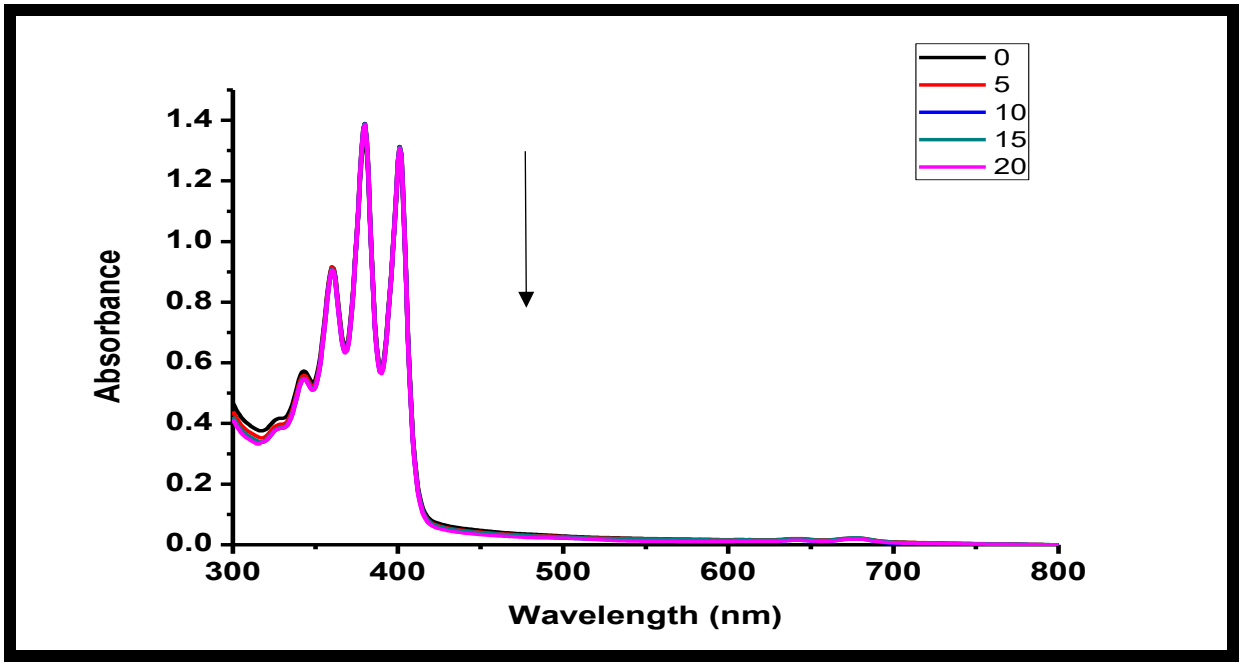

*Figure 4.4 – Absorption spectra changes of ADMA in DMSO in the presence of complex **1** (5 min intervals)*

For the functionalised fibres, ADMA was used as a singlet oxygen quencher and its spectra were monitored at ~380 nm (**Figure 4.4**). The Φ_{Δ} values in water were 0.03 and 0.02 for **1**-PAN and **2**-PAN (embedded) respectively, while the immersed fibres tend to show an increase Φ_{Δ} when compared to the embedded fibres with values of 0.06 and 0.05 of complexes **1**-PAN and **2**-PAN respectively. This may be due to an increased presence of the Pc on the surface of the immersed fibres compared to embedded fibres. The significantly lower values in water may be attributed to aggregation of the Pcs within the fibres and a quenching of the triplet state [107].

4.2 Porphyrins and their Fibres

4.2.1 Fluorescence Quantum Yields and Lifetimes

The Φ_F value for compound **3** was evaluated to be 0.28 in DMF, a significantly higher value then the value obtained for complex **4** being 0.12 due to the insertion of a heavy atom zinc in its central cavity, **Table 4.1.**

Table 4.1 – Photophysical properties of complexes and conjugates = Solvent – DMF unless otherwise stated

Compound	Φ_F	τ_F (ns)	Φ_T	τ_T (ns)	Φ_Δ
1	<0.01	0.29	0.79	155	0.35
2	0.12	2.45	0.68	323	0.21
1-PAN (embedded)	-	-	-	-	0.03[a]
2-PAN (embedded)	-	-	-	-	0.02[a]
1-PAN (immersed)	-	-	-	-	0.06[a]
2-PAN (immersed)	-	-	-	-	0.05[a]
3	0.28	1.66	-	-	0.62
4	0.12	1.03	-	-	0.70
4-PAN	-	-	-	-	0.39[a]

[a] *solvent = water*

The fluorescence lifetime (τ_F) values for compound **3** and complex **4** were determined using a time correlated single photon count (TCSPC) (**Figure 4.5 –** complex **4** as an example) method, by excitation at the emission maxima. For the porphyrin complexes **3** and **4**, mono-exponential fluorescence decay curves were obtained with values of 1.66 and 1.03 ns respectively. An expected observed decrease was due to metallation of the complex.

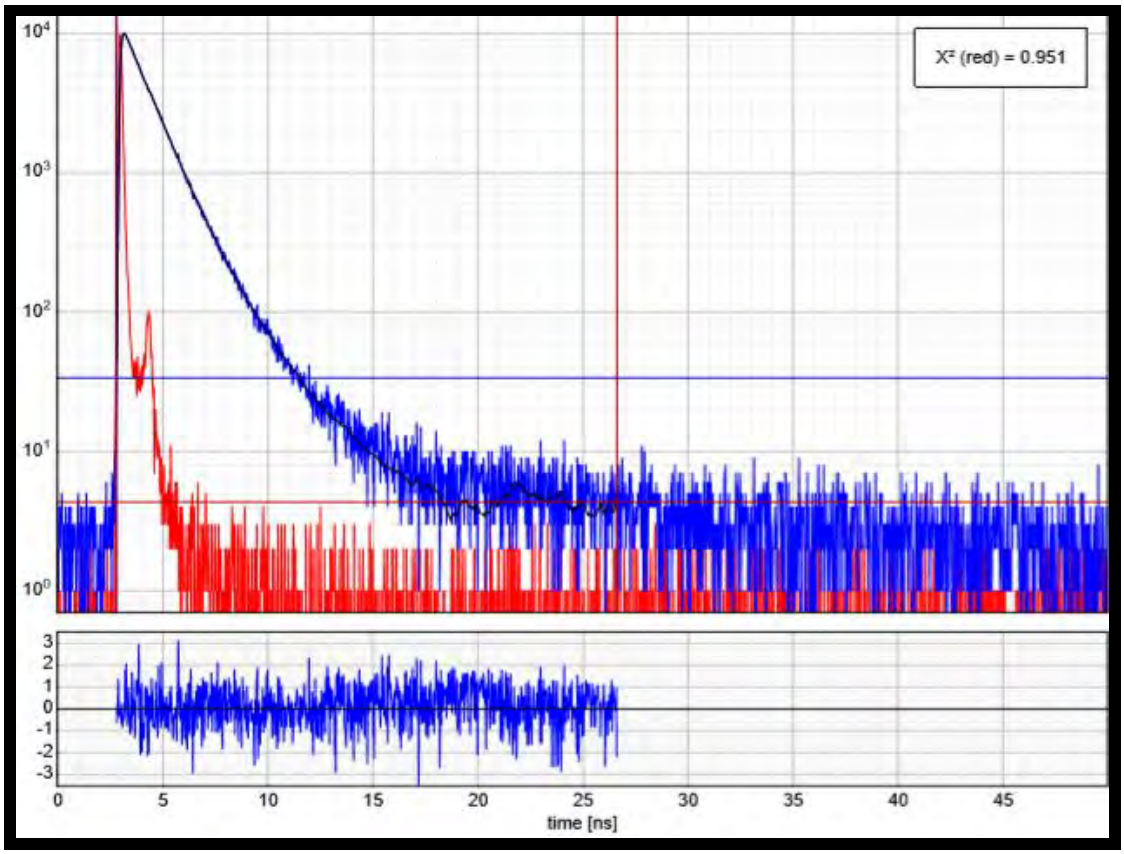

*Figure 4.5 – Fluorescence decay curve for complex **4** in DMSO at 705 nm.*

4.2.2 Singlet Oxygen Quantum Yields

The Φ_Δ of **3** and **4** were determined using DMA as a quencher for singlet oxygen in DMF, **Figure 4.6** (complex **4** as an example). There were no significant changes observed of the B or Q-bands for either **3** or **4**, indicating that they are photostable. However, the steady decrease of the DMA band at 379 nm was observed and this can be attributed to the production of singlet oxygen. The rate of production of singlet oxygen is directly proportional to the rate of degradation of DMA. The values obtained are 0.62 and 0.70 respectively (**Table 4.1**). The slightly increased value for complex **4** is due to the insertion of a heavy atom inside the central cavity of the porphyrin.

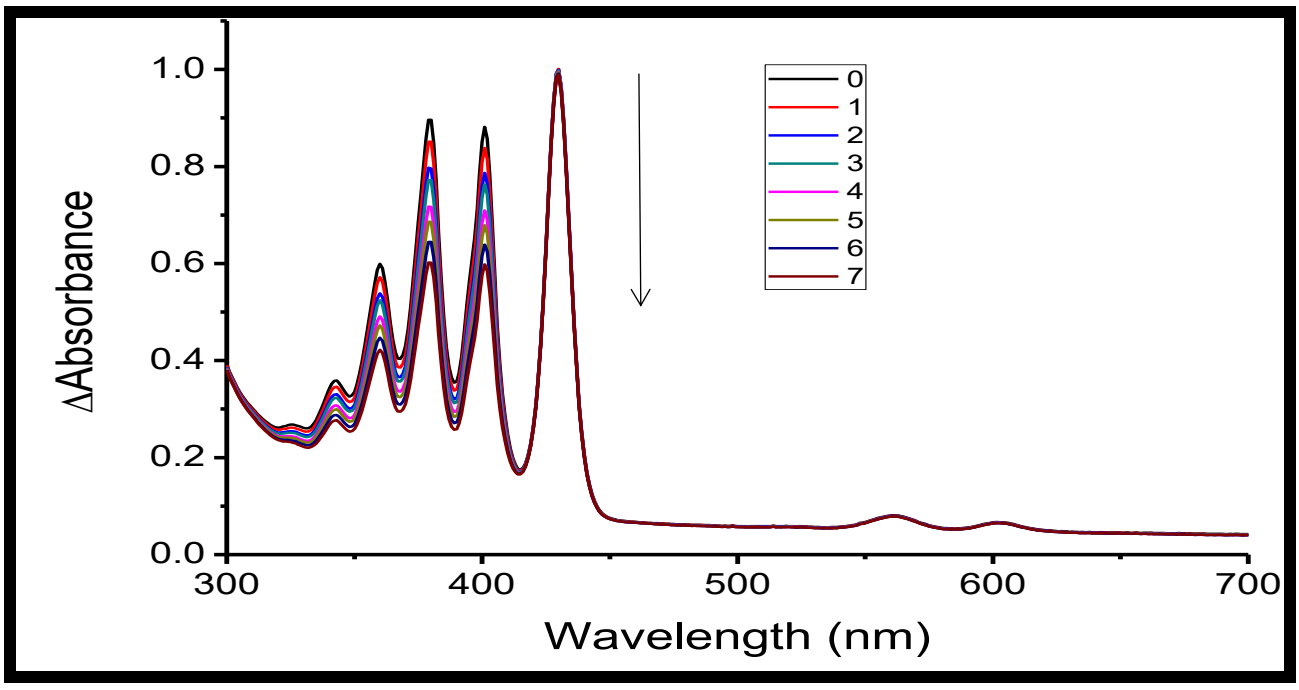

*Figure 4.6 – Spectral changes of DMA in DMF in the presence of complex **4***

ADMA degradation was monitored at 380 nm for determination of the singlet oxygen quantum yield of the modified fibres in water, **Figure 4.7** (complex **4** as an example).

The Φ_{Δ} value for **4**-PAN is 0.39 in water, **Table 4.1**. The significantly lower values in water may also be attributed to the aggregation of the complex within the fibre [107].

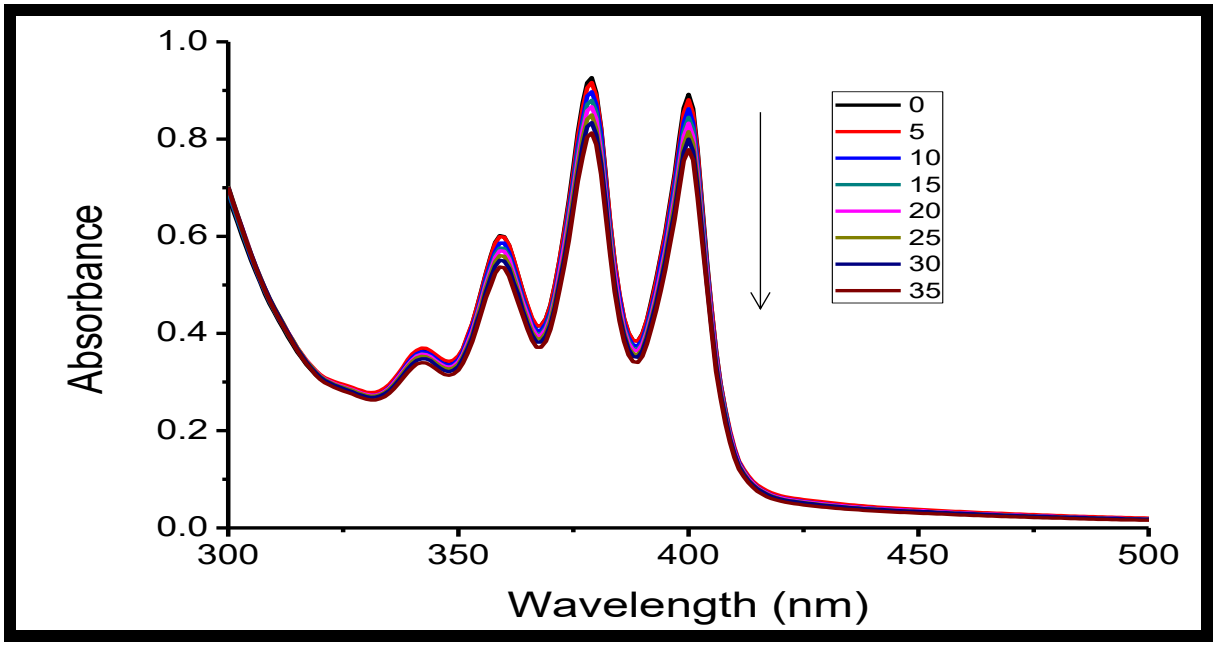

*Figure 4.7 – Spectral changes of ADMA in water in the presence of **4**-PAN.*

4.3 Conclusions for the chapter

Triplet quantum yields and lifetimes were determined for the Pc complexes. The higher quantum yields had shorter lifetimes as expected. Fluorescence quantum yields and lifetimes were determined for all complexes. Upon metalation a general decrease in lifetime and quantum yield was observed. Φ_{Δ} values were obtained for porphyrins. A decrease of Φ_{Δ} in the fibre counterparts is due to the aggregation and possible quenching of singlet oxygen in water.

Chapter 5

Photodegradation and Kinetics

This chapter provides the photodegradation and kinetics of 4-chlorophenol and 4-nonylphenol in the presence of the phthalocyanine and porphyrin functionalised fibres

5.1 pH determination of studies

It has been reported that when phenols are in their deprotonated form when immersed in basic media, they are more prone to oxidation leading to higher quantum yields for the photo-oxidation process [108,109]. A range of pHs was tried to investigate the effects it has on the pollutants.

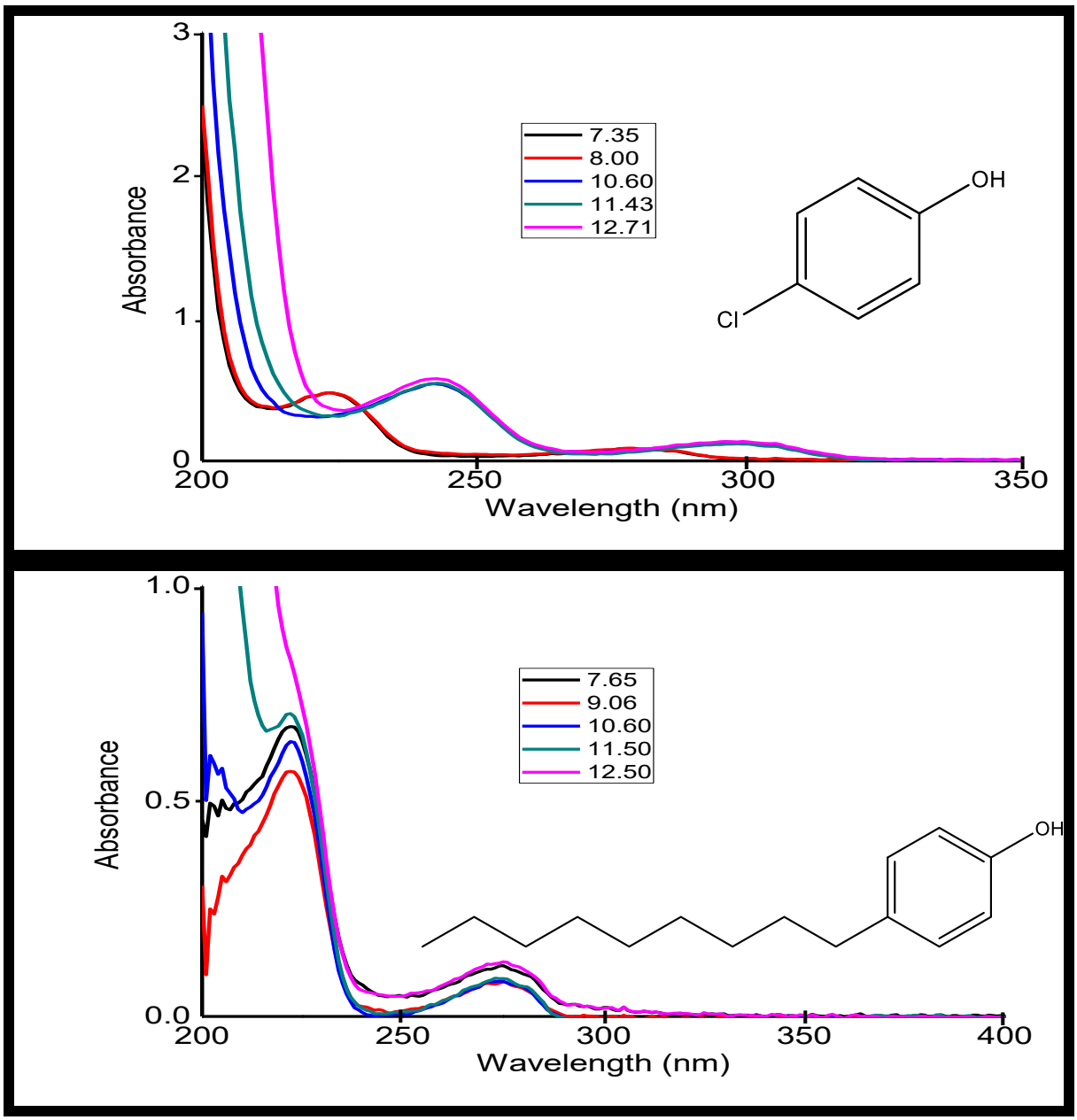

Figure 5.1 - UV-vis spectra of 4-chlorophenol (above) and 4-nonylphenol (below) at different pHs.

4-*n*-NP molecule has two peaks at ~ 225 nm and 275 nm, **Figure 5.1** similar to literature reports [110]. **Figure 5.1** illustrates that at pHs greater than 10.60 the main absorption band (near 225 nm) of the nonylphenol is distorted and would not be able to be monitored. Hence pH 10.60 was employed in this work for 4-*n*-NP. The initial spectrum for 4-CP shows two characteristic bands at 244 and 300 nm [111]. At the pH of 10.60 used for 4-*n*-NP, 4-chlorophenol undergoes a red shift indicating that deprotonation has taken place. Thus both 4-CP and 4-*n*-CP were studied at the pH of 10.60.

5.2 UV-vis absorption spectral changes

5.2.1 Photocatalysis of 4-chlorophenol

Please note that for the phthalocyanine functionalised fibres, these studies were done only for **1**-PAN (embedded) and **2**-PAN (embedded) since there was leaching of the Pcs for the immersed fibres thus showing the importance of embedding the Pcs within the fibres.

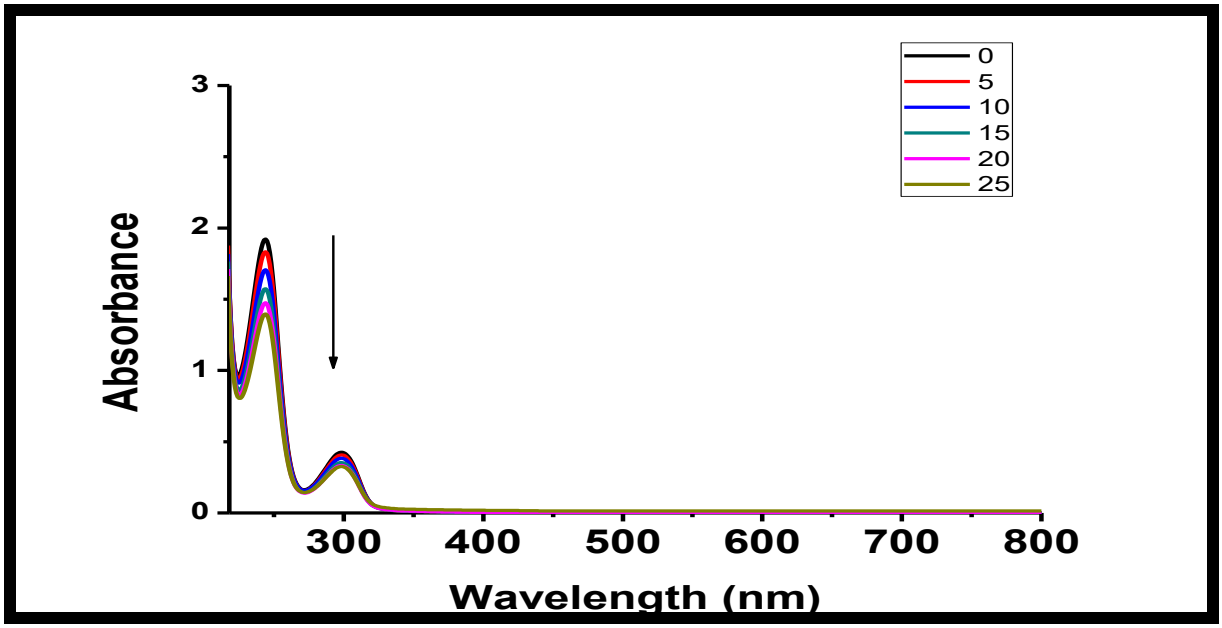

*Figure 5.2 - Absorption spectral changes of 4-CP in water in the presence of complex **1**-PAN embedded fibres at pH 10.60 (5 min intervals).*

Figure 5.2 shows changes in spectra during irradiation of 4-CP in the presence of **1**-PAN (embedded) over time, as an example. The initial spectrum for 4-CP shows two characteristic bands [111] at 244 and 300 nm at pH 10.60. These bands are shifted compared to 225 nm and 280 nm reported in literature [111] due to differences in solvents. As stated above the deprotonated form of 4-CP is more oxidizable by singlet oxygen than in its protonated or neutral forms. 4-CP with a pKa = 9.4 [112] is in its deprotonated form at pH 10.60. **1**-PAN (embedded) and **2**-PAN (embedded) were employed for the photodegradation of 4-CP. There was a decrease in both peaks at 244 and 300 nm with photolysis time (**Figure 5.2**). The decrease in peak intensity is due to the degradation of 4-CP. Usually the decrease is accompanied by the emergence of two new absorbance bands at ~ 230 and ~280 nm due to benzoquinone and hydroquinone (**Scheme 5.1**), respectively [111,113], which are intermediates but these were not observed. If 4-CP degrades with no new peaks

forms, then this implies that there were no intermediates or by-products formed [111].

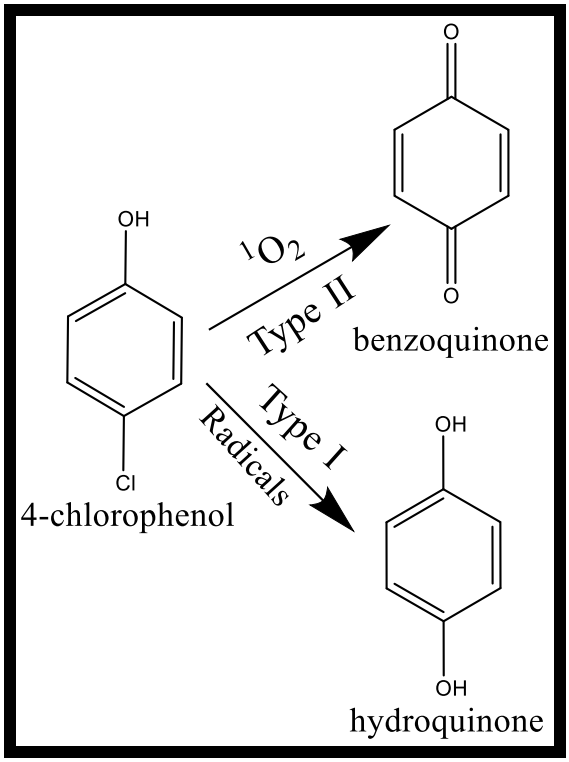

Scheme 5.1 – Phototransformation pathways of 4-CP

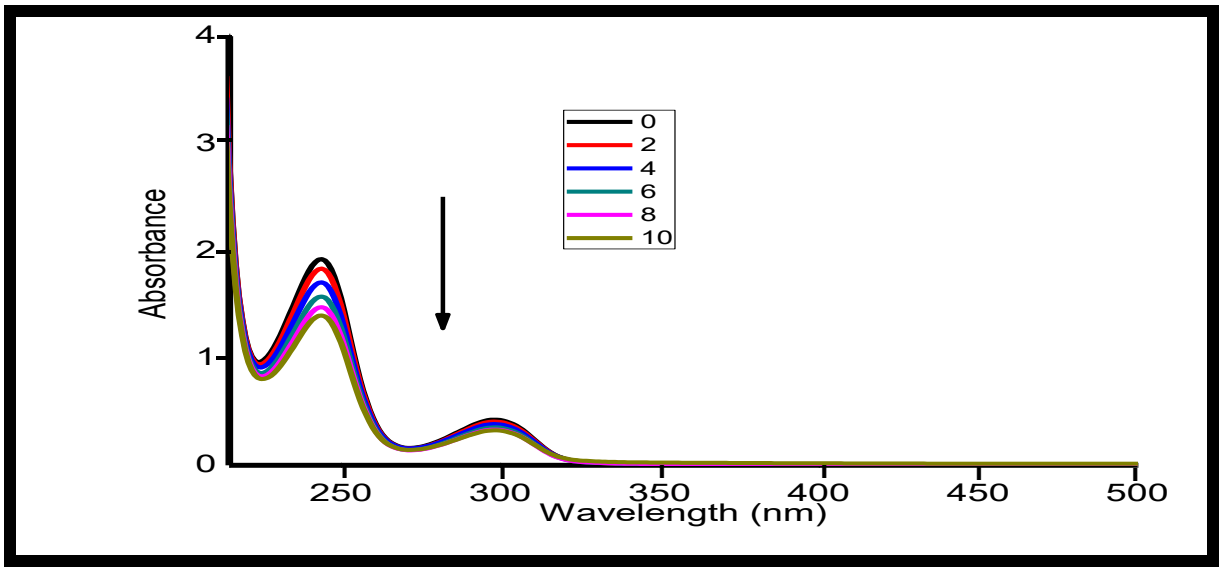

*Figure 5.3 - Absorption spectral changes of 4-chlorophenol in the presence of **4**-PAN at 2 min intervals at pH 10.60*

With the porphyrinated fibres, **Figure 5.3** shows changes in absorption spectra during irradiation of 4-CP in the presence of **4**-PAN over time. As stated above, the spectrum shows the two characteristic bands of 4-CP at 244 and 300 nm. There was an observed decrease with both absorption bands over time which again proposes that no intermediates or by-products were formed. The possible mechanism has been previously reported, **Scheme 5.2** [114].

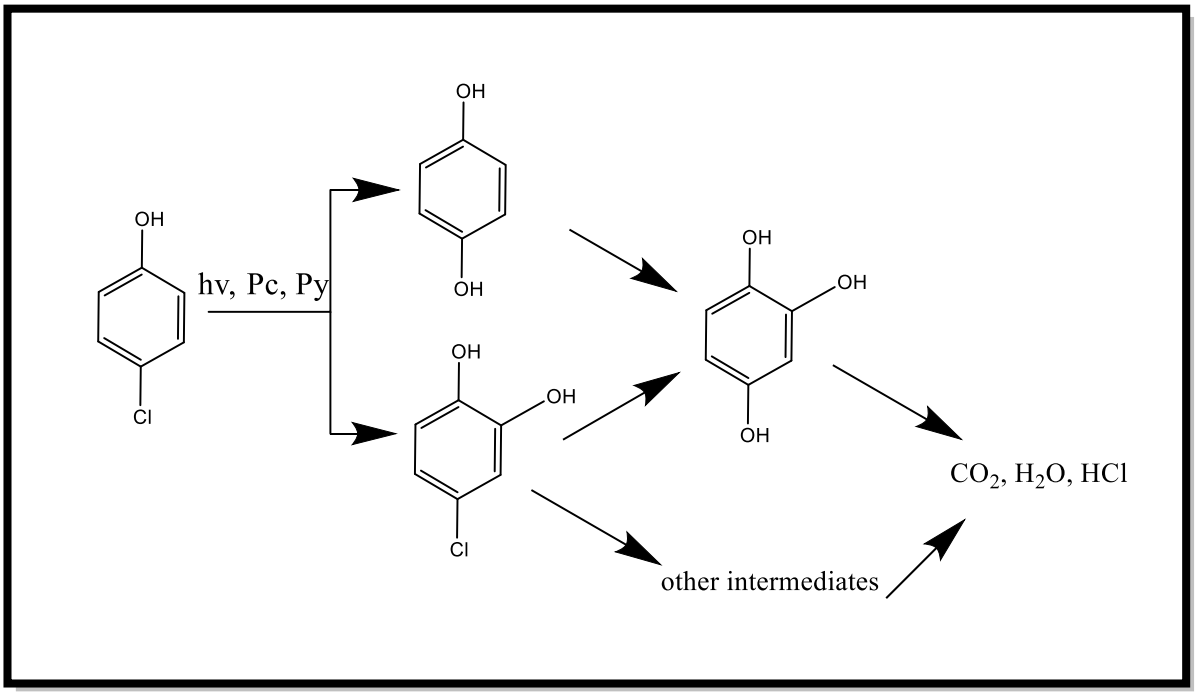

Scheme 5.2 – Possible degradation pathway of 4-CP

5.2.2 Photocatalysis of 4-nonylphenol

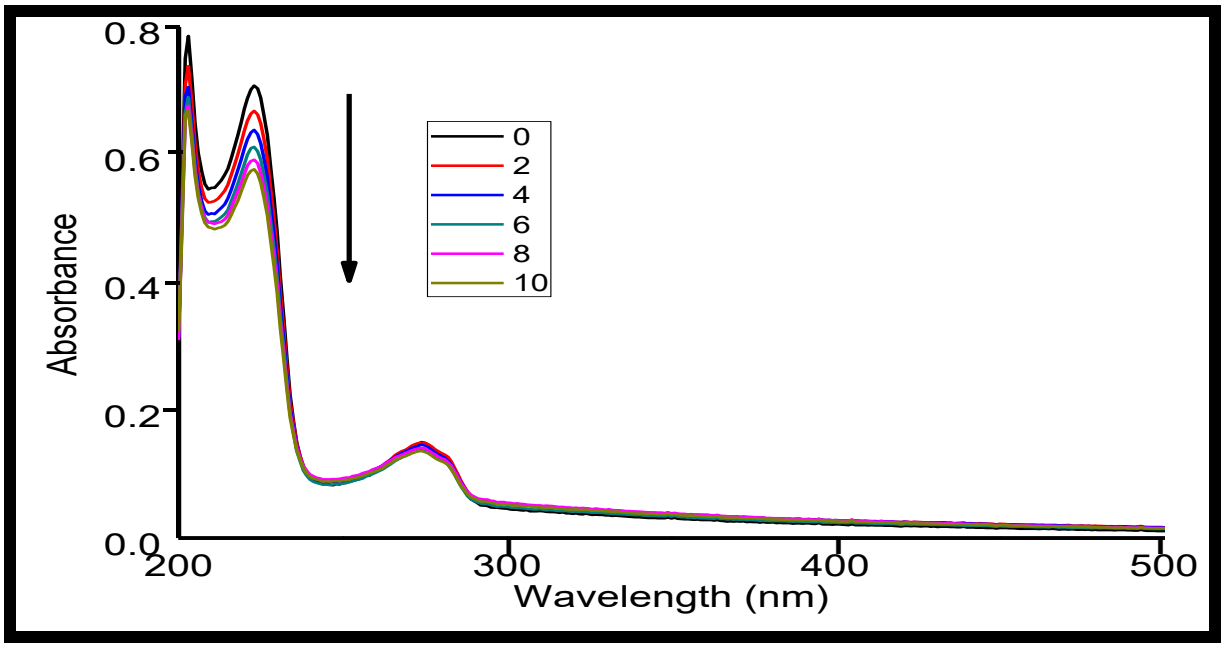

*Figure 5.4 – Absorption spectral changes of 4-nonylphenol in the presence of **4**-PAN with 2 min intervals at pH 10.60*

Pcs were tried for 4-*n*-NP, but significantly slower rates were observed hence porphyrins were employed as they displayed higher yields of degradation. **Figure 5.4** displays changes in spectra during the irradiation of nonylphenol in the presence of **4**-PAN over time as an example. What can be observed is the spectral bands at ~225 nm undergoing a significant decrease in concentration which can be related to the degradation of 4-*n*-NP. It has been reported that phenol, 1,4-dihydroxylbenzene and 1,4-benzoquinone are possible intermediate products of the photodegradation process [115]. Because no new absorption bands were observed, it is possible that no intermediates were formed, and the final products are CO_2 and H_2O, as seen in literature with other phenols [111,114].

5.3 Kinetic studies

5.3.1 Photodegradation kinetics for 4-CP with Pc fibres

Table 5.1 – Photodegradation kinetics for 4-CP with the Pc fibres

[4-CP] (mol.L^{-1})	Initial Rate (mol L^{-1}min^{-1}) [K_{Obs}] (10^{-3}.min^{-1})		Degradation % (η) (% at 25 min)	
	1-PAN (embedded)	**2**-PAN (embedded)	**1**-PAN (embedded)	**2**-PAN (embedded)
0.20	2.69 ×10^{-3} [13.3]	2.38 ×10^{-3} [11.8]	28.1	26.3
0.19	2.07 ×10^{-3} [11.6]	1.72 ×10^{-3} [9.8]	25.7	22.4
0.11	8.16 ×10^{-4} [7.2]	6.85×10^{-4} [6.1]	16.3	14.6
0.10	6.62 ×10^{-4} [6.8]	4.53 ×10^{-4} [4.6]	15.8	10.9
0.09	4.53 ×10^{-4} [5.1]	3.29 ×10^{-4} [3.7]	11.6	8.7

Kinetic studies for the degradation of 4-CP were performed. The data for the Pc fibres are listed in **Table 5.1**. The concentrations of 4-CP used are: 0.20, 0.19, 0.11, 0.10, 0.09 mol L^{-1}. The plots obtained for ln(C_O/C) versus irradiation time, **Figure 5.5 A** and **B** are linear, an indication that the reactions follow pseudo-first order kinetics. Both k_{obs} and initial rate increase with increase in concentration, **Figure 5.6**. Complex **1** shows larger k_{obs} and initial rate compared to **2**, due to the larger singlet oxygen quantum yield. The increase of k_{obs} and initial rate with concentration can be related to the photodegradation percentage (η) using **Equation 5.1** [49]:

$$\eta = \left(1 - \frac{C}{C_0}\right).100 \qquad \textbf{(5.1)}$$

where C_0 is the initial concentration, and C_t is the concentration at a time t. It was seen that both complexes **1** and **2** showed an increase in their degradation efficiency with the increase in concentration. Complex **1** has larger η compared to complex **2** due to improved Φ_Δ.

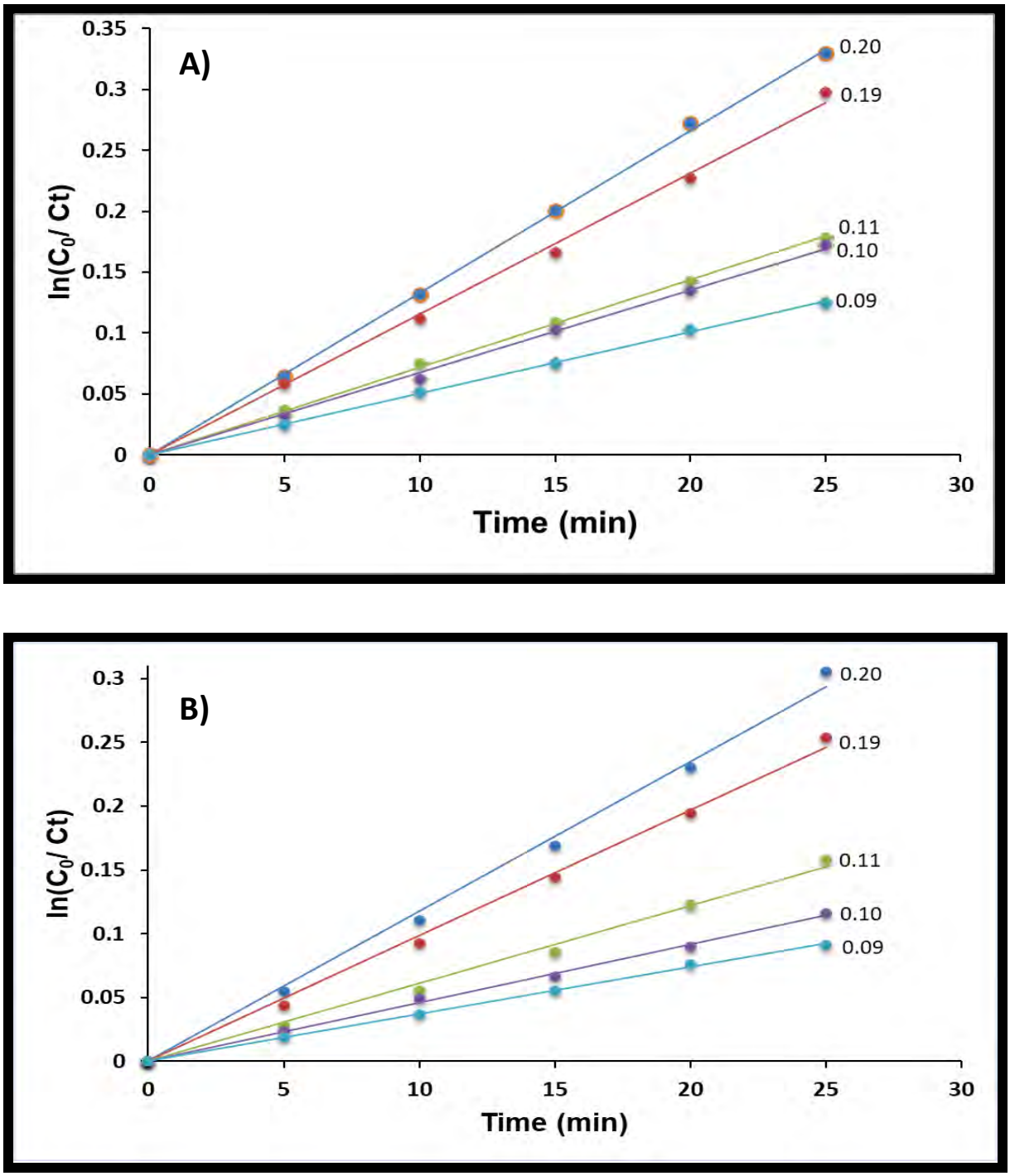

*Figure 5.5 - First order kinetic plots of photodegradation of 4-chlorophenol using (A) **1**-PAN (embedded) and (B) **2**-PAN (embedded).*

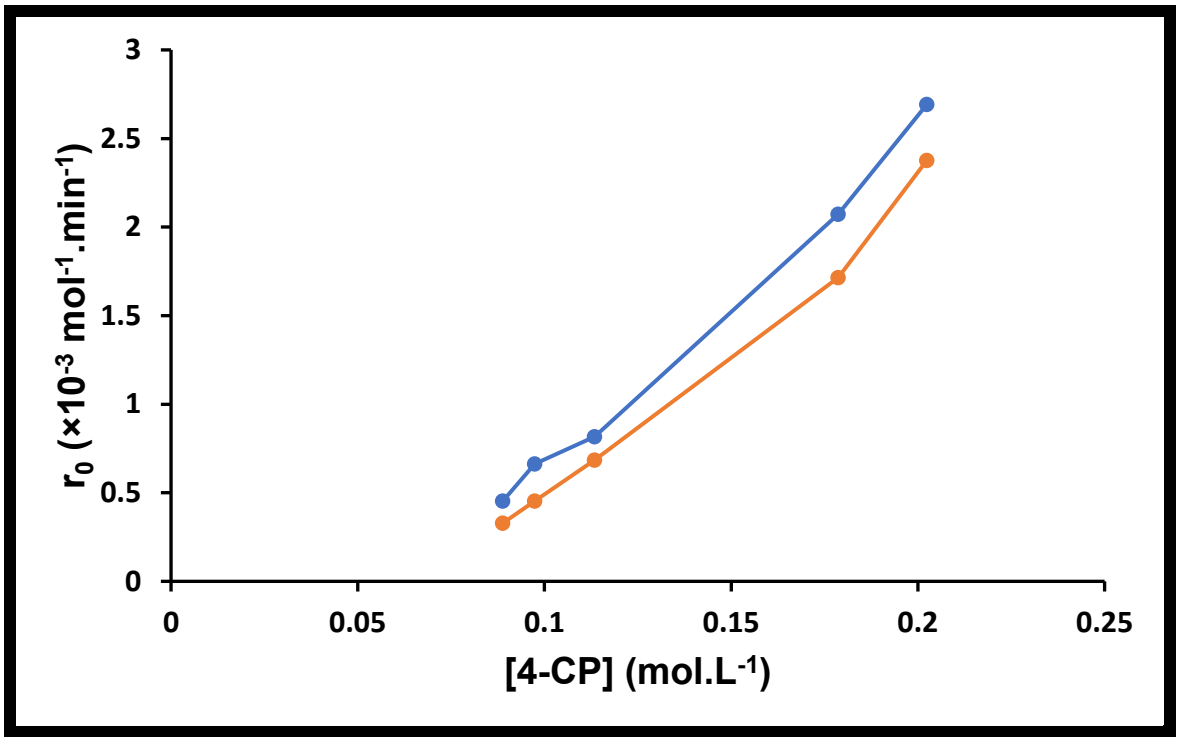

*Figure 5.6 - Plots of initial rate versus initial concentration for photodegradation of 4-chlorophenol for **1**-PAN (embedded, blue) and **2**-PAN (embedded, orange).*

The Langmuir–Hinshelwood kinetic model has been successfully applied in solid-liquid reactions, particularly heterogeneous photocatalytic degradation reactions [116] and is expressed as **Equation 5.2**:

$$\frac{1}{r_0} = \frac{1}{kK_A}\frac{1}{C_0} + \frac{1}{k} \qquad (\mathbf{5.2})$$

where r_0 is the initial photocatalytic degradation rate (mol L^{-1} min^{-1}), C_0 is the initial concentration of 4-CP, k is the apparent reaction rate constant (mol L^{-1} min^{-1}) and K_A is the adsorption coefficient. Using data from the degradation, $1/r_0$ was plotted against $1/C_0$, linear fits were not obtained for embedded **1**-PAN and **2**-PAN **Figure 5.7**. The Langmuir–Hinshelwood kinetics model assumes uniformity of active

centres [117]. The fact that this model is not obeyed in this work, suggests non-uniformity.

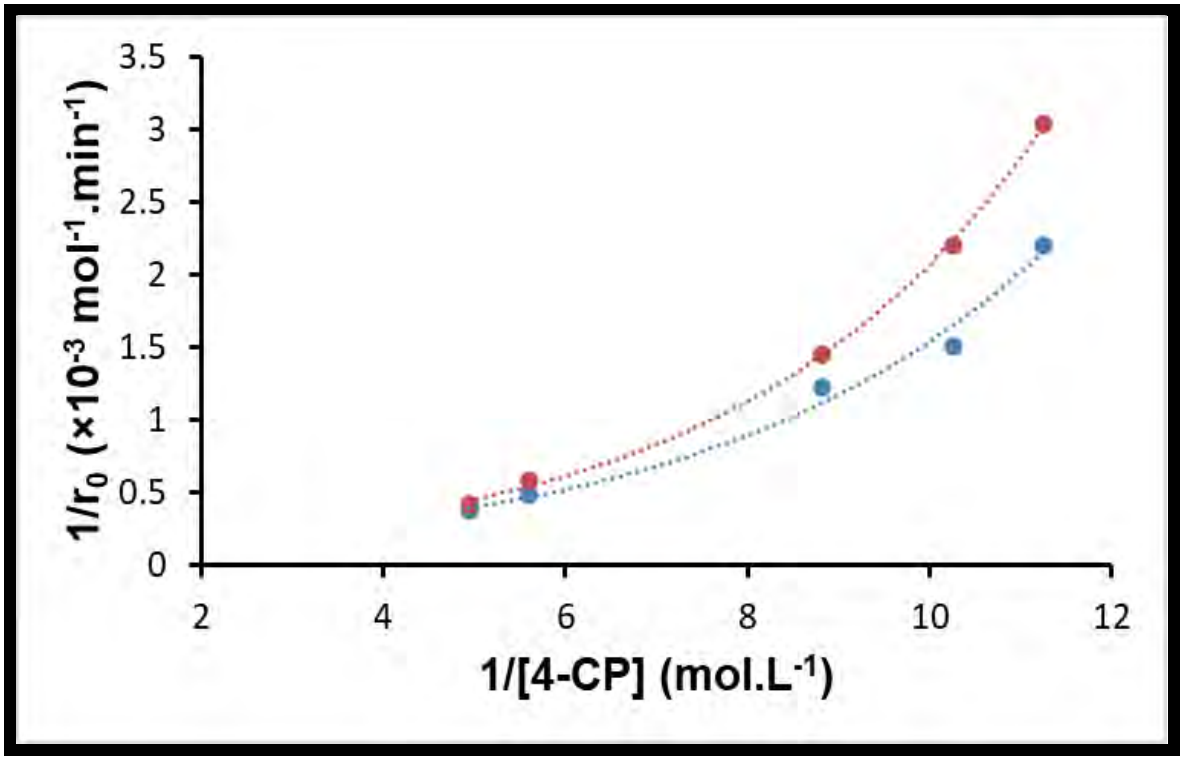

*Figure 5.7 - Plots of the inverse of the initial rate versus the inverse of the initial concentration for photodegradation of 4-CP for **1**-PAN (embedded, blue) and **2**-PAN (embedded, red).*

5.3.2 Photodegradation kinetic for 4-CP and 4-*n*-NP with porphyrin fibres

Kinetic studies for the degradation of 4-CP and 4-*n*-NP were performed with **4-**PAN. The data listed are in **Tables 5.2** and **5.3**. The concentrations for 4-CP used were 0.20, 0.17, 0.13, 0.10, 0.09 mol. L^{-1} while the concentrations for 4-*n*-N*P* are 0.17, 0.16, 0.14, 0.09, 0.07 mol. L^{-1}

Table 5.2: Photodegradation kinetics for 4-CP

[4-CP] (mol.L^{-1})	Initial Rate (mol L^{-1}min^{-1})	Degradation % (η) (% at 10 min)
	[K_{Obs}] (10^{-3}.min^{-1})	
	4-PAN	**4**-PAN
0.20	6.94×10^{-3} [34.3]	29.1
0.17	5.46×10^{-3} [30.6]	26.8
0.13	3.41×10^{-3} [25.4]	22.3
0.10	1.64×10^{-3} [16.9]	15.9
0.09	1.12×10^{-3} [12.6]	11.8

Table 5.3: Photodegradation kinetics for 4-*n*-NP

[NP] (mol.L^{-1})	Initial Rate (mol L^{-1}min^{-1})	Degradation % (η) (% at 10 min)
	[K_{Obs}] (10^{-3}.min^{-1})	
	4-PAN	**4**-PAN
0.17	5.56×10^{-3} [32.0]	26.7
0.16	3.86×10^{-3} [24.4]	20.9
0.14	3.22×10^{-3} [23.7]	20.6
0.09	1.98×10^{-3} [22.1]	18.8
0.07	1.41×10^{-3} [19.0]	17.8

Plots of ln(C_O/C) versus irradiation times, **Figure 5.8 A** and **B**, are both linear. This indicates that both reactions follow pseudo-first order kinetics. It was observed that both the initial rate and K_{obs} increased with an increase in concentration for both 4-CP and 4-*n*-NP. The (η) was recalculated for each phenol and displayed an observed increase with increased concentration.

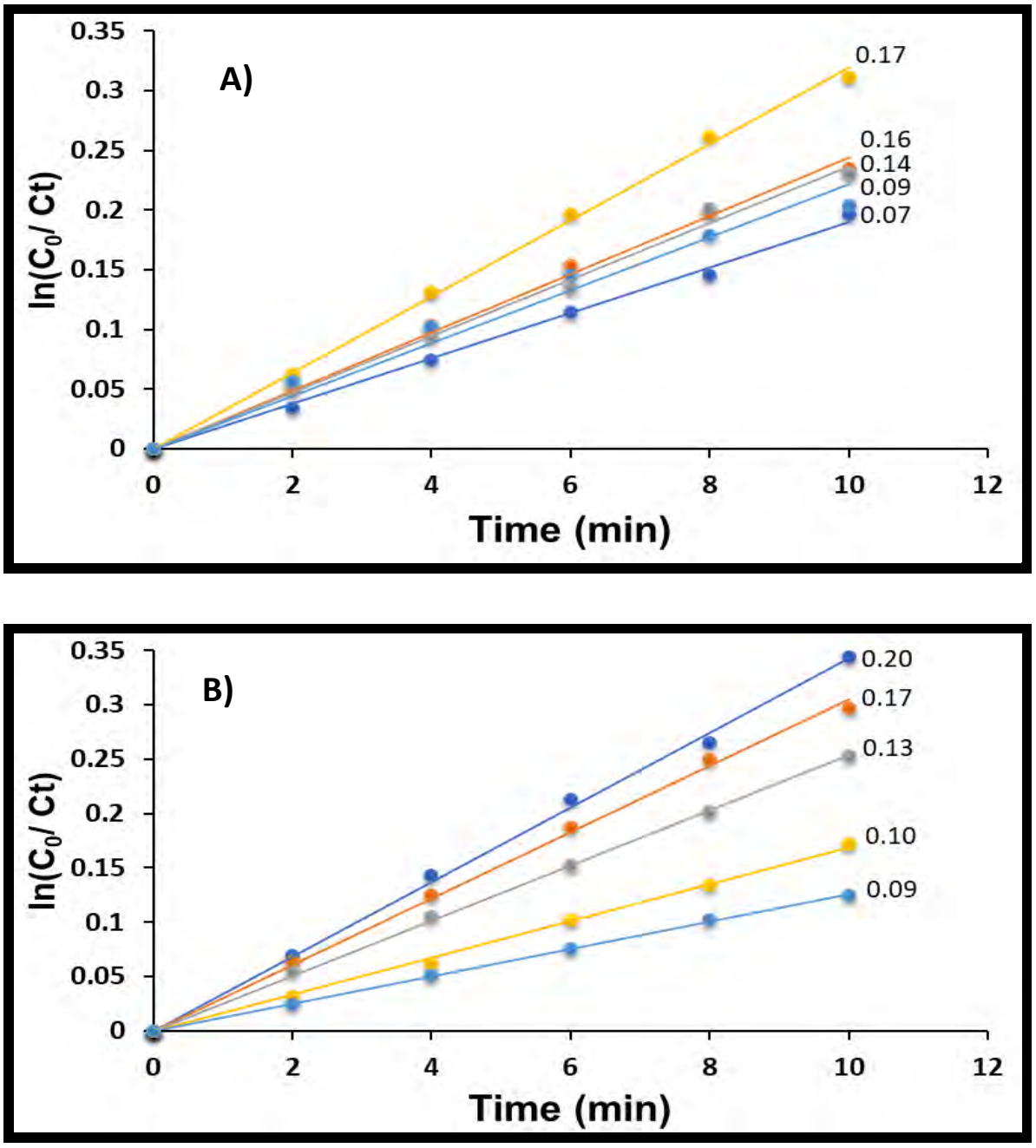

*Figure 5.8 - First order kinetic plots of photodegradation of A) nonylphenol and B) 4-chlorophenol using **4**-PAN*

Langmuir-Hinshelwood kinetics were also applied to both experiments and it was observed that neither 4-CP nor 4-*n*-NP obeyed this model (**Figure 5.9 A** and **B**).

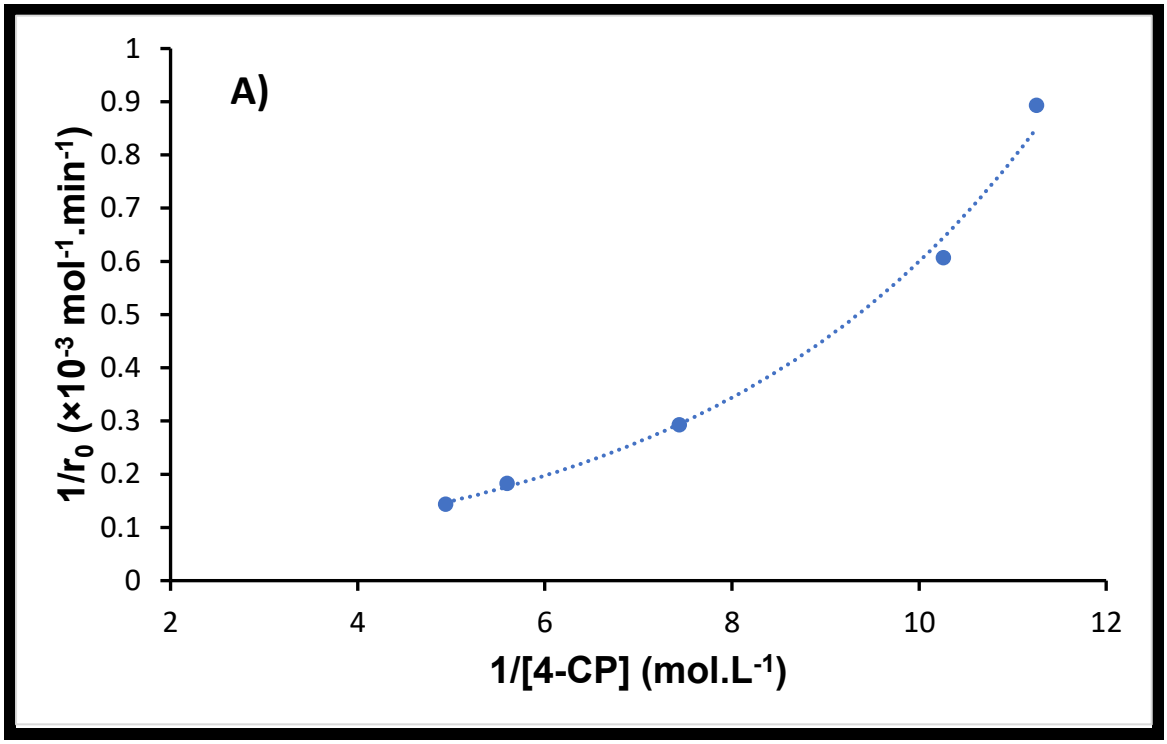

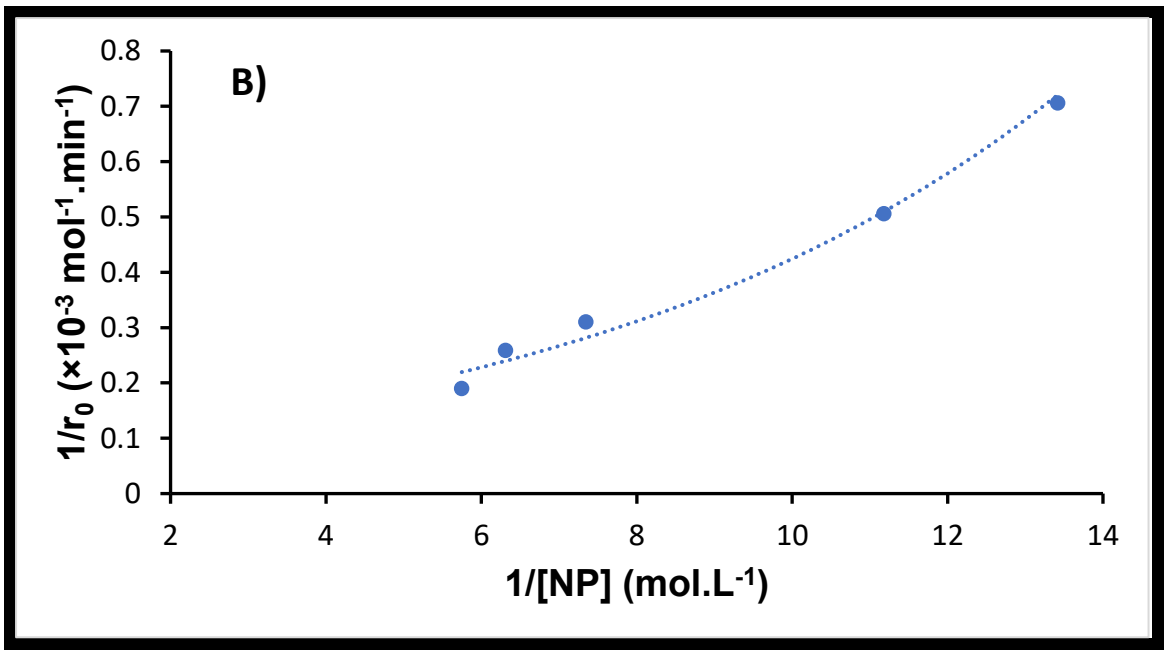

*Figure 5.9 - Plots of the inverse of the initial rate versus the inverse of the initial concentration of A) 4-n-NP and B) 4-CP both in the presence of **4**-PAN.*

5.3.3 Comparison of phthalocyanines to porphyrins

The initial rates, K_{obs} and degradation efficiencies (η) were compared between the Pcs and porphyrins with respect to 4-CP. Upon inspection, the porphyrins exhibited significantly higher values for all measured parameters. The largest η values for **4**-PAN were 29.1% against 28.1% for **1**-PAN even though it was irradiated for 10 mins as opposed to 25 min for **1**-PAN. The reasons for this may be attributed to the porphyrin molecules being asymmetrical which is known to increase their singlet oxygen quantum yields. It must also be noted that the porphyrinated fibres are irradiated at significantly lower wavelengths (430 nm as opposed to 690 nm for Pcs). Lower wavelengths consequently use higher frequencies resulting in greater energy transferred to the fibres during this process. **1-**PAN, **2**-PAN and **4**-PAN exhibited higher initial rates and k_{obs} values when compared to other photodegradation attempts using Pcs on 4-chlorophenol [76,118] and similar dyes on other pollutants [49].

Chapter 6

Conclusion and Future Prospects

The summary of this thesis is presented in this chapter along with prospects.

6.1 Conclusions

This work has successfully presented a series of novel In and Zn phthalocyanines and novel free-base and Zn porphyrins. It is also the first time polyacrylonitrile has been linked to an asymmetric porphyrin employed in the photodegradation of 4-CP and 4-*n*-CP. Both the phthalocyanines, porphyrins and their fibre counterparts were fully characterized using ^{1}NMR, FT-IR, SEM, EDS, UV-vis, solid-state UV-vis, TOF-SIMS, MALDI-TOF and several other powerful tools. The photocatalytic activity of the porphyrinated fibres showed higher degradation percentages of degradation than the Pc fibres with shorter irradiation times with the highest values being 29.1% of 4-CP in 10 min against 28.1% in 25 min. 4-*n*-NP was also successfully degraded with the porphyrinated fibres showing a decrease of 26.7% after 10 min. It must be noted that both fibres showed higher rates of degradation and increased rate constants at higher concentrations for both pollutants.

6.2 Future Prospects

I have observed that linking a photosensitiser than alternatively embedding in electrospun fibres has obvious advantages in water purification. Detailed studies should be conducted on the modification of various photosensitisers and their fibres to accelerate the process of utilising these promising techniques in cleaning up wastewater pollutants.

Bibliography

[1] A. Braun, J. Tcherniac, Über die Produkte der Einwirkung von Acetanhydrid auf Phthalamid, Berichte Der Dtsch. Chem. Gesellschaft. 40 (1907) 2709–2714. https://doi.org/10.1002/cber.190704002202.

[2] H. de Diesbach, E. von der Weid, Quelques sels complexes des o-dinitriles avec le cuivre et la pyridine, Helv. Chim. Acta. 10 (1927) 886–888. https://doi.org/10.1002/hlca.192701001110.

[3] R.P. Linstead, Phthalocyanines. Part I. A new type of synthetic colouring matters, J. Chem. Soc. 212 (1934) 1016–1017. https://doi.org/10.1039/jr9340001016.

[4] J.M. Robertson, An x-ray study of the phthalocyanines. Part II. Quantitative structure determination of the metal-free compound, J. Chem. Soc. 255 (1936) 1195–1209. https://doi.org/10.1039/jr9360001195.

[5] T.K. Horne, H. Abrahamse, M.J. Cronjé, Investigating the efficiency of novel metallo-phthalocyanine PDT-induced cell death in MCF-7 breast cancer cells, Photodiagnosis Photodyn. Ther. 9 (2012) 215–224. https://doi.org/10.1016/j.pdpdt.2011.12.008.

[6] D. Akyüz, Ü. Demirbaş, A. Koca, F. Çelik, H. Kantekin, Electrochemistry, electropolymerization and electrochromism of novel phthalocyanines bearing morpholine groups, J. Mol. Struct. 1206 (2020) 127674. https://doi.org/10.1016/j.molstruc.2019.127674.

[7] I. Maliszewska, W. Kałas, E. Wysokińska, W. Tylus, N. Pietrzyk, K. Popko, K. Palewska, Enhancement of photo-bactericidal effect of tetrasulfonated

hydroxyaluminum phthalocyanine on Pseudomonas aeruginosa, Lasers Med. Sci. 33 (2018) 79–88. https://doi.org/10.1007/s10103-017-2337-0.

[8] B. Ali, T. McCormac, C. Maccato, D. Barreca, G. Carraro, Multilayer assemblies of a Cu-phthalocyanine with Dawson type polyoxometalates (POMs) for the electrocatalytic reduction of phosphate, J. Electroanal. Chem. 858 (2020) 113770. https://doi.org/10.1016/j.jelechem.2019.113770.

[9] S. Gorduk, A. Altindal, Non-peripherally tetra substituted phthalocyanines bearing carboxylic acid anchoring groups as photosensitizer for high efficient dye-sensitized solar cells, J. Mol. Struct. 1204 (2020) 127636. https://doi.org/10.1016/j.molstruc.2019.127636.

[10] N. Nwaji, B. Jones, J. Mack, D.O. Oluwole, T. Nyokong, Nonlinear optical dynamics of benzothiazole derivatized phthalocyanines in solution, thin films and when conjugated to nanoparticles, J. Photochem. Photobiol. A Chem. 346 (2017) 46–59. https://doi.org/10.1016/j.jphotochem.2017.05.042.

[11] D.M. Mafukidze, T. Nyokong, Graphene quantum dot-phthalocyanine polystyrene conjugate embedded in asymmetric polymer membranes for photocatalytic oxidation of 4-chlorophenol, J. Coord. Chem. 70 (2017) 3598–3618. https://doi.org/10.1080/00958972.2017.1400664.

[12] B.D. Berezii, L.P. Shorlyialgova, Synthesis and optical behaviour of complex compounds of polymeric phthalocyanines, Vysok. Soyed. 10 (1967) 384–389.

[13] I.M. Denekamp, P. Jungbacker, G. Rothenberg, A simple synthesis of symmetric phthalocyanines and their respective perfluoro and transition metal complexes, Appl. Organomet. Chem. 33 (2019) e4872. https://doi.org/10.1002/aoc.4872.

[14] T. Furuyama, K. Satoh, T. Kushiya, N. Kobayashi, Design , Synthesis , and Properties of Phthalocyanine Complexes with Main-Group Elements Showing Main Absorption beyond 1000 nm plexes with Main-Group Elements Showing Main Absorption beyond 1000 nm, J. Am. Chem. Soc. 136 (2013) 765–776.

[15] N. Kobayashi, T. Furuyama, K. Satoh, Rationally Designed Phthalocyanines Having Their Main Absorption Band beyond 1000 nm, J. Am. Chem. Soc. 133 (2011) 19642–19645. https://doi.org/10.1021/ja208481q.

[16] V.N. Nemykin, E.A. Lukyanets, Synthesis of substituted phthalocyanines, Arkivoc. (i) (2010) 136–208.

[17] M. Gouterman, Spectra of porphyrins, J. Mol. Spectrosc. 6 (1961) 138–163. https://doi.org/10.1016/0022-2852(61)90236-3.

[18] D.K. Lavallee, A Review of: “Porphyrins and Metalloporphyrins, Edited by K.M. Smith, in: Synthesis and Reactivity in Inorganic and Metal-Organic Chemistry, Elsevier Scientific Publishing Company, New York, 8, in: 1978: pp. 97–98. https://doi.org/10.1080/00945717808057392.

[19] V.L. Goedken, G. Dessy, C. Ercolani, V. Fares, L. Gastaldi, Synthesis, Reactivity, and X-ray Crystal Structure of Dichloro(phthalocyaninato)titanium(IV), Inorg. Chem. 24 (1985) 991–995. https://doi.org/10.1021/ic00201a006.

[20] P.E. McGovern, R.H. Michel, Royal Purple Dye: Tracing Chemical Origins of the Industry, Anal. Chem. 57 (1985) 1514–1522. https://doi.org/10.1021/ac00291a002.

[21] W. Kuster, Einführung in die Chemie der Hämine, Physiol. Chem. Phys. 82

(1913) 6–22. https://doi.org/10.1007/BF02164281.

[22] H. Fischer, K. Zeile, Synthese des Hämatoporphyrins, Protoporphyrins und Hämins, Justus Liebigs Ann. Chem. 468 (1929) 98–116. https://doi.org/10.1002/jlac.19294680104.

[23] T.D. Lash, Origin of aromatic character in porphyrinoid systems, J. Porphyr. Phthalocyanines. 15 (2011) 1093–1115. https://doi.org/10.1142/S1088424611004063.

[24] M.J. Warren, A.G. Smith, M.R. Moore, An Historical Introduction to Porphyrin and Chlorophyll Synthesis, in: Tetrapyrroles, Springer-Verlag, New York, 2009: pp. 1–28. https://doi.org/10.1007/978-0-387-78518-9_1.

[25] J. Min Park, J.H. Lee, W.D. Jang, Applications of porphyrins in emerging energy conversion technologies, Coord. Chem. Rev. 407 (2020) 213157. https://doi.org/10.1016/j.ccr.2019.213157.

[26] N. Rabiee, M.T. Yaraki, S.M. Garakani, S.M. Garakani, S. Ahmadi, A. Lajevardi, M. Bagherzadeh, M. Rabiee, L. Tayebi, M. Tahriri, M.R. Hamblin, Recent advances in porphyrin-based nanocomposites for effective targeted imaging and therapy, Biomaterials. 232 (2020) 119707. https://doi.org/10.1016/j.biomaterials.2019.119707.

[27] V. Pandey, D. Jain, N. Pareek, I. Gupta, Pd(II) porphyrins: Synthesis, singlet oxygen generation and photoassisted oxidation of aldehydes to carboxilic acids, Inorg. Chim. Acta. 502 (2020) 119339. https://doi.org/10.1016/j.ica.2019.119339.

[28] C.M.B. Neves, O.M.S. Filipe, N. Mota, S.A.O. Santos, A.J.D. Silvestre, E.B.H.

Santos, M.G.P.M.S. Neves, M.M.Q. Simões, Photodegradation of metoprolol using a porphyrin as photosensitizer under homogeneous and heterogeneous conditions, J. Hazard. Mater. 370 (2019) 13–23. https://doi.org/10.1016/j.jhazmat.2018.11.055.

[29] K. Xie, N. An, Y. Zhang, G. Liu, F. Zhang, Y. Zhang, F. Jiao, Two-dimensional porphyrin sheet as an electric and optical sensor material for pH detection: A DFT study, Comput. Mater. Sci. 174 (2020) 109485. https://doi.org/10.1016/j.commatsci.2019.109485.

[30] M. Wierzchowski, D. Łażewski, T. Tardowski, M. Grochocka, R. Czajkowski, S. Sobiak, L. Sobotta, Nanomolar photodynamic activity of porphyrins bearing 1,4,7-trioxanonyl and 2-methyl-5-nitroimidazole moieties against cancer cells, J. Photochem. Photobiol. B Biol. 202 (2020) 111703. https://doi.org/10.1016/j.jphotobiol.2019.111703.

[31] G.K. Couto, B.S. Pacheco, V.M. Borba, J.C.R. Junior, T.L. Oliveira, N.V. Segatto, F.K. Seixas, T. V. Acunha, B.A. Iglesias, T. Collares, Tetra-cationic platinum(II) porphyrins like a candidate photosensitizers to bind, selective and drug delivery for metastatic melanoma, J. Photochem. Photobiol. B Biol. 202 (2020) 111725. https://doi.org/10.1016/j.jphotobiol.2019.111725.

[32] F. Cheng, X. He, L. Yin, B. Xie, Y. Li, Design and structural modification of narrow-bandgap small molecules based on asymmetric porphyrin-diketopyrrolopyrrole backbone for solution-processed organic solar cells, Dye. Pigment. (2020) 108211. https://doi.org/10.1016/j.dyepig.2020.108211.

[33] A.D. Adler, F.R. Longo, F. Kampas, J. Kim, On the preparation of metalloporphyrins, J. Inorg. Nucl. Chem. 32 (1970) 2443–2445.

https://doi.org/10.1016/0022-1902(70)80535-8.

[34] E. Rabinowitch, Spectra of porphyrins and chlorophyll, Rev. Mod. Phys. 16 (1944) 226. https://doi.org/10.1103/RevModPhys.16.226.

[35] W.T. Simpson, On the theory of the π-electron system in porphines, J. Chem. Phys. 17 (1949) 1218–1221. https://doi.org/10.1063/1.1747145.

[36] M. Pera-Titus, V. García-Molina, M.A. Baños, J. Giménez, S. Esplugas, Degradation of chlorophenols by means of advanced oxidation processes: A general review, Appl. Catal. B Environ. 47 (2004) 219–256. https://doi.org/10.1016/j.apcatb.2003.09.010.

[37] P.Y. Chan, M. Gamal El-Din, J.R. Bolton, A solar-driven UV/Chlorine advanced oxidation process, Water Res. 46 (2012) 5672–5682. https://doi.org/10.1016/j.watres.2012.07.047.

[38] T. Robinson, G. McMullan, R. Marchant, P. Nigam, Remediation of dyes in textile effluent: A critical review on current treatment technologies with a proposed alternative, Bioresour. Technol. 77 (2001) 247–255. https://doi.org/10.1016/S0960-8524(00)00080-8.

[39] V.K. Sharma, G.A.K. Anquandah, R.A. Yngard, H. Kim, J. Fekete, K. Bouzek, A.K. Ray, D. Golovko, Nonylphenol, octylphenol, and bisphenol-A in the aquatic environment: A review on occurrence, fate, and treatment, J. Environ. Sci. Heal. - Part A Toxic/Hazardous Subst. Environ. Eng. 44 (2009) 423–442. https://doi.org/10.1080/10934520902719704.

[40] C.G. Okkerman P.C, Towards the establishment of a priority list of substances for further evaluation of their role in endocrine disruption, Eur. Comm. Env. 1

(2000) 1–29. https://doi.org/M0355008/1786Q/10/11/00.

[41] M.P. Sárria, M.M. Santos, M.A. Reis-Henriques, N.M. Vieira, N.M. Monteiro, The unpredictable effects of mixtures of androgenic and estrogenic chemicals on fish early life, Environ. Int. 37 (2011) 418–424. https://doi.org/10.1016/j.envint.2010.11.004.

[42] A. Soares, B. Guieysse, B. Jefferson, E. Cartmell, J.N. Lester, Nonylphenol in the environment: A critical review on occurrence, fate, toxicity and treatment in wastewaters, Environ. Int. 34 (2008) 1033–1049. https://doi.org/10.1016/j.envint.2008.01.004.

[43] C. Vogelsang, M. Grung, T.G. Jantsch, K.E. Tollefsen, H.L. Ã, Occurrence and removal of selected organic micropollutants at mechanical , chemical and advanced wastewater treatment plants in Norway, Water Res. 40 (2006) 3559–3570. https://doi.org/10.1016/j.watres.2006.07.022.

[44] C. Tai, G. Jiang, J. Liu, Q. Zhou, J. Liu, Rapid degradation of bisphenol A using air as the oxidant catalyzed by polynuclear phthalocyanine complexes under visible light irradiation, J. Photochem. Photobiol. A Chem. 172 (2005) 275–282. https://doi.org/10.1016/j.jphotochem.2004.12.015.

[45] J. Cooley, Improved methods of and apparatus for electrically separating the relatively volatile liquid component from the component of relatively fixed substances of composite, Pat. GB, United Kingdom Pat. #6385. (1900).

[46] Z.O. Makinde, M. Louzada, P. Mashazi, T. Nyokong, S. Khene, Electrocatalytic behaviour of surface confined pentanethio cobalt (II) binuclear phthalocyanines towards the oxidation of 4-chlorophenol, Appl. Surf. Sci. 425 (2017) 702–712. https://doi.org/https://doi.org/10.1016/j.apsusc.2017.06.271.

[47] A.E. Pirbazari, Sensitization of Tio2 Nanoparticles With Cobalt Phthalocyanine: An Active Photocatalyst for Degradation of 4-Chlorophenol under Visible Light, Procedia Mater. Sci. 11 (2015) 622–627. https://doi.org/https://doi.org/10.1016/j.mspro.2015.11.096.

[48] S. Khene, K. Lobb, T. Nyokong, Characterization of nickel tetrahydroxy phthalocyanine complexes and the electrocatalytic oxidation of 4-chlorophenol: Correlation of theory with experiments, Inorg. Chim. Acta. 362 (2009) 5055–5063. https://doi.org/https://doi.org/10.1016/j.ica.2009.08.019.

[49] A.K. Lebechi, T. Nyokong, J. Mack, BODIPY dye embedded electrospun polystyrene nanofibers for the photocatalytic degradation of orange G in industrial wastewaters, Macroheterocycles. 10 (2017) 460–466. https://doi.org/10.6060/mhc171143n.

[50] A. Sułek, B. Pucelik, J. Kuncewicz, G. Dubin, J.M. Dąbrowski, Sensitization of TiO2 by halogenated porphyrin derivatives for visible light biomedical and environmental photocatalysis, Catal. Today. 335 (2019) 538–549. https://doi.org/https://doi.org/10.1016/j.cattod.2019.02.070.

[51] T. Shiragami, J. Matsumoto, H. Inoue, M. Yasuda, Antimony porphyrin complexes as visible-light driven photocatalyst, J. Photochem. Photobiol. C Photochem. Rev. 6 (2005) 227–248. https://doi.org/https://doi.org/10.1016/j.jphotochemrev.2005.12.001.

[52] R. Sasai, D. Sugiyama, S. Takahashi, Z. Tong, T. Shichi, H. Itoh, K. Takagi, The removal and photodecomposition of n-nonylphenol using hydrophobic clay incorporated with copper-phthalocyanine in aqueous media, J. Photochem. Photobiol. A Chem. 155 (2003) 223–229.

https://doi.org/https://doi.org/10.1016/S1010-6030(02)00372-6.

[53] N. Tucker, J.J. Stanger, M.P. Staiger, The History of the Science and Technology of Electrospinning from 1600 to 1995, J. Eng. Fiber. Fabr. 7 (1995) 63–73.

[54] N. Basson, Free volume of electrospun organic-inorganic, MSc thesis, University of Stellenbosch, (2014).

[55] Z.M. Huang, Y.Z. Zhang, M. Kotaki, S. Ramakrishna, A review on polymer nanofibers by electrospinning and their applications in nanocomposites, Compos. Sci. Technol. 63 (2003) 2223–2253. https://doi.org/10.1016/S0266-3538(03)00178-7.

[56] J. Doshi, D.H. Reneker, Electrospinning process and applications of electrospun fibers, Conf. Rec. - IAS Annu. Meet. (IEEE Ind. Appl. Soc. 3 (1993) 1698–1703. https://doi.org/10.1109/ias.1993.299067.

[57] I.C. Audrey Frenot, Polymer nanofibers assembled by electrospinning, Curr. Opin. Colloid Interface Sci. 8 (2003) 64–75. https://doi.org/10.1016/S1359-0294.

[58] M.G. McKee, G.L. Wilkes, R.H. Colby, T.E. Long, Correlations of Solution Rheology with Electrospun Fiber Formation of Linear and Branched Polyesters, Macromolecules. 37 (2004) 1760–1767. https://doi.org/10.1021/ma035689h.

[59] E.S. Medeiros, L.H.C. Mattoso, R.D. Offeman, D.F. Wood, W.J. Orts, Effect of relative humidity on the morphology of electrospun polymer fibers, Can. J. Chem. 86 (2008) 590–599. https://doi.org/10.1139/V08-029.

[60] V. Pillay, C. Dott, Y.E. Choonara, C. Tyagi, L. Tomar, P. Kumar, L.C. Du Toit, V.M.K. Ndesendo, A review of the effect of processing variables on the fabrication of electrospun nanofibers for drug delivery applications, J. Nanomater. (2013) 1–22. https://doi.org/10.1155/2013/789289.

[61] S.A. Mirmohammad Sadeghi, S. Borhani, A. Zadhoush, M. Dinari, Single nozzle electrospinning of encapsulated epoxy and mercaptan in PAN for self-healing application, Polymer (Guildf). 186 (2020) 122007. https://doi.org/10.1016/j.polymer.2019.122007.

[62] H. Rodríguez-Tobías, G. Morales, D. Grande, Comprehensive review on electrospinning techniques as versatile approaches toward antimicrobial biopolymeric composite fibers, Mater. Sci. Eng. C. 101 (2019) 306–322. https://doi.org/10.1016/j.msec.2019.03.099.

[63] S. Chao, Y. Li, R. Zhao, L. Zhang, Y. Li, C. Wang, X. Li, Synthesis and characterization of tigecycline-loaded sericin/poly(vinyl alcohol) composite fibers via electrospinning as antibacterial wound dressings, J. Drug Deliv. Sci. Technol. 44 (2018) 440–447. https://doi.org/https://doi.org/10.1016/j.jddst.2018.01.022.

[64] G. Zheng, J. Jiang, X. Wang, W. Li, J. Liu, G. Fu, L. Lin, Nanofiber membranes by multi-jet electrospinning arranged as arc-array with sheath gas for electrodialysis applications, Mater. Des. 189 (2020) 108504. https://doi.org/10.1016/j.matdes.2020.108504.

[65] S. Hong, L.Y. Lin, Fabrication of TiO2 nanoparticle/TiO2 microcone array photoanode for fiber-type dye-sensitized solar cells: Effect of acid concentration on morphology of microcone, Electrochim. Acta. 331 (2020)

135278. https://doi.org/https://doi.org/10.1016/j.electacta.2019.135278.

[66] S. Jiang, H. Hou, S. Agarwal, A. Greiner, Polyimide Nanofibers by “green” Electrospinning via Aqueous Solution for Filtration Applications, ACS Sustain. Chem. Eng. 4 (2016) 4797–4804. https://doi.org/10.1021/acssuschemeng.6b01031.

[67] B. Trajkovski, A. Petersen, P. Strube, M. Mehta, G.N. Duda, Intra-operatively customized implant coating strategies for local and controlled drug delivery to bone, Adv. Drug Deliv. Rev. 64 (2012) 1142–1151. https://doi.org/10.1016/j.addr.2012.05.016.

[68] L. Shao, J. Chen, L. He, G. Xing, W. Lv, Z. Chen, C. Qi, Preparation of porphyrinated polyacrylonitrile fiber mat supported TiO2 photocatalyst and its photocatalytic activities, Turkish J. Chem. 36 (2012) 700–708. https://doi.org/10.3906/kim-1112-32.

[69] L.S. Wan, J. Wu, Z.K. Xu, Porphyrinated nanofibers via copolymerization and electrospinning, Macromol. Rapid Commun. 27 (2006) 1533–1538. https://doi.org/10.1002/marc.200600381.

[70] A. Sindelo, T. Nyokong, Magnetic nanoparticle - indium phthalocyanine conjugate embedded in electrospun fiber for photodynamic antimicrobial chemotherapy and photodegradation of methyl red, Heliyon. 5 (2019) e02352. https://doi.org/10.1016/j.heliyon.2019.e02352.

[71] O.L. Osifeko, T. Nyokong, Effects of symmetry and the number of positive charges on the photocatalytic activity of indium phthalocyanines when embedded in electrospun fibers, Inorg. Chim. Acta. 458 (2017) 50–57. https://doi.org/10.1016/j.ica.2016.12.025.

[72] N. Masilela, P. Kleyi, Z. Tshentu, G. Priniotakis, P. Westbroek, T. Nyokong, Photodynamic inactivation of Staphylococcus aureus using low symmetrically substituted phthalocyanines supported on a polystyrene polymer fiber, Dye. Pigment. 96 (2013) 500–508. https://doi.org/10.1016/j.dyepig.2012.10.001.

[73] P. Modisha, T. Nyokong, Fabrication of phthalocyanine-magnetic nanoparticles hybrid nanofibers for degradation of Orange-G, J. Mol. Catal. A Chem. 381 (2014) 132–137. https://doi.org/10.1016/j.molcata.2013.10.012.

[74] T. Arai, M. Tanaka, H. Kawakami, Porphyrin-containing electrospun nanofibers: Positional control of porphyrin molecules in nanofibers and their catalytic application, ACS Appl. Mater. Interfaces. 4 (2012) 5453–5457. https://doi.org/10.1021/am3013664.

[75] J. Avossa, R. Paolesse, C. Di Natale, E. Zampetti, G. Bertoni, F. De Cesare, G. Scarascia-Mugnozza, A. Macagnano, Electrospinning of polystyrene/polyhydroxybutyrate nanofibers doped with porphyrin and graphene for chemiresistor gas sensors, Nanomaterials. 9 (2019) 280. https://doi.org/10.3390/nano9020280.

[76] R. Zugle, T. Nyokong, Comparative phototransformation of environmental pollutants using metallophthalocyanines supported on electrospun polymer fibers, J. Appl. Polym. Sci. 128 (2013) 1131–1142. https://doi.org/10.1002/app.38381.

[77] Z.H. Iksan, A. Sarji, A. Hamed, Knowledge , Practice and Involvement of University Community in Environmental Activities Connected to Polystyrene, Creat. Educ. 10 (2019) 1777–1791. https://doi.org/10.4236/ce.2019.108127.

[78] A.S. Oliveira, D. Licsandru, R. Boscencu, R. Socoteanu, V. Nacea, L.F. Vieira

Ferreira, A singlet oxygen photogeneration and luminescence study of unsymmetrically substituted mesoporphyrinic compounds, Int. J. Photoenergy. 41 (2009) 413915. https://doi.org/10.1155/2009/413915.

[79] A. Jablonski, Efficiency of Anti-Stokes Fluorescence in Dyes, Nature. 131 (1933) 839–840. https://doi.org/10.1038/131839b0.

[80] S.P. Stratton, D.C. Liebler, Determination of singlet oxygen-specific versus radical-mediated lipid peroxidation in photosensitized oxidation of lipid bilayers: Effect of β- carotene and α-tocopherol, Biochemistry. 36 (1997) 12911–12920. https://doi.org/10.1021/bi9708646.

[81] O. Abimbola, J.Y. Chen, T. Nyokong, Photophysical and Photochemical Studies of Pyridoxamine, New J. Chem. 28 (2004) 822–827. https://doi.org/10.1002/hlca.200390279.

[82] M. Shi, J. Tian, C. Mkhize, G. Kubheka, J. Zhou, J. Mack, T. Nyokong, Z. Shen, Synthesis, characterization and photodynamic therapy properties of an octa-4-tert-butylphenoxy-substituted phosphorus(V) triazatetrabenzcorrole, J. Porphyr. Phthalocyanines. 18 (2014) 698–707. https://doi.org/10.1142/S1088424614500436.

[83] R.L. Brookfield, H. Ellul, A. Harriman, G. Porter, Luminescence of porphyrins and metalloporphyrins. Part 11. - Energy transfer in zinc-metal-free porphyrin dimers, J. Chem. Soc. Faraday Trans. 2 Mol. Chem. Phys. 82 (1986) 219–233. https://doi.org/10.1039/F29868200219.

[84] H.C. Gerritsen, R. Sanders, A. Draaijer, C. Ince, Y.K. Levine, Fluorescence lifetime imaging of oxygen in living cells, J. Fluoresc. 7 (1997) 11–15. https://doi.org/10.1007/BF02764572.

[85] T. Nyokong, E. Antunes, Photochemical and Photophysical Properties of Metallophthalocyanines, in: K. Kadish, K. Smith, R. Guilard (Eds.), Handb. Porphyr. Sci., 7th ed., Singapore, 2010: pp. 247–349. https://doi.org/10.1142/9789814307246_0006.

[86] N.A. Kuznetsova, N.S. Gretsova, O.A. Yuzhakova, V.M. Negrimovskii, O.L. Kaliya, E.A. Luk'yanets, New reagents for determination of the quantum efficiency of singlet oxygen generation in aqueous media, Russ. J. Gen. Chem. 71 (2001) 36–41. https://doi.org/10.1023/A:1012369120376.

[87] M.S. Patterson, S.J. Madsen, B.C. Wilson, Experimental tests of the feasibility of singlet oxygen luminescence monitoring in vivo during photodynamic therapy, J. Photochem. Photobiol. B Biol. 5 (1990) 69–84. https://doi.org/10.1016/1011-1344(90)85006-I.

[88] T.C. Zhu, B. Liu, M.M. Kim, D. McMillan, X. Liang, J.C. Finlay, T.M. Busch, Comparison of singlet oxygen threshold dose for PDT, Opt. Methods Tumor Treat. Detect. Mech. Tech. Photodyn. Ther. XXIII. 8931 (2014) 89310I. https://doi.org/10.1117/12.2039719.

[89] W. Spiller, H. Kliesch, D. Wöhrle, S. Hackbarth, B. Röder, G. Schnurpfeil, Singlet oxygen quantum yields of different photo-sensitizers in polar solvents and micellar solutions, J. Porphyr. Phthalocyanines. 2 (1998) 145–158. https://doi.org/10.1002/(SICI)1099-1409(199803/04)2:2<145::AID-JPP60>3.0.CO;2-2.

[90] J.G. Young, W. Onyebuagu, Synthesis and characterization of di-substituted phthalocyanines, J. Org. Chem. 55 (1990) 2155–2159. https://doi.org/https://doi.org/10.1021/jo00294a032.

[91] T. Pan, Y. Sun, G. Jiang, P. Luo, S. Wang; X. Zhang, Y. Du, Yuchang, Chinese Patent, CN104788355, 2015.

[92] M.J. Stilman, T. Nyokong, Phthalocyanines, in: Leznoff, C. C., A.B.P. Lever (Eds.), Phthalocyanines Prop. Appl., VCH Publishers, 1989: pp. 133–137.

[93] E. Gürel, M. Pişkin, S. Altun, Z. Odabaş, M. Durmuş, Synthesis, characterization and investigation of the photophysical and photochemical properties of highly soluble novel metal-free, zinc(ii), and indium(iii) phthalocyanines substituted with 2,3,6-trimethylphenoxy moieties, Dalt. Trans. 44 (2015) 6202–6211. https://doi.org/10.1039/C5DT00304K.

[94] A.D. Adler, F.R. Longo, J.D. Finarelli, J. Goldmacher, J. Assour, L. Korsakoff, A Simplified Synthesis for Meso-Tetraphenylporphine, J. Org. Chem. 32 (1967) 476. https://doi.org/10.1021/jo01288a053.

[95] K. Hirao, Theoretical study of the Q and B bands of free-base, magnesium, and zinc porphyrins, and their derivatives, J. Phys. Chem. A. 103 (1999) 1894–1904. https://doi.org/10.1021/jp984807d.

[96] L. Alagna, A. Capobianchi, M.P. Casaletto, G. Mattogno, A.M. Paoletti, G. Pennesi, G. Rossi, Effect of molecular packing on the solid state spectra of ruthenium phthalocyanine: Anomalous behaviour of a monodimensional stacked assembly, J. Mater. Chem. 11 (2001) 1928–1935. https://doi.org/10.1039/b100041l.

[97] A. Auger, P.M. Burnham, I. Chambrier, M.J. Cook, D.L. Hughes, X-Ray crystallographic studies of three substituted indium(iii) phthalocyanines: effect of ring substitution and the axial ligand on molecular geometry and packing, J. Mater. Chem. 15 (2005) 168–176. https://doi.org/10.1039/B413189B.

[98] M. Kasha, H.R. Rawls, M.A. El-Bayoumi, The Exciton Model In Molecular Spectroscopy, Pure Appl. Chem. 11 (1965) 371–392. https://doi.org/10.1351/pac196511030371.

[99] R.L. Musselman, R.W. Larsen, B.M. Hoffman, Electronic spectra of porphyrins in the solid state: Newly observed transitions, collective and structural effects, and protein-mimicking environments, Coord. Chem. Rev. 257 (2013) 369–380. https://doi.org/10.1016/j.ccr.2012.08.015.

[100] X. Wang, M. Lu, C. Huo, H. Li, Y. Wang, Z. Li, Solvent effects on the absorption, circular dichroism and Raman spectroscopy of meso-tetrakis [3-methoxy-4-(N-carbazyl)n-hexyloxyphenyl] porphyrin in water-THF solution, Spectrochim. Acta - Part A Mol. Biomol. Spectrosc. 73 (2009) 581–586. https://doi.org/10.1016/j.saa.2009.01.012.

[101] M.A. Mateos-Timoneda, M. Crego-Calama, D.N. Reinhoudt, Supramolecular chirality of self-assembled systems in solution, Chem. Soc. Rev. 33 (2004) 363–372. https://doi.org/10.1039/B305550G.

[102] M. Shirakawa, S. Kawano, N. Fujita, K. Sada, S. Shinkai, Hydrogen-Bond-Assisted Control of H versus J Aggregation Mode of Porphyrins Stacks in an Organogel System, J. Org. Chem. 68 (2003) 5037–5044. https://doi.org/10.1021/jo0341822.

[103] Z.N. Erol, P. Atienzar, Y. Arslanoğlu, E. Hamuryudan, H. García, Synthesis and photophysical properties of phthalocyanines having calixpyrrole units, RSC Adv. 5 (2015) 55901–55908. https://doi.org/10.1039/C5RA05830A.

[104] C. Öztürk, A. Erdoğmuş, M. Durmuş, A.L. Uğur, F.A. Kılıçarslan, İ. Erden, Highly soluble 3,4-(dimethoxyphenylthio) substituted phthalocyanines:

Synthesis, photophysical and photochemical studies, Spectrochim. Acta Part A Mol. Biomol. Spectrosc. 86 (2012) 423–431. https://doi.org/https://doi.org/10.1016/j.saa.2011.10.062.

[105] J.R. Darwent, P. Douglas, A. Harriman, G. Porter, M.-C. Richoux, Metal phthalocyanines and porphyrins as photosensitizers for reduction of water to hydrogen, Coord. Chem. Rev. 44 (1982) 83–126. https://doi.org/https://doi.org/10.1016/S0010-8545(00)80518-4.

[106] X.-F. Zhang, Y. Di, F. Zhang, Photoinduced single- and double-electron transfer in a photosynthetic model consisting of one-acceptor with four equally linked donors (D4–A), J. Photochem. Photobiol. A Chem. 203 (2009) 216–221. https://doi.org/https://doi.org/10.1016/j.jphotochem.2009.02.009.

[107] C. Tanielian, C. Wolff, M. Esch, Singlet oxygen production in water: Aggregation and charge-transfer effects, J. Phys. Chem. 100 (1996) 6555–6560. https://doi.org/10.1021/jp952107s.

[108] K. Ozoemena, N. Kuznetsova, T. Nyokong, Photosensitized transformation of 4-chlorophenol in the presence of aggregated and non-aggregated metallophthalocyanines, J. Photochem. Photobiol. A Chem. 139 (2001) 217–224. https://doi.org/https://doi.org/10.1016/S1010-6030(01)00383-5.

[109] Y. Li, X. Duan, X. Li, D. Zhang, Photodegradation of nonylphenol by simulated sunlight, Mar. Pollut. Bull. 66 (2013) 47–52. https://doi.org/https://doi.org/10.1016/j.marpolbul.2012.11.014.

[110] Z. Noorimotlagh, I. Kazeminezhad, N. Jaafarzadeh, M. Ahmadi, Z. Ramezani, S.S. Martinez, The visible-light photodegradation of nonylphenol in the presence of carbon-doped TiO2 with rutile/anatase ratio coated on GAC: Effect

of parameters and degradation mechanism, J. Hazard. Mater. 350 (2018) 108–120. https://doi.org/https://doi.org/10.1016/j.jhazmat.2018.02.022.

[111] K. Bustos-ramírez, C.E. Barrera-díaz, M. De Icaza-herrera, A.L. Martínez-hernández, R. Natividad-rangel, C. Velasco-santos, 4-chlorophenol removal from water using graphite and graphene oxides as photocatalysts, J. Environ. Heal. Sci. Eng. 13 (2015) 33. https://doi.org/10.1186/s40201-015-0184-0.

[112] A.-P. Durand, R.G. Brown, D. Worrall, F. Wilkinson, A nanosecond laser flash photolysis study of aqueous 4-chlorophenol, J. Photochem. Photobiol. A Chem. 96 (1996) 35–43. https://doi.org/https://doi.org/10.1016/1010-6030(95)04289-X.

[113] R. Zugle, E. Antunes, S. Khene, T. Nyokong, Photooxidation of 4-chlorophenol sensitized by lutetium tetraphenoxy phthalocyanine anchored on electrospun polystyrene polymer fiber, Polyhedron. 33 (2012) 74–81. https://doi.org/https://doi.org/10.1016/j.poly.2011.11.005.

[114] X. Li, J.W. Cubbage, W.S. Jenks, Photocatalytic Degradation of 4-Chlorophenol. 2. The 4-Chlorocatechol Pathway, J. Org. Chem. 64 (1999) 8525–8536. https://doi.org/10.1021/jo990912n.

[115] M. Neamţu, D.-M. Popa, F.H. Frimmel, Simulated solar UV-irradiation of endocrine disrupting chemical octylphenol, J. Hazard. Mater. 164 (2009) 1561–1567. https://doi.org/https://doi.org/10.1016/j.jhazmat.2008.08.024.

[116] K.V. Kumar, K. Porkodi, F. Rocha, Langmuir–Hinshelwood kinetics – A theoretical study, Catal. Commun. 9 (2008) 82–84. https://doi.org/https://doi.org/10.1016/j.catcom.2007.05.019.

[117] L. Beránek, An Examination of the Langmuir-Hinshelwood Model Using Ion Exchange Catalysts, Catal. Rev. 16 (1977) 1–35. https://doi.org/10.1080/03602457708079633.

[118] S. Tombe, E. Antunes, T. Nyokong, Electrospun fibers functionalized with phthalocyanine-gold nanoparticle conjugates for photocatalytic applications, J. Mol. Catal. A Chem. 371 (2013) 125–134. https://doi.org/10.1016/j.molcata.2013.01.033.